https://lib.uliege.be https://matheo.uliege.be

Master thesis and internship[BR]- Master's Thesis : On the use of different test gases in the longshot tunnel to simulate different planetary entries[BR]- Internship (linked to master's thesis)

Auteur : Purnode, Martin
Promoteur(s) : Dimitriadis, Grigorios
Faculté : Faculté des Sciences appliquées
Diplôme : Master en ingénieur civil en aérospatiale, à finalité spécialisée en "aerospace engineering"
Année académique : 2019-2020
URI/URL : http://hdl.handle.net/2268.2/9045

Avertissement à l'attention des usagers :

Tous les documents placés en accès ouvert sur le site le site MatheO sont protégés par le droit d'auteur. Conformément aux principes énoncés par la "Budapest Open Access Initiative"(BOAI, 2002), l'utilisateur du site peut lire, télécharger, copier, transmettre, imprimer, chercher ou faire un lien vers le texte intégral de ces documents, les disséquer pour les indexer, s'en servir de données pour un logiciel, ou s'en servir à toute autre fin légale (ou prévue par la réglementation relative au droit d'auteur). Toute utilisation du document à des fins commerciales est strictement interdite.

Par ailleurs, l'utilisateur s'engage à respecter les droits moraux de l'auteur, principalement le droit à l'intégrité de l'oeuvre et le droit de paternité et ce dans toute utilisation que l'utilisateur entreprend. Ainsi, à titre d'exemple, lorsqu'il reproduira un document par extrait ou dans son intégralité, l'utilisateur citera de manière complète les sources telles que mentionnées ci-dessus. Toute utilisation non explicitement autorisée ci-avant (telle que par exemple, la modification du document ou son résumé) nécessite l'autorisation préalable et expresse des auteurs ou de leurs ayants droit.

U-VKI 2020-01

ON THE USE OF DIFFERENT TEST GASES IN THE LONGSHOT TUNNEL TO SIMULATE DIFFERENT PLANETARY ENTRIES

Graduation Studies conducted for obtaining the Master's degree in Aerospace Engineering, by

Purnode Martin

Supervisors: Dr. Grossir Guillaume & Pr. Dimitriadis Grigorios
Member of the Jury: Pr. Koen Hillewaert

Academic year 2019-2020
University of Liège - Faculty of Applied Sciences

von KARMAN INSTITUTE FOR FLUID DYNAMICS

LIÈGE université

Abstract

In order to increase the simulation capabilities of the Longshot wind tunnel, different gases are proposed to duplicate the conditions encountered during an atmospheric entry. Hydrogen, argon, oxygen, air, methane and a mixture equation of state are presented. The thermodynamic results are compared to the reference data provided by the Nist or the experimental measurements. These equations of state are accurate on a large temperatures and pressures range. The mixture equation is tested for several concentration of oxygen and nitrogen with the same type of error in all the cases. Hydrogen safety recommendations highlight the flammability and detonability hazard of this gas. The second risk of this gas is linked to the embrittlement this gas causes in several materials. Health hazards are limited to the general asphyxiant risks. A series of simulations using hydrogen as test gas is performed inside a L1D program that simulate the behaviour of the gas inside the Longshot. The behaviour of hydrogen differs from nitrogen. The velocity of the shock wave, the maximum temperature and the maximum pressure are higher in the case of hydrogen, while the compression due to the passage of the shock is far lower than when using nitrogen. New initial conditions should be designed for a pertinent use of hydrogen inside the Longshot.

Acknowledgments

The author wants to acknowledge the contributions of several Professors of the University of Liege. First, Professor Nathalie Job for her help regarding the thermodynamic behaviour of hydrogen. Then, the contribution of Pr. Gregoire Leonard in the domain of the mixing equations is also greatly appreciated. The help of Pr. Pierre Rochus must also be noticed. I also want to thanks the different people in my family who provided support and help in the final verification of the form of this report. The contribution of my academic supervisor, Pr. Grigorios Dimitriadis has also to be highlighted. I greatly appreciate the opportunity the von Karman Institute offered me to participate in the aerospace engineering field with this first contribution.

One person has to be thank with a higher intelligibility. This acknowledgement review would not be complete without highlighting the help, availability and support of Dr. Guillaume Grossir. I am very grateful to him for his contribution to this work.

Contents

Abstract iii

Nomenclature xi

1 Introduction 1

1.1 Framework and motivations 1

1.2 Objectives 1

1.3 Outlines 1

2 Wind tunnel families 3

2.1 Similitude parameters 3

2.2 Low enthalpy flows 4

2.2.1 Blowdown tunnels 5

2.2.2 Ludwieg tube 5

2.2.3 Hotshot 6

2.2.4 Gun tunnels 6

2.3 High enthaly flows 6

2.4 Very high enthalpy flows 8

2.4.1 Non reflective shock tunnels 8

2.4.2 Shock tubes 8

2.4.3 Expansion tubes/tunnels 8

2.5 Longhsot wind tunnel 8

2.5.1 Overview 9

2.5.2 Operational scheme 10

2.5.3 Valves system 12

2.5.4 Nozzles 13

2.5.5 Test gases 13

2.6 Summary 14

3 Influence of test gas on aerodynamics **15**

3.1 Atmosphere of the different planet of our Solar system 15

3.2 Analyse of different entry trajectories 18

3.2.1 Galileo mission 19

3.2.2 Galileo's trajectory reconstruction 21

3.3 Influence of the test gas on the aerodynamics 24

3.4 Icy Giants mission 28

3.5 Conclusions 29

4 Implementation and verification of the equations of state **31**

4.1 Hydrogen 31

4.1.1 General form of the equations of state 31

4.1.2 Specific form of the hydrogen 32

4.1.3 Verification of the equation of state 35

4.1.4 Safety aspects and advice for Longshot use 38

4.2 Oxygen 43

4.2.1 Equation of state 43

4.2.2 Verification of the equation of state 46

4.3 Argon 48

4.3.1 Equation of state 48

4.3.2 Verification of the equation of state 50

4.4 Air 52

4.4.1 Equation of state for air 52

4.4.2 Verification of the equation of state 53

4.5 Mixture equation 55

4.5.1 Mixing rules 55

4.5.2 Validation of the mixing equation 58

4.6 Other gases 61

4.6.1 Methane 61

4.6.2 Tetrafluoromethane 63

4.7 Summary 65

5 On the use of the Lagrangian 1d program **67**

5.1 Introduction to the Lagrangian 1d code 67

5.2 Convergence study 70

5.3 Introduction of the hydrogen 72

5.3.1 Approximations on the gases used 72

5.3.2 Results and discussions 74

5.3.3 Effect of a modification of the initial parameters 81

5.4 Conclusions 82

6 Conclusions and propositions of future investigations **85**

6.1 Conclusions 85

6.2 Propositions of future investigations 86

A Derivatives of the equations of states **87**

A.1 Hydrogen equation of states 87

B Hypervelocity Free Fligh Aerodynamic Facility **89**

B.1 HFFAF components 89

B.1.1 Launcher tubes 89

B.1.2 Separation chamber 91

B.1.3 Test section 91

B.1.4 Impact chamber 91

B.1.5 Shock tunnel 91

B.2 Simulation capabilities 92

B.3 Summary 92

References **93**

Nomenclature

Latin Symbols

A	Area, m^2
a	Helmholtz energy, J/mol
a_D	Deceleration, m/s^2
C	Chapman-Rubesin linear viscosity law constant, –
C_D	Drag coefficient, –
c_p	Constant pressure heat capacity, J/kg/K
c_v	Constant volume heat capacity, J/kg/K
e	Internal energy per unit mass, J/kg
g	Local gravitational acceleration, m/s^2
h	Enthalpy per unit mass, J/kg/K
He	Helium
Kn	Knudsen number, –
L	Reference length, m
M	Mach number, –
m	Mass, kg
M_w	Molecular weight, kg/mol
p	Pressure, Pa
Q	Arbitrary dimensionless quantity, –
R	Prefect gas constant, J/mol/K
r	Specific gas constant, J/kg/K
Re	Reynolds number, –
s	Entropy, J/K
St	Stanton number,–
t	Time, ms
T	Temperature, K
u	Velocity, m/s
$\overline{V}$	Viscous parameter, –
w	Speed of sound, m/s
z	Altitude, km
z_0	Reference altitude, km

Greek Symbols

α	Reduced Helmholtz energy, –
β	Shock angle, –
γ	Specific heat ratio, –
δ	Reduced density, –
ζ	Reentry flight path angle, –

κ	Atmospheric density decay, m^{-1}
λ	Mean free path, m
μ	Dynamic viscosity, Pa.s
ρ	Density, kg/m^3
τ	Reduced temperature, $-$
ψ	Mass fraction of dissociated molecules, $-$
$\overline{\chi}$	Viscous Interaction parameter, $-$

Superscripts

0	Ideal gas property
r	residual

Subscripts

c	Critical
L	Based on the length L
max	Maximum condition
ref	Taken at reference conditions
re	Reentry condition
w	At the wall
∞	Free stream value
$\left(\frac{\partial}{\partial}\right)_\delta$	(derivative of ...) at constant reduced density
$\left(\frac{\partial}{\partial}\right)_\tau$	(derivative of ...) at constant reduced temperature

Abbreviations

AFE	Aeroassit Flight Experiment
EoS	Equation of state
ESA	European Space Agency
FAA	Federal Aviation Administration
GRAM	Global Reference Atmospheric Model
HFFAF	Hypervelocity Free Flight Aerodynamic Facility
INRS	Institut National de recherches et de securite
IPCC	Intergovernmental Panel on Climate Change
L1d	Lagrangian 1-dimensional code
NASA	National Air and Space Agency
NIST	National Institute of Standards and technology
VKI	von Karman Institute for Fluid Dynamics

1 Introduction

1.1 Framework and motivations

The von Karman Institute for Fluid Dynamics is a major actor in the European research landscape for many topics, such as the turbomachinery and propulsion, the environmental research and the aeronautics and aerospace thermodynamics. The latter offers a unique expertise in the reentry domain thanks to several super and hyper sonic wind tunnels. These different facilities offer opportunities of investigations in several areas of the atmospheric reentry. The Longshot hypersonic wind tunnel focuses its experimental campaigns on the determination of the aerodynamic coefficients of a spacecraft at hypersonic speeds. This competence is currently used to simulate the conditions encountered during a part of the reentry on Earth and in the Martian atmosphere. These capabilities could however be extended to several other planet atmosphere, such as Venus or Neptune thanks to the introduction of new gases inside this wind tunnel. This increase of competence could then serves for future missions on different planets, such as the new collaboration between the ESA and the NASA with the objective of sending a probe inside the Icy Giants.

1.2 Objectives

The objective of this work is the extension of the simulation capabilities of the Longshot wind tunnel by the presentation and the study of several gases that could be used to simulate the conditions met by a spacecraft during atmospheric entries. The selection of these gases is done through the review of the composition of the atmospheres of different planets inside our solar system. Several other gases used by different wind tunnels around the world were also investigated. This study will then present more deeply the possibilities of the use of hydrogen to simulate entries on the Gaseous and Icy Giants. The second most important improvement for the Longshot simulation is the introduction of a mixing rule that would allow the use of more complex test gases inside the Longshot wind tunnel.

1.3 Outlines

This study starts in § 2 by presenting the different varieties of hypersonic wind tunnels existing, as well as the types of measurements they offer and the limitations they are submitted to. A particular attention is then given in § 2.5 to the Longshot wind tunnel. The influence of the test gas on aerodynamics is then presented by § 3. Next, the different atmospheres that would support an atmospheric entry are introduced in § 3.1. The entry trajectory and the reconstruction process of the temperature, pressure and density profile of a barely known atmosphere is then depicted in § 3.2, with a particular attention on the Galileo probe, which entered inside the Jovian atmosphere 35 years ago. The influence of the test gas, the Reynolds number and the Mach number on the duplication of the aerodynamic coefficients is finally highlighted by § 3.3.

Several gases are studied in § 4. The general form of equation of state already used for the current tests real, as well as the relations that link this type of equation to the different thermodynamic parameters are presented in § 4.1. The specific form of this equation of states for hydrogen is then presented in § 4.1.2 and compared to reference data in § 4.1.3 in order to validate the approach proposed by this equation. Several safety warnings and advice are provided by § 4.1.4. The specific equations of states of oxygen, argon and air are presented respectively in § 4.2, § 4.3 and § 4.4. A mixture equation of state using the same formulation is then presented in § 4.5. Two other gases, methane and tetrafluoromethane are also introduced in § 4.6.

The Lagrangian one dimensional program used to simulate the conditions inside the Longshot wind tunnel during a test is presented by § 5. A convergence study is then proposed in § 5.2. Afterwards, the study of the results obtained using hydrogen in the L1d program is presented in § 5.3. The conclusions of this study and several propositions of future works are finally presented in § 6.

2 Wind tunnel families

The wind tunnels used to simulate the atmospheric reentry are usually not able to duplicate the full conditions encountered during this entry. They are however able to duplicate several of these conditions thanks to the use of similitude parameters. Depending on several criteria, different families of wind tunnels can be described. In this section, the major families will be quickly exposed, with the maximal enthalpies and operation schemes as differentiation parameters, as presented by Olivier and Gu (2018). The different wind tunnels offer different possibilities and limitations in terms of test time, stagnation point temperature and velocity of the flow. Starting with the wind tunnels operating in low enthalpy flows, the high and very high enthalpy flows operating wind tunnels will be introduced. A special attention is then given to the Longshot wind tunnel, since this hypersonic tunnel is the one considered in the simulations presented in § 5.

2.1 Similitude parameters

Thanks to several examples based on the historical flights of American spacecrafts, Lukasiewicz (1973) presented a method of similitude parameter to simulate the different part of hypersonic reentries. This topic was also discussed by Hornung (2010) with a special attention devoted to high enthalpy wind tunnels and by Grossir (2015), where the low enthalpy VKI Longshot tunnel was the support of the study.

The duplication of the whole entry, in terms of heat shield ablation, real gas phenomena or aerodynamic parameters is impossible using a single wind tunnel, due to the high quantity of energy it would required. For this reason, these different aspects of the atmospheric reentry are studied separately and by different types of wind tunnels. The categorisation of the different types of wind tunnels can be made in different ways. Some of these differences imply the flow velocity, the maximal enthalpy, the test time or the stagnation point temperature. Figure 1 presents one type of differentiation that can be made to classify the types of wind tunnels.

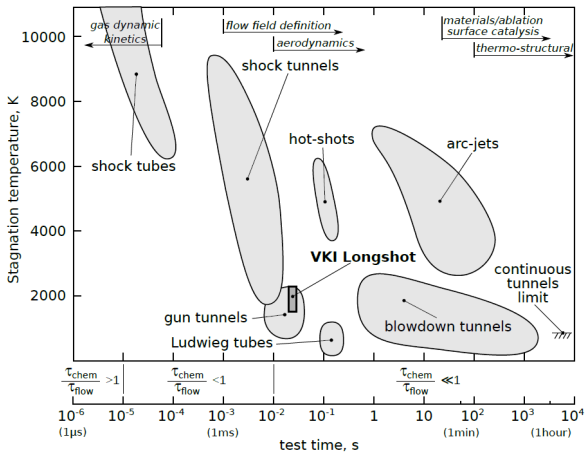

Figure 1: Stagnation point temperature vs test time (Grossir, 2015)

Making assumptions on the behaviour of the gas can also be seen as another trail to differentiate the type of similitude parameters that would be needed to obtain accurate data. Studies presented by Lukasiewicz (1973) have shown that, with the price of a careful interpretation, several data, such as the hypersonic forces, can be obtained thanks to appropriate similitude parameters.

The Reynolds number $Re_{L,\infty} = \frac{u_\infty L_{ref} \rho_\infty}{\mu_\infty}$ naturally comes from dimensional analysis when aerodynamic studies are considered. This parameter offers a representation of the viscosity effect on a model having a reference length of L. The Mach number $M = \frac{u_\infty}{w_\infty}$ can be used to represent the compressibility effects. For an ideal gas, i.e. thermally and calorically perfect, other parameters could be considered, such as the Knudsen $Kn = \frac{\lambda}{L}$, with λ the mean free path, well suited for the rarefied environment where the higher Mach numbers are measured. The viscous interaction parameter $\overline{\chi} = \frac{M_\infty^3}{\sqrt{Re_{L,\infty}}}\sqrt{C}$ or the viscous parameter $\overline{V}_\infty = M_\infty \sqrt{\frac{C}{Re_{L,\infty}}}$, where $C = \frac{\mu_w}{\mu_\infty}\frac{T_\infty}{T_w}$ is the Chapman-Rubesin linear viscosity law constant, can also be used. However, either Kn, $\overline{\chi}$ or $\overline{V}_\infty$ can be obtained by thanks to Re, M and the wall to free-stream temperature ratio $\frac{T_w}{T_\infty}$..

The use of the Mach and Reynolds numbers is well suited for the study of aerodynamic forces/coefficients, but is not enough when it comes to the study of the real gas phenomena or the heat transfer. The former includes the studies of the ionisation and dissociation effects, that can alter the measurement of these duplication parameters. In that case, the real flight conditions must be replicated. If the heat transfer are matter of interest, the real flow enthalpy as well as the real flow density become the important parameters.

2.2 Low enthalpy flows

These wind tunnels are characterised by a maximal enthalpy of 2 MJ/kg and the assumption of a perfect gas behaviour[1]. The variation of the specific heat ratio γ is not yet influence by the pressure and the modification of its value is due to the vibrational excitation of gas. The behaviour of this quantity in presented in Fig. 2 for air[2]. In this "perfect gas" configuration, an arbitrary dimensionless quantity Q can be expressed in term of other dimensionless parameters as

$$Q = Q\left(M_\infty, Re, \frac{T_w}{T_0}, F_q\right) \tag{1}$$

where M_∞ is the free stream value of the Mach number, Re the Reynolds number, T_w/T_0 the wall to total temperature ratio and F_q was defined by Olivier and Gu (2018) as a "*set of dimensionless parameters defining the flow quality in the wind tunnel*". Thanks to this dependency, the skin friction coefficient, the Stanton number, the laminar viscous interaction

[1]Perfect gas behaviour must here be understood as a behaviour where chemical reactions due to the temperature do not appear. For air, these rel gas effects appears at T=2000 K with the dissociation of oxygen

[2]Thermally perfect

parameters, etc can easily be computed. These wind tunnels are then performing *Mach-Reynolds* simulations. The Longshot wind tunnel is part of this category and is described in § 2.5. The main families of low enthalpy tunnels are the blowdown tunnels, the Ludwieg tubes, the hotshots and the gun tunnels.

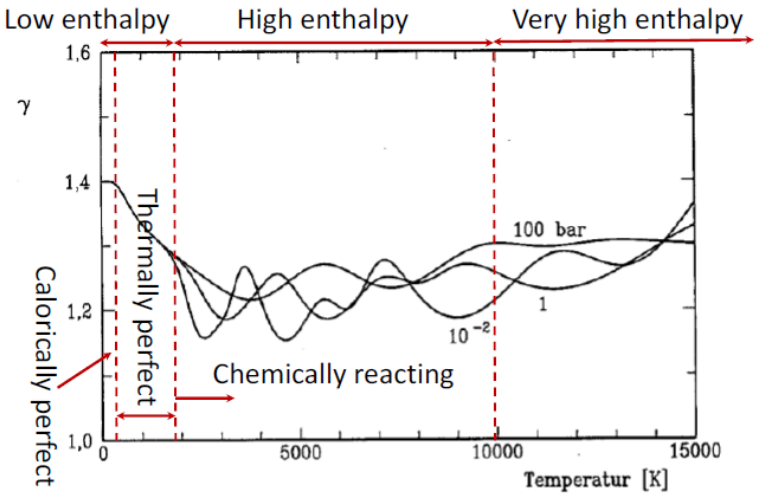

Figure 2: Variation of the specific heat ratio γ of air with temperature and pressure (Olivier and Gu, 2018)

2.2.1 Blowdown tunnels

The principle of operation of a *blowdown tunnel* is simple. A high-pressure tank is separated from the test section by a diaphragm or a high pressure valve, and a nozzle. Before the beginning of the test, both the nozzle and the test section are set to a low pressure. The gas inside the tank is heated to obtain the desired pressure and temperature. The exact parameters depend on the test. When these conditions are reached, the diaphragm ruptures or the high pressure valve is opened. Then, the expansion gas passes over the model. A low equivalent velocity and a low to moderate stagnation temperature are characteristics of this blowdown wind tunnel. This is also the type of wind tunnel that offers the highest test time, as it is presented in Fig. 1. It is used by the AEDC tunnel 9 of the Arnolds Air Force Base (Tennessee, USA) or by the VKI H3 Mach 6 tunnel (Rhode-Saint-Genèse, Belgium).

2.2.2 Ludwieg tube

A second family of low enthalpy tunnel is known as the *Ludwieg tube*. It uses a similar heated gas contained in a tank before the beginning of the test. A vacuum tank is added after the test section, increasing the pressure difference between the test section and the tank containing the test gas. The high-pressure gas experiences an unsteady expansion when the diaphragm is broken. The expansion wave moves upstream until its reflection at the end of the tube. When this reflecting wave reaches the nozzle, the test is over. Examples of this

type of blowdown wind tunnel are the HHK of the HTG company (Göttingen, Germany), or the TU (Delft, Netherlands). This type of wind tunnel was described by Reynier (2016) and Olivier and Gu (2018).

2.2.3 Hotshot

Another type of low enthalpy wind tunnel currently used is the *Hotshot*, where the test gas is heated thanks to an electric arc. This type of wind tunnel was used the ONERA F4 (Le Fagua, France). This facility conducted interesting studies including several test gases, such as air, argon or carbon-dioxide to offer measurements of aerodynamic and aeroheating on different models. Russia also uses this type of tunnels with its ITAM IT-302M, dedicated to combustion studies. Another example is the Russian TSAGI IT2 tunnel, that also uses, among other, argon to simulate aerodynamic behaviour of several configurations.

2.2.4 Gun tunnels

The *gun tunnel* uses a system of light piston to compress and heat the test gas contained in a driven section. A driver tube, located upstream the driven tube and separated from the latter by the piston, is filled with a high pressure gas. When the test starts, the piston is released and accelerated by the pressure difference between the driver and the driven tube. The gas contained in the latter is compressed until a certain pressure that triggers the rupture of a diaphragm located at the end of the driven tube. The piston continues to compress the gas in the driven tube, while a part of this gas is ejected through a nozzle in the test section, where is the model. The Cranfield University[3], UK, uses several wind tunnel, one of them being a gun tunnel.

The Longshot variant of this gun tunnel uses the series of check valves, which increases the test time by preventing the gas trapped in the reservoir to be influenced by the rebound of the piston. This type of gun tunnel is illustrated and detailed in § 2.5 with the VKI Longshot (Rhode-Saint-Genèse, Belgium).

2.3 High enthaly flows

When the enthalpy increases, the vibrational excitation of the test gas is not longer the only real gas effect that must be taken into account. Indeed, the temperatures reached during the tests are high enough to allow chemical reactions, such as dissociation and recombination of the gas. Fig. 2 shows the variation of γ with temperature and pressure for air. For temperatures below 2000 K, the chemical reactions do not occur in air and a low enthalpy flow can be considered, as discussed above. When this critical temperature is reached, γ does

[3]Cranfield University website, URL

not only depend on the temperature, but also on the pressure, due to these chemical reactions. In this type of flow, a dimensionless parameter Q can be obtained by a combination of several other parameters, in the same way than for a low enthalpy flow. However, its dependency parameters are here different and thus

$$Q = Q\left(u_\infty, \rho_\infty, L, \psi_\infty, \frac{T_w}{T_\infty}\right) \tag{2}$$

where u_∞ is the free stream velocity, ρ_∞ the free stream density, L the characteristic length and ψ_∞ is the mass fraction of the dissociated molecules in the free stream. Moreover, an important parameter is the product $\rho_\infty L$. Indeed, when combined with u_∞, it automatically satisfies the post-shock Reynolds number. According to Olivier and Gu (2018), the velocities that can be reached by this type of tunnels range from 2 to 7 km/s. However, due to the strong shocks created by blunt bodies, the Mach number becomes irrelevant for these types of measurements.The main type of high enthalpy flow wind tunnel is the *reflected shock tunnel*.

The precise operational scheme of the reflected shock tunnels was reported by Olivier and Gu (2018); Holder and Schultz (1960). It consists of a driver tube separated from the driven tube by a first diaphragm. Inside the driver tube, the driver gas is heated to reach the desired conditions. The driven tube contained the test gas and is separated from the test section by second diaphragm and a converging diverging nozzle. The test begins when the primary diaphragm ruptures. A strong shock wave is then created. When it reaches the second diaphragm, a reflected shock wave forms and creates a stagnated nozzle inlet condition. This type of tunnels require higher pressure and temperature than the low enthalpy wind tunnels. According to Olivier and Gu (2018), these conditions are currently achieved by three methods:

- The first method, used by the NASA EAST at the Ames Research Center, USA, or by the Russian TSAGI ADST, uses an electric discharge to heat the driver gas. This type of wind tunnel is then known as *Electric arc driver*.

- The *Stalker tunnel* is a second solution to increase the temperature and pressure of the gas. It uses a heavy piston to compress almost adiabatically and isentropically the driver gas. This type of wind tunnel is very popular and used in every continent. The HEG wind tunnel in Germany, the T4 in Australia, or the FD21 in China can be mentioned as examples.

- The last method used for this type of wind tunnel relies on the detonation of a hydrogen-oxygen mixture. This method, known as *detonation driver*, is not largely used, due to its poor performance with respect to the Stalker tunnels, the risk of the storage and use of hydrogen, or the maintenance the detonation process requires. However, its attractive price can be a reason to prefer this method to the Stalker tunnel.

2.4 Very high enthalpy flows

In order to generate even higher temperature and pressure, the stagnated test gas condition at the reservoir created by the previously presented method have to be overcome. Practically, this objective can be realised following types of wind tunnels.

2.4.1 Non reflective shock tunnels

This configuration, almost identical to the reflected shock tunnels, does no longer use a converging diverging nozzle, but a purely diverging nozzle. Thanks to this configuration, the gas does not stagnate at the entrance of the nozzle but continues its motion without interruption. Even if this configuration offers higher performances than the reflected shock tunnels, Olivier and Gu (2018) reported an absence of this type of facility.

2.4.2 Shock tubes

This type of wind tunnel is similar to the shock tunnel, but does not use a nozzle. They are mostly used to study thermochemical kinetics and radiations. Unlike the previous facilities, this type of wind tunnel usually focuses its study on the flow itself and do not uses models. The two main advantages of this configuration is the 1 dimensional flow configuration, allowing simple studies, and the accurate definition of the free stream. However, the structure of the tunnel itself limits the variety of experiments that can be conducted in this type of wind tunnel.

2.4.3 Expansion tubes/tunnels

This configuration can be seen as a shock tube with an additional acceleration tube at low pressure. This acceleration tube is separated by a thin diaphragm. When the latter is broken by the shock generated by the driver and driven sections, the test gas experience an unsteady expansion, increasing the total pressure and enthalpy. Depending on the use or not of a nozzle, this type of wind tunnel is called respectively expansion tunnel or tube.

2.5 Longhsot wind tunnel

The Longshot wind tunnel occupies a particular attention here, since this is the facility used by the von Karman Institute to simulate the conditions encountered during a part of the atmospheric entries in terms of Mach and Reynolds numbers. This section introduces this wind tunnel, starting with an overview of its history and components. Its operational scheme is then depicted, with a particular attention given on the qualitative behaviour of the flow, the check valve system, the different nozzles and the test gases currently used. The particular attention given to this wind tunnel is explained by the important role it plays in this study, as the different test gases that will be described in § 4 have possible applications in this facility.

2.5.1 Overview

The Longshot hypersonic facility is based on the gun tunnel principle presented by § 2.2.4. It was conceived by R.W. Perry and his team (Perry, 1964) at the Republic Aviation Corporation (USA) before being moved to the VKI premises in 1967, where it has been used for different applications ever since. Its fields of application include aerothermodynamic characterisation of space probes, creation of aerothermodynamic databases for reentry vehicles, experiments of hypersonic phenomena on several configuration or, since a few years, aerothermodynamic measurements on space debris and meteorites (Grossir and Ilich, 2018).

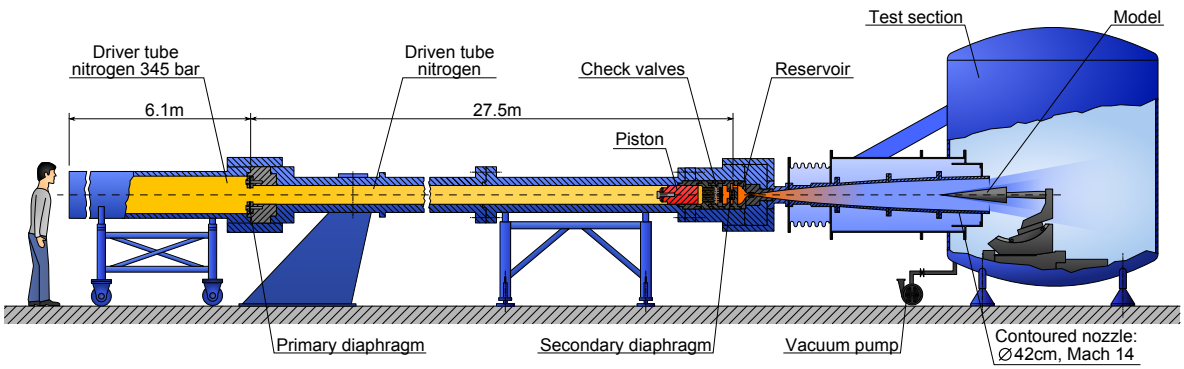

Figure 3: Sketch of the VKI Longshot hypersonic gun tunnel (Grossir, 2015).

This short-duration facility is composed of the following main elements with reference to the sketch given in Fig. 3:

- a driver tube (initially filled with nitrogen at high pressure),
- a long driven tube, containing the test gas initially at ambient temperature and at moderate pressure,
- a piston, initially located at the interface between the driver and driven tubes and preventing gas mixing between the two tubes,
- a set of 48 check valves at the end of the driven tube which is used to trap the gas near the peak stagnation conditions in the reservoir,
- a conical or a contoured nozzle,
- a test section, vacuumed prior to an experiment, and in which instrumented models and probes are located,
- and two diaphragms: a primary one attached to the piston and maintaining the latter until the beginning of the test, and a secondary one isolating the driven tube from the reservoir.

2.5.2 Operational scheme

The initial conditions in the driver tube are usually taken at approximately 300 K and a high pressure of 34.5 MPa. The only gas used in this driver tube until now is nitrogen. The same gas is also currently used in the driven tube to simulated Earth reentries, but carbon dioxide can also be considered to simulate entries in the Martian atmosphere. Before a test run using nitrogen, the initial temperature in the driven tube is set to $\sim$ 293 K, while the initial pressure depends on the desired flow conditions in the test section. It usually ranges from 144.1 to 275.8 kPa. The mass of the piston used depends on the pressure, as a too heavy piston coupled with a too low pressure could result in a final deceleration that is not be able to prevent a collision between the piston and the valves set. Three pistons are currently used, having masses of 1.59 kg, 3.215 kg and 4.592 kg. Grossir (2015) highlighted that the use of a heavier piston, and thus a higher pressure in the driven tube, results in a higher Reynolds number reached in the test section. In the latter, the pressure is lowered to be smaller than 1 Pa (Grossir, 2015; Grossir and Ilich, 2018). Similar conditions were reported by Ilich et al. (2019) for Martian reentry. If carbon dioxide is used, the pressure in the driven tube is usually set 140 and 300 kPa. The initial temperature in the driven tube and the conditions in the driver tube are the same than in the case of nitrogen. The mass of the piston used with this gas is usually between 1.3 and 3.8 kg.

When the initial parameters are reached (Fig. 4a), the operator ruptures the primary diaphragm that separates the driver and the driven tubes. This diaphragm, made of a 3 mm thick layer of aluminium, is attached to the piston. The free piston will then be accelerated by the pressure difference between the two tubes. The peak acceleration is of the order of 50 km/s^2. Expansion waves are created behind the piston, while compression waves appear in front of the latter (Fig. 4b). At this stage, most of the gas inside the driven tube is not influenced yet by the compression waves.

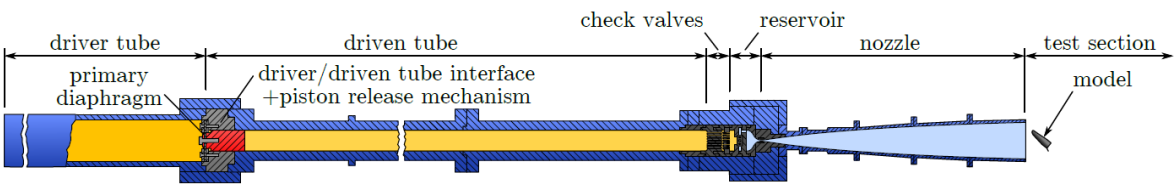

(a) Initial conditions

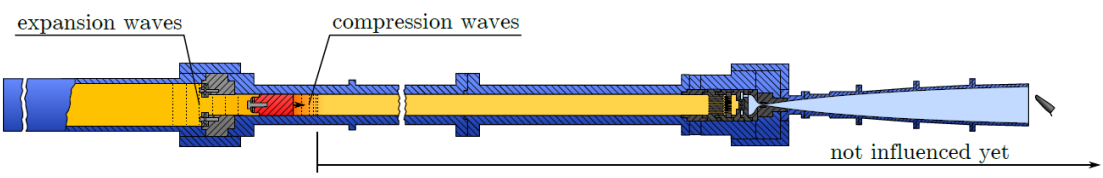

(b) Release of the piston, creation of compression wave in front of it

The speed of the piston becomes supersonic to finally reach a peak velocity of the order of 600 m/s. Due to this speed, the driven gas compression can be considered nearly adiabatic.

The compression waves merge into a shock wave with a velocity higher than the piston itself (Fig. 4c). The shock wave finally reaches the downstream extremity of the driven tube (Fig. 4d), where a part is transmitted to the valves system, and another part is reflected upstream to the piston. When the shock wave reaches the piston, it is reflected back and fourth between the piston and the end of the driven tube. The piston decelerates, giving its energy to the driven gas. The pressure quickly rises and, at a certain pressure level (12 MPa), breaks the 1 mm thick copper diaphragm. Then, the test gas begins to enter inside the reservoir.

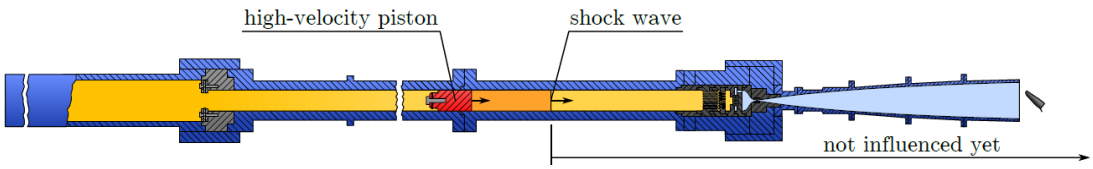

(c) Compression waves merge into a shock wave

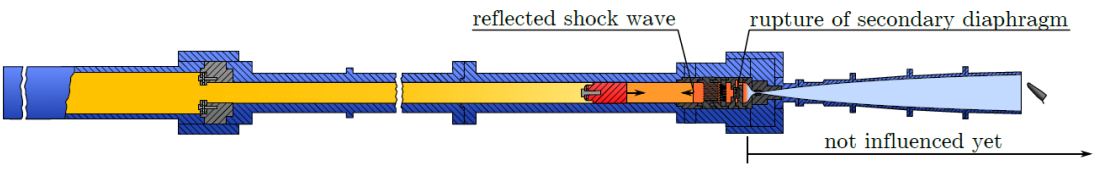

(d) The shock wave reaches the reservoir and is partially reflected backward

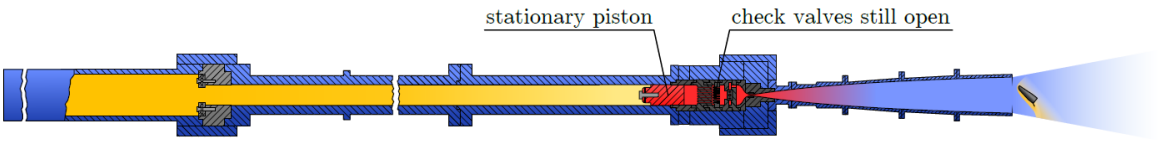

(e) Rupture of the secondary diaphragm, introduction of the test gas inside the nozzle and rebound of the piston

Figure 4: Sketch of the compression process of the VKI Longshot wind tunnel (Grossir and Ilich, 2018)

In Fig. 4e, the pressure between the piston and the reservoir is so high that a peak deceleration of the order of 500 km/s^2 is experienced by the piston. The latter is then stopped before impacting the valves set and the reservoir. The nozzle flow is quickly established. The pressure difference pushes the piston upstream. Thanks to a set of valves, the pressure in the reservoir is not reduced when the piston moves backward. This system increases the test time by an order of magnitude compared to the simplier gun tunnel described in § 2.2.4. Inside the reservoir, the stagnation conditions gradually decreases, as the amount of test gas in this constant volume decreases. This allows the duplication of a large variety of Reynolds number during a single test. Moreover, the Longshot experiment can be seen as a series of quasi-steady flow configurations, since the flow establishment time over the different models is smaller than the characteristic time of this flow (Grossir, 2015; Grossir and Ilich, 2018).

2.5.3 Valves system

Several components of the Longshot architecture will be deeply introduced. First, the system of valves. The latter is composed of a set of 48 valves with a length of the order of the centimetre, placed at the end of the driven tube and before the reservoir. The role of these valves is to trap the test gas in the reservoir at its largest stagnation conditions. When the piston moves backward, the pressure difference automatically closes the valves, enhancing the test time by preventing the test gas to go back with the piston. Due to the short test time, the motions of these valves have to be very fast, which explain the preference of a large number of small valves to the consideration of a small number of larger ones. However, in the scope of maintaining an appropriate sealing of the reservoir, these valves are replaced after each test. The valves system is presented in Fig. 5, (Grossir and Ilich, 2018).

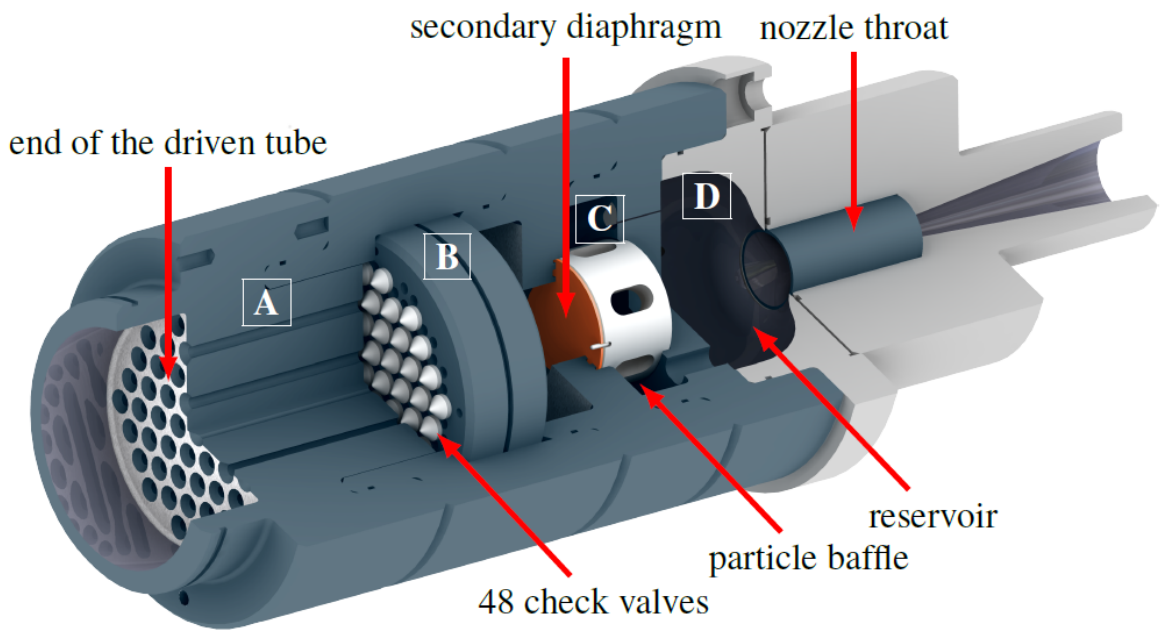

Figure 5: 3D sketch of the valves system, reservoir and secondary diaphragm of the VKI Longshot (Grossir and Ilich, 2018)

The test gas enters the reservoir by the 48 holes drilled in zone A. The downstream extremities of these drilled holes have a conical form in order to be blocked by the valves when the piston is pushed upstream by the high pressure difference discussed above. These valves are held by 48 holes in the second zone (B), to which are added 132 holes drilled to allow the test gas to pass through to the second diaphragm. When the pressure reaches 12 MPa, this second diaphragm ruptures. The particle baffle (zone C) was created to trap the copper particles resulting from this rupture. This diaphragm, as well as the reservoir behind, form the last part of the Longshot wind tunnel before the nozzle.

2.5.4 Nozzles

Three nozzles are currently used in the Longshot wind tunnel. The simplest one is a conical nozzle that has two main advantages: the Mach number at its outlet can be selected by modifying the inlet/outlet area ratio, allowing then a large variety of tests. Contrary to the two other nozzles that were shaped to be used with nitrogen only, this nozzle can be used with different gases. However, its major drawback turns out to be its shape itself. Indeed, the flux coming from this nozzle diverges, which is not representative of the real conditions experienced by a vehicle in reentry. To palliate this problem, a solution could be to use shaped nozzle that creates a parallel outlet flow, which ensures a closer reproduction of the real flight environment. The Longshot wind tunnel has two of these nozzles at its disposition, offering parallel flux at Mach number of 12 and 14. Nevertheless, the use of these nozzles is very rigid, as they only allow a single outlet Mach number and for a single test gas. These two shaped nozzles were designed for the use of nitrogen. At this stage, the use of the conical nozzle is the best option for the use of gases other than nitrogen and for Mach number different from those of the shaped nozzles. A shaped nozzle could also be designed for the different gas or Mach number to take advantage of the better approximation of the flight environment offered by this type of nozzle. A more advance study could however be made on the possibility of the use of these shaped nozzle with a gas having a specific heat ratio similar to nitrogen.

2.5.5 Test gases

The test gases used in the VKI Longshot are mostly nitrogen and carbon dioxide, even if several test were conducted using helium. The use of the former was decided after strong problems of oxidation experienced using air. These problems were attributed to the oxygen dissociation and recombination in the reservoir. The nitrogen is found relevant for Earth reentry tests, since it composes the vast majority of its atmosphere. Moreover, the oxidation of the nitrogen occurs at higher temperature and its ratio of specific heat is very close to the one of the air at the same temperature. This can be easily explained by the large portion of nitrogen in the "standard" air composition, which is also very close to the specific heat ratio of the oxygen (≈ 1.4 in both cases). Grossir (2015) exposed the purity level of the nitrogen to be as high as 99.999%, while the contamination of di-oxygen and water are respectively less 5 ppm and 2 ppm. The use of a substitute test gas can be considered to duplicate the condition of air. Indeed, the moderate enthalpy effects are not the interest of this wind tunnel, dedicated to the study of reentry aerodynamics by the duplication of Reynolds and Mach number.

With a first simulation conducted in 1995, carbon-dioxide is also used as a test gas in the Longshot wind tunnel to simulate Martian entries. Ilich et al. (2019) presented the boundary and initial conditions used when this gas is introduced in the driven tube. It also highlights the results obtained using this test gas, and compared them to the numerical results obtained thanks to a modified version of the Lagrangian 1-dimensional code (L1d) already used for nitrogen simulations. An introduction of this program is presented in § 5. For both test gases,

a strong correlation between the numerical model and the experimental measurements tends to validate this approach. Ilich (2018) also presented a study with Helium as test gas, even if the objective of this study was not the simulation of aerodynamic behaviour, but rather to improve the understanding of the nozzle flow of the VKI Longshot.

Even if the law of the perfect gas can be used as a first crude approximation, the extreme conditions met in the wind tunnel require the use of more accurate equations of states. The nitrogen behaviour is then simulated by the Span and Wagner equation of state (EoS), that is applicable up to a temperature of 1000K and a pressure of 2200 MPa (Span et al., 2000). The EoS used for carbon dioxide was also described by Span and Wagner (Span and Wagner, 1996). The helium equation of state was presented by Ortiz Vega (2013). Even if the temperature met at the extreme reservoir conditions is above the upper limits of these equations of states, the thermodynamic behaviour of these gas can be extrapolated with a good accuracy.

2.6 Summary

The atmospheric reentry cannot be simulated using a single type of wind tunnel due to the energy requested to duplicate every parameter encountered. Several type of wind tunnels are then used to proceed to different type of experiments. The low enthalpy wind tunnels that are the blowdown, the Ludwieg tube, the hotshot and the gun tunnels are more suited for Mach-Reynolds simulations. Consequently, they are usually used for aerodynamic studies. The high and very high enthalpy wind tunnels, more interested in radiation and thermochemical phenomena, use higher temperatures and pressures that lead to chemical reaction of the test gases. The importance of the aerodynamic studies can be highlighted in several re-entry applications. This is the subject of § 3.3.

The hypersonic wind tunnel used at the von Karman Institute, the Longshot, is composed of a driver tube, a driven tube, a reservoir, a nozzle and a test section. The former is filled at high pressure and quasi ambient temperature with nitrogen. This gas is used to propel a piston that compress a test gas along the driven section. The gases currently used inside this driven tube are nitrogen, carbon dioxide and several tests were run with helium. A set of check valves traps the compressed gas inside a reservoir. When a certain pressure is reached, a second diaphragm ruptures and the gas is released through a nozzle. The latter expand the gas on the model in the test section. This tunnel currently provides aerodynamics measurements for reentry testing on Earth and on Mars. Depending on the gas used inside the driven tube, the initial conditions in this tube, as well as the piston employed, are different. The dissociation of gases in this facility has to be avoided, because of the damages it causes to the reservoir of the wind tunnel during the recombination of this gas. A particular attention should then be given in the choice of alternative test gases to ensure that their real gas effects (dissociation, ionisation) do not appear or do not lead to damages in the wind tunnel.

3 Influence of test gas on aerodynamics

This section introduces the composition of several planets and satellite atmospheres, those that are thick enough to make re-entry phenomena important. An analyse of the entry trajectory of Galileo is then introduced, along with the method used to reconstruct the atmosphere of a planet using in-situ measurement gathered during the reentry. The influence of the test gas on the aerodynamic parameters is finally discussed.

3.1 Atmosphere of the different planet of our Solar system

The knowledge of the different planetary atmospheres is of major concern when a reentry mission is considered. The objectives of these missions can be divided into four categories:

- The slowing down of a vehicle in order to land on a planet. This type of mission is frequent, as reentries on Earth occurs several times a year, to bring astronauts back for example. Similar reentries were experienced during missions on Venus (Soviet Venera program, American Pioneer Venus missions), Mars (Soviet Mars 3, American Viking 1 & 2, European Beagle 2,...) or Titan (European Huygens). The importance of these reentry simulations mainly lies on the survival of the crew/equipment of the reentry itself.
- The measurement of the precise atmospheric composition. Theoretical models are used to estimate unknown atmospheric composition, but the latter needs to be confirmed by in situ measurements. One of the most famous example of this type of reentry was performed by the American probe Galileo, which entered Jupiter atmosphere on the 7th of December 1995. The Cassini-Huygens or the Venera program can also be cited here, since at least a part of their missions was to analyse the atmospheric composition of their "target". This type of missions is detailed with the exposure of the Galileo mission.
- The aerobreaking or aerocapture of a satellite. This method consisting of performing a controlled atmospheric reentry on a planet and to use the aerobreaking due to the atmospheric drag to reduce an hyperbolic orbit into a close elliptic orbit around the considered planet/satellite. Even if this technique was not yet used with other planet atmosphere, the soviet spacecrafts Zond 6 and 7 used it when they came back from the Moon. According to Justus et al. (2006), aerocapture can by performed on eight different locations that are three of the four rocky planets (Mercury[4] has a very thin atmosphere, with a surface pressure as low as 0.5 nPa), the gaseous giants and the Saturn's biggest satellite, Titan. The atmospheres of the different other satellites of the solar system are also too thin to consider for an effective aerocapture or other reentry. Lockwood (2003) and Starr et al. (2004) exposed studies of the aerocapture capabilities respectively on Neptune and Titan.

[4]Data obtained from NASA fact sheet: Mercury

- The destructive reentry. This type of reentry is by far the most frequent, since a large number of meteorites of various sizes enter the atmosphere of the Earth every day. This type of reentry can also be extended to involve the destructive reentry of satellites in disposal phase.

The eight destinations mentioned in this brief description of aerocapture are the only one in the solar system that present an atmosphere dense enough to allow a pertinent atmospheric entry study. The mean composition of these atmospheres are depicted by Table 1. When it is possible, the atmospheric compositions reported in this table were obtained thanks to in situ measurements. Venus's atmosphere was obtained thanks to the Soviet Venera program and the occidental Venus pioneer and Mariner missions. This atmospheric composition was reported by VonZahn et al. (1983) and David C. Catling (2019). Mars atmospheric data are those measured by Curiosity and presented by Mahaffy et al. (2013) and David C. Catling (2019). Galileo probe, when it entered in the Jovian atmosphere, offered measurements of the planet atmosphere that was reported by Niemann et al. (1996) and Niemann et al. (1998). Flasar (1998) estimated the composition of the atmosphere of Titan and these data were corrected by the measurements carried by Huygens probe, reported by Niemann et al. (2005) and David C. Catling (2019). The atmospheric compositions of Saturn and the Icy Giants are known theoretically, namely thanks to spectroscopy, but since no atmospheric probes had been sent in these locations to provide in situ measurements, the data exposed in Table 1 are mean theoretical data provided by the NASA fact sheets. An approximation of these atmospheres is alos provided by Curry and Webster (1998) These last two planets are at the centre of attention of the American and European space agencies, according to Bavon (2019). The scientific objective of this mission are presented in § 3.4.

Location	Element abundance (volume ratio)			Source
	Main	second	Third	
Venus	CO_2 (96.5 %)	N_2 (3.5 %)	He (12 ppm)	(David C. Catling, 2019)
Earth	N_2 (78.08 %)	O_2 (20.95 %)	Ar (0.93 %)	(David C. Catling, 2019)
Mars	CO_2 (95.7 %)	Ar (2.07%)	N_2 (2.03%)	(David C. Catling, 2019)
Jupiter	H_2 (89.8 %)	He (10.2 %)	CH_4 (3000 ppm)	(Niemann et al., 1998)
Saturn	H_2 (96.3 %)	He (3.25 %)	CH_4 (5000 ppm)	(Williams, 2018b)
Titan	N_2 (94.2 %)	CH_4 (5.65 %)	H_2 (0.1 %)	(David C. Catling, 2019)
Uranus	H_2 (82.5 %)	He (15.2 %)	CH_4 (2.3 %)	(Williams, 2018c)
Neptune	H_2 (80 %)	He (19 %)	CH_4 (1 %)	(Williams, 2018a)

Table 1: Mean composition of the different planetary atmospheres, (David C. Catling, 2019; Niemann et al., 1998; Curry and Webster, 1998)

At this stage, it is important to remind that these compositions are variable with the altitude or the distance from the sun, in the same way than inside the Earth heterosphere. A visual example of the composition difference with altitude is presented in Fig. 6 in the case of the gaseous giants. This summary of the different atmosphere compositions highlights that the simulation of the behaviour of helium and hydrogen mixtures is a necessary step for

the simulation of the atmospheric entry on the Gaseous and Icy Giants. Ilich (2018) already presented a possible use of helium in the Longshot wind tunnel, even if the first objective of its work was more linked to non equilibrium flow phenomena than in the simulation of outer planet entries. This study will then introduce, among others, the possibility of the use of hydrogen inside the Longshot wind tunnel. The introduction of this gas inside the Longshot is discussed by § 4.1 and § 5.3.

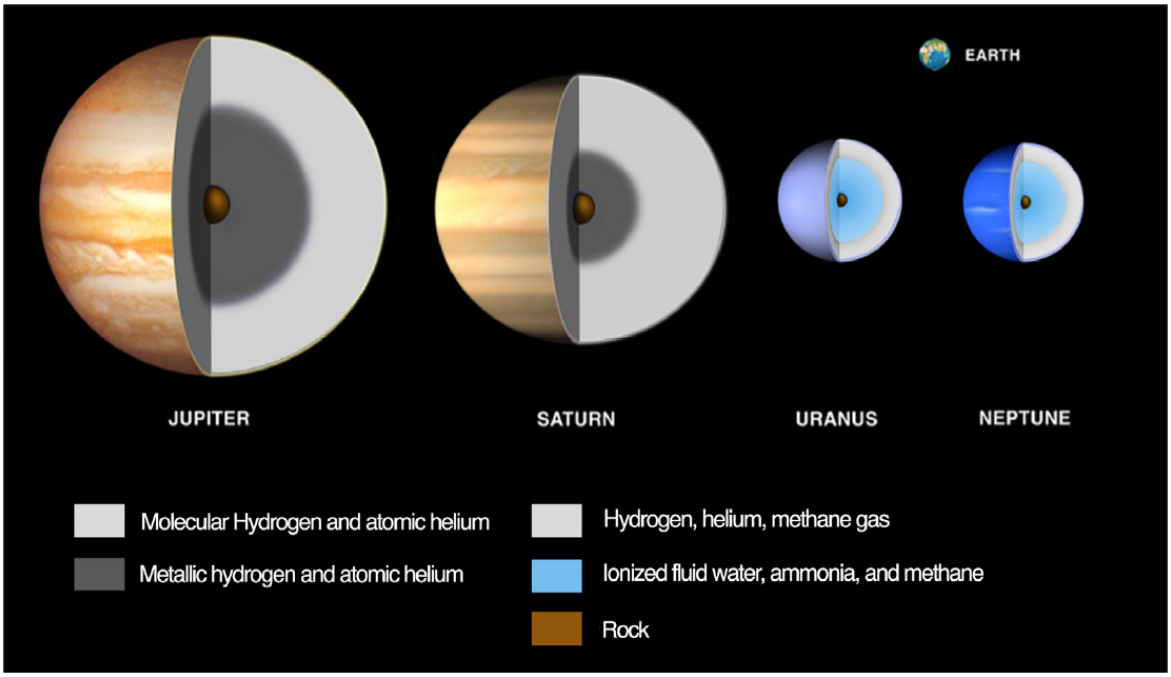

Figure 6: Illustration of the atmospheric composition of the different gaseous giants with their relative size (Hofstadter et al., 2017)

In order to simulate the behaviour of the different planet atmospheres in terms of temperatures, pressures and densities, several models were created. Taking the case of Neptune as an example, the Jean-Paul Huot atmospheric model can be cited. However, this model does not include uncertainties and is now being replaced by the Neptune Global Reference Atmospheric Model (Neptun-GRAM), (Bavon, 2019). These GRAM models, developed by the Marshall Space Flight Center, had already been developed for Venus, the Earth, Mars, Titan and Neptune, (Justh et al., 2006; Justh, 2017; Justh and Dwyer Cianciolo, 2017). These models simulate the density variation due to longitude, latitude, season, diurnal activity,... either directly or by the use of an interpolation function (in the case of Triton and Neptune). The main strength of these models is their ability to simulate quasi-random density perturbation. This allows Monte Carlo analyses of thermal design, guidance and navigation and control algorithm. They are currently used for the primarily design of the thermal protection system on these different planets and are often updated with the new data obtained during in-situ measurements. The type of reconstruction offered by these models is presented by Fig. 7

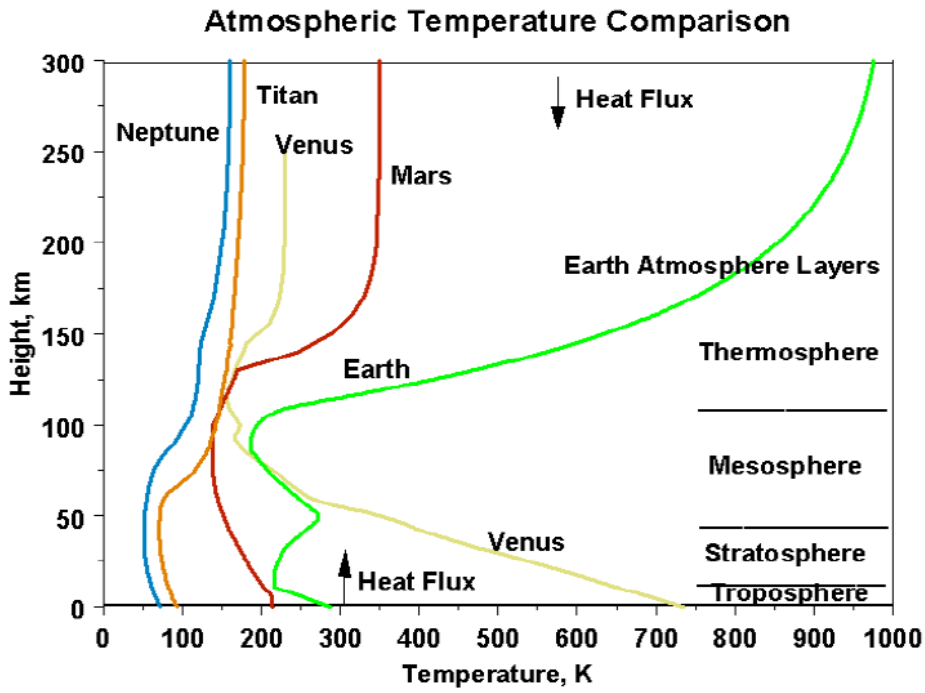

Figure 7: Reconstruction of the temperature profile on the atmosphere of several planets and satellites using the GRAM models (Justus et al., 2005)

3.2 Analyse of different entry trajectories

The trajectory of the spacecraft during re-entry is of major importance, since it can decide of the success or the failure of a long run mission. The maximum deceleration and the maximal heat encountered during this phase of a mission flux depend on several parameters, such as the composition of the atmosphere, the entry speed or the re-entry flight path. For superorbital entries, the guidance accuracy also becomes a major problem, since achieving the desired entry manoeuvre ensure that the deceleration will be neither too low or too high. Indeed, the first goal of the deceleration of a spacecraft arriving from this type of orbit is to ensure that the vehicle will not pass through the atmosphere and get lost. In this case, a deceleration smaller than requested results in the undershoot phenomenon. An interesting use of this slowing down is the aerocapture that could be used on Neptune to slow down a spacecraft to circularise an orbit either around the planet or Triton, according to a scenario proposed by Bavon (2019). However, when a probe mission, such as Galileo or Cassini-Huygens, is considered, a too low deceleration would result in the loss of the vehicle after its rebound on the atmosphere. In contrast, the heat flux increasing with the deceleration, a drag coefficient that would have been design too high would result in a advanced deterioration of the thermal protection system too early in the descent. This could then lead to severe damages or even the destruction of the payload. According to the Federal Aviation Administration (FAA)[5]

[5]FAA website, Chapter 4.1.7 Returning from space, available at URL

and Chapman (1960), the maximal deceleration can be obtained by the relation

$$a_{max} = \frac{u_{re}^2 \kappa \sin \zeta}{2e} \tag{3}$$

where u_{re} is the velocity of the spacecraft at the beginning of the re-entry, ζ the re-entry flight path angle and κ is the atmospheric density decay parameter, calculated using different planetary constant, such as the local temperature, molecular mass or gravitational acceleration. By knowing the velocity of the spacecraft during the re-entry, the flight path angle and the drag coefficient of the vehicle, it becomes possible to estimate the trajectory of the spacecraft during its journey across the atmosphere of the target planet. Chapman (1960) describes a part of this method that will be exposed using the case study of Galileo.

3.2.1 Galileo mission

One of the objective of the re-entry presented above is the determination of the composition of a barely known planet's atmosphere. If spectroscopy can offer a first estimation of the overall composition, in situ measurements precise the structure of this atmosphere. Cortesi et al. (2016) and Chapman (1960) presented different methods used for the reconstruction of the temperature, pressure and density profiles of an atmosphere from the different measurements taken during the entry, descent and landing. These reconstructed profiles are computed statistically thanks to the measurement of pressure, heat flux or deceleration. It presented the design of an atmospheric entry as an exercise mainly dependent of the atmospheric conditions and the vehicle aerodynamic. A similar method was used by Galileo probe reconstruction after its entry into Jupiter atmosphere on December 7, 1995.

The entry velocity on Jupiter was reported by Seiff et al. (1996) to be as high as 60 km/s. However, by taking advantage of the rotation of the planet, this local entry velocity was reduced to 47.5 km/s. These conditions being the more extreme in the solar system, a specific attention was given to the thermal protection system of the probe. This extreme entry velocity has major consequences on the measurement techniques used by the probe during its descent. First, the temperature resulting from the very high heat flux on the probe would destroy conventional thermometers, (Reynier, 2008; Cortesi et al., 2016). A similar issue is also noticed for the measurement of the atmospheric pressure. Indeed, the extreme velocity of the spacecraft generates a dynamic pressure so high that the static pressure contribution of the total pressure is extracted with a very large error. The method used to obtain atmospheric data of the Jovian atmosphere during the hypersonic part of the Galileo flight relied on a series of accurate accelerometers and ablation sensors. The latter were used to reconstruct the modification of the shape of the probe during the reentry in order to accurately select the drag coefficient associated with the ablated shapes. Knowing the mass m of the spacecraft, its reference area A_{ref} and drag coefficient C_D, the deceleration a_D and the velocity u_∞^2 at a

particular moment, it becomes possible to estimate the atmospheric conditions. Indeed, the density can be obtained by reconstruction procedure as

$$\rho_\infty = 2\frac{m\,|a_D|}{C_D A_{ref} u_\infty^2}. \tag{4}$$

The temperature and pressure can then be defined as functions of the altitude z, the local gravitational acceleration g and the molecular weight of the atmosphere M_w. Cortesi et al. (2016) presents the expression of the reconstructed pressure and temperature profiles as

$$p_\infty(z) = p_\infty(z_0) - \int_{z_0}^{z} g\rho_\infty \mathrm{d}h \tag{5}$$

and

$$T_\infty = \frac{M_w p_\infty}{R\rho_\infty} \tag{6}$$

where R is the perfect gas constant. The importance of the drag coefficient C_D is then highlighted, since an error on the computation of the latter impacts the value of the density and then the pressure and temperature. For non lifting vehicle, such as the probe used for Galileo or Pioneer Venus missions, depicted by Fig. 8, the lift is negligible and the measurement of the drag coefficient is of prior necessity. This aerodynamic coefficient is then measured before the flight for different configuration, mainly before and after ablation. The difference of geometry due to the ablation is presented by Fig. 9 for the case of Galileo. After the flight, the data obtained by the ablation sensors are used to describe the shape of the thermal protection system (TPS) across time. Coupled with the computation of the drag coefficient for these configurations, the atmosphere of the planet can be reconstructed.

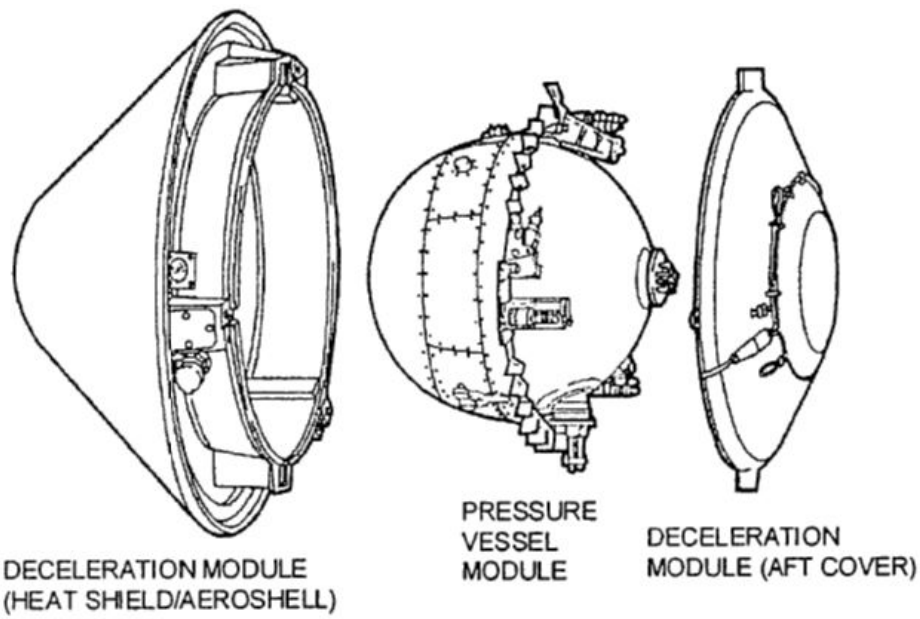

Figure 8: Heatshield, vessel module and cover of probe used for Galileo and Pioneer Venus missions (Bienstock, 2004)

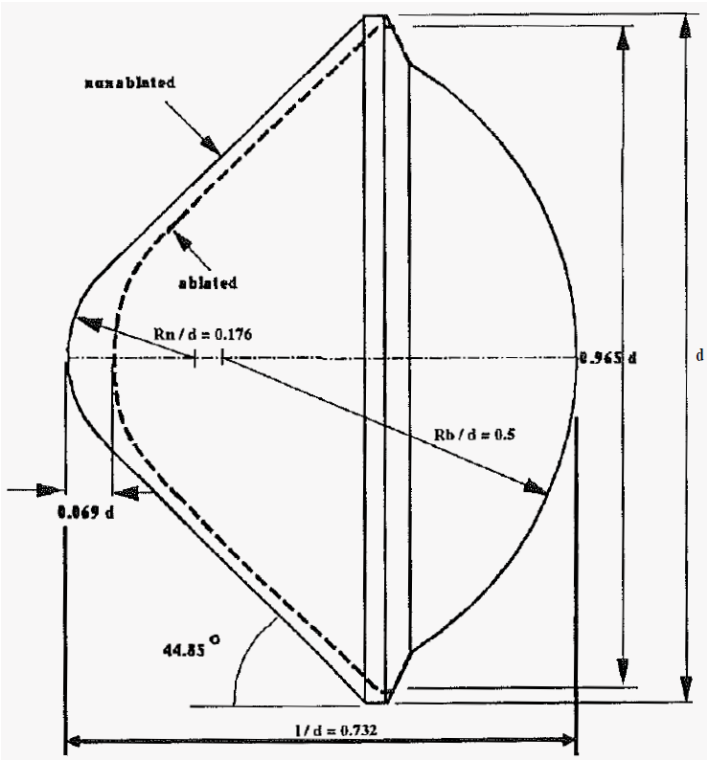

Figure 9: Probe geometry, before and after ablation (Seiff et al., 1996)

3.2.2 Galileo's trajectory reconstruction

The reconstruction of the Galileo's trajectory had been discussed by several references, such as (Moss, 1980), (Collicott and Bauer, 1983), (Reynier, 2012) or (Seiff et al., 1996). Thanks to the data included in these references and the method of reconstruction presented above, the temperature, pressure, velocity or density profiles can be described for the hypersonic part of the entry. The latter lasted 110 seconds and began at an inertial velocity of 60 km/s, reduced to 48 by taking the rotation of the planet into account, and a flight path angle $\zeta = -6.835^o$. The trajectory of the probe in terms of altitude and velocity are presented in Fig. 10 for the hypersonic part of the reentry. The reference altitude of this graph was selected by the NASA to be the isobaric altitude of 1 bar. After the first 110 seconds, the probe velocity was reduced under the speed of sound at 740 m/s. The probe itself was then separated from its heat shield after the deployment of the probe's parachutes. The measurements of the density, pressure, temperature and composition of the Jovian atmosphere was then made using "conventional" measurement methods. The different data collected by the probe during its descent and until its destruction due to the very high pressure reached inside Jupiter were sent to the orbiter and then back to Earth, where the reconstruction process was made.

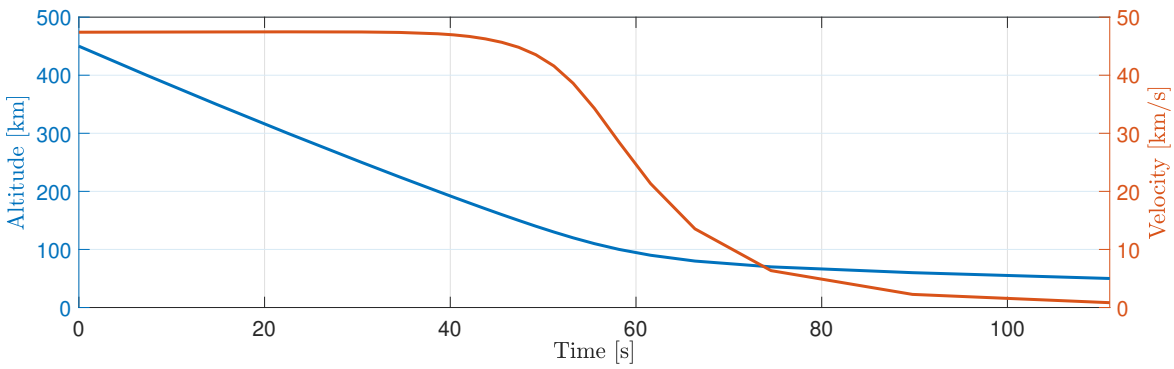

Figure 10: Altitude above the 1 bar reference and velocity of the Galileo probe during its hypersonic entry in the Jovian atmosphere until the deployment of the parachutes, (Reynier, 2012)

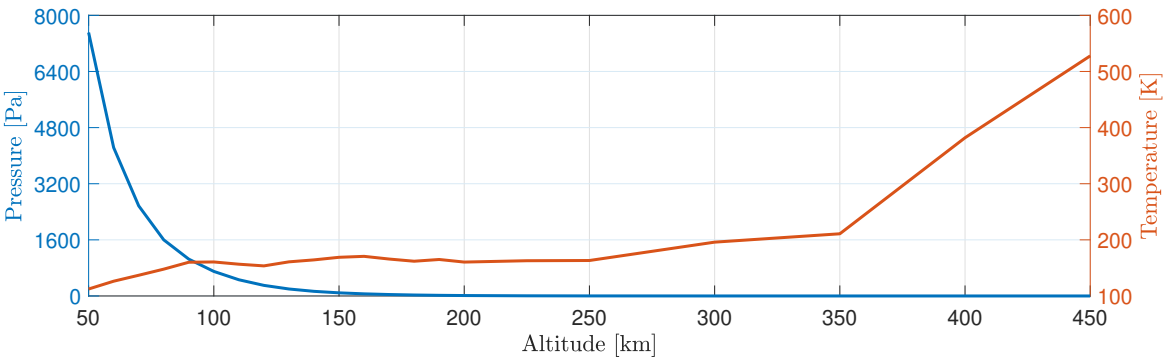

Figure 11: Reconstruction of the temperature and pressure profile of the Jovian atmosphere between 50 and 450 km above the 1 bar reference altitude, (Reynier, 2012)

The reconstruction of the Galileo trajectory was investigated several time. The temperature and pressure profile is presented by Fig. 11 using the data provided by Reynier (2012). Another type of reconstruction is presented by Seiff et al. (1996) that proposes a reconstruction of the Galileo entry in terms of several adimentional numbers, such as the Knudsen[6], the Mach number or the Reynolds number. The former is found well adapted to describe the region where the Reynolds number is low (below 1000). Indeed, it is used to represent the passage of the probe in the rarefied environment of the Jovian high atmosphere. The formulation in terms of Mach and Reynolds is particularly interesting for the VKI Longshot. This trajectory is presented by Fig. 12 for a Reynolds number based on the diameter of the front heat shield. The ablation started approximately 215 km above the 1 bar reference altitude, to end 123 km lower. Determining the real accurate rate of ablation is a complex task that was simulated by direct Monte Carlo Simulation and verified thanks to the ablation sensors on the heat shield of the probe.

[6]This non-dimensional number was there defined as $Kn = \frac{\lambda}{D} = 1.49\frac{M}{Re}$, where D is the diameter of the probe's heatshield and λ the mean free path

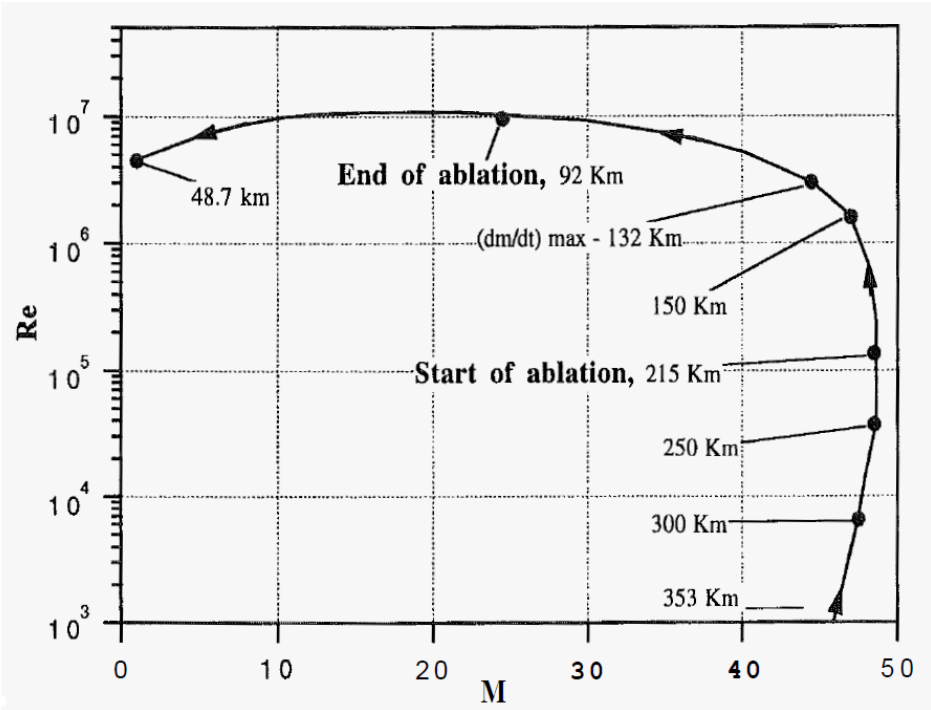

Figure 12: Reconstruction of the Galileo entry into Jupiter in terms of Mach and Reynolds numbers, (Seiff et al., 1996)

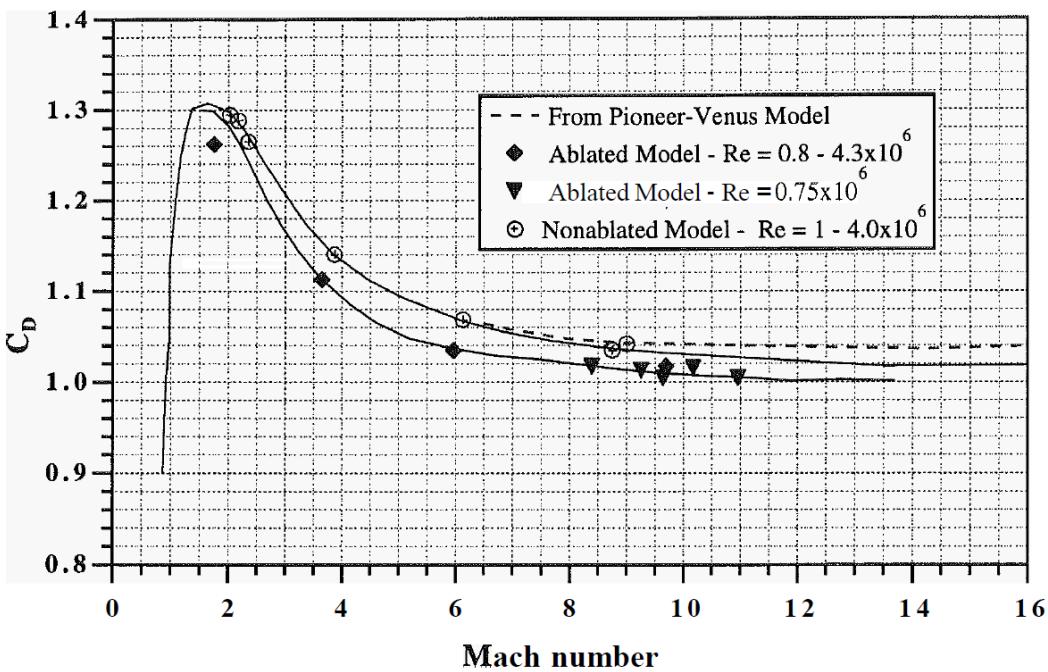

Figure 13: Drag coefficient as a function of the Mach number at several Reynolds number for the pre and post ablated models of the Galileo probe. The data of Pioneer Venus probe are also shown for comparison, (Seiff et al., 1996)

The type of Mach numbers reached by the probe during the atmospheric entry into the Jovian atmosphere can be seen as too high to be simulated inside the Longshot wind tunnel. However, the pre-flight series of tests and the reconstruction studies that follows show that the value of the drag coefficient stabilises at a constant value when the Mach number increases. The same type of behaviour had been observed with the Reynolds number. These behaviours are presented by Fig. 13 and Fig. 14 respectively for the Mach number and the Reynolds number.

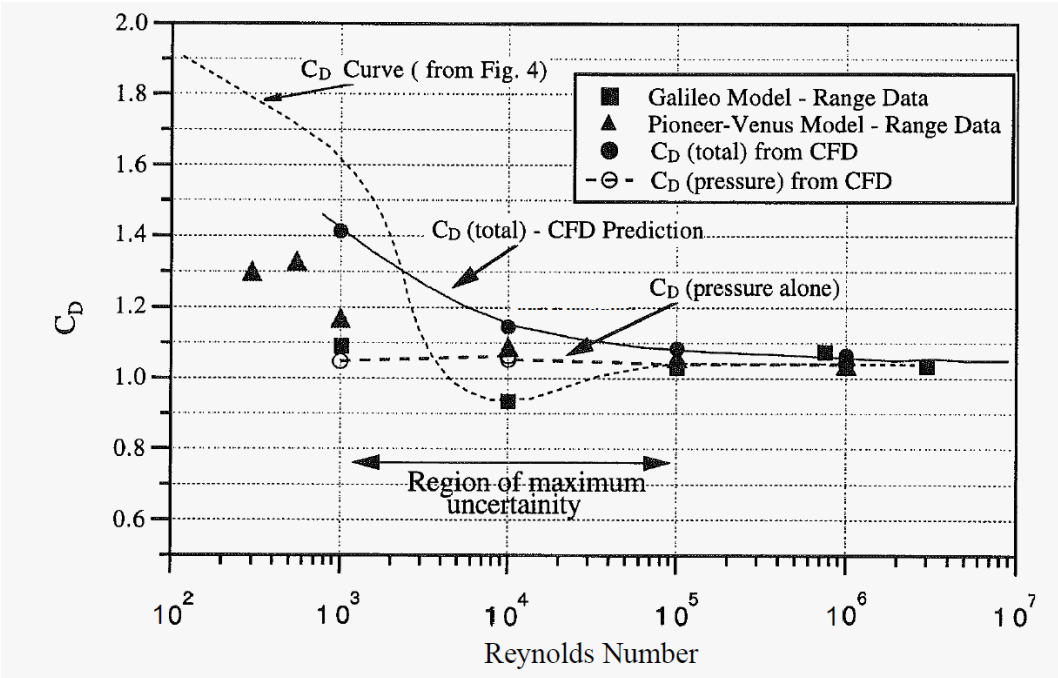

Figure 14: Drag coefficient of the Galileo and the Venus Pioneer probes as a function of the Reynolds number, (Seiff et al., 1996)

The stabilisation of the drag coefficient to a constant value when the Mach and Reynolds number increases can be linked to the Mach number independence principle that is discussed in the next section and to predominance of the pressure drag over the friction drag for the blunt bodies. These two behaviours would offer the opportunity to simulate the same type of entry than Galileo at lower Mach and Reynolds number than those encountered by the probe. A series of tests should however be led to check the minimum Mach and Reynolds number necessary to consider the drag coefficient to be a constant.

3.3 Influence of the test gas on the aerodynamics

Using the data obtained during the test campaign of the Galileo probe, the effect of the test gas on the aerodynamic measurements of blunt bodies is discussed here. The selection of an alternative gas to simulate the different atmospheres presented by Table 1 will then be introduced.

During re-entry, the very high velocity of the spacecraft coupled with the rarefied conditions of the atmospheres can lead to the very high Mach numbers presented by Fig. 13. The case of Galileo presented above even reaches M47 at approximately 215 km above the 1 bar reference altitude. At these velocities, a bow shock forms in front of the probe. Several relations are available to describe the density, pressure or temperature before and after this shock. These are extensively presented by Neice (1948) and Anderson Jr (2006). From the presentation of the Galileo probe mission, the importance of the drag coefficient in the reconstruction of a planetary atmosphere was highlighted. The accuracy of this parameter is then of major importance to obtain the best reconstruction of a barely known atmosphere. The drag coefficient can be divided into a friction and a pressure contribution. For blunt bodies, Hunt and Jones (1969) reported that the aerodynamic characteristics are almost exclusively a function of the flow over the forebody. This is confirmed by the fact that the contribution of the pressure drag is higher than the influence of the friction drag when a blunt body is considered. Jones and Hunt (1973) and Hunt and Jones (1969) show that the distribution of pressure correlates with the density ratio across the bow shock. An approximation of this correlation is given by the Rankine Hugoniot equations. The ratio of density through shock can be expressed as a function of the Mach number, the shock angle β and the ratio of specific heat γ by

$$\frac{\rho_2}{\rho_1} = \frac{(\gamma+1)M_1^2 \sin^2\beta}{(\gamma-1)\,M_1^2 \sin^2\beta + 2} \tag{7}$$

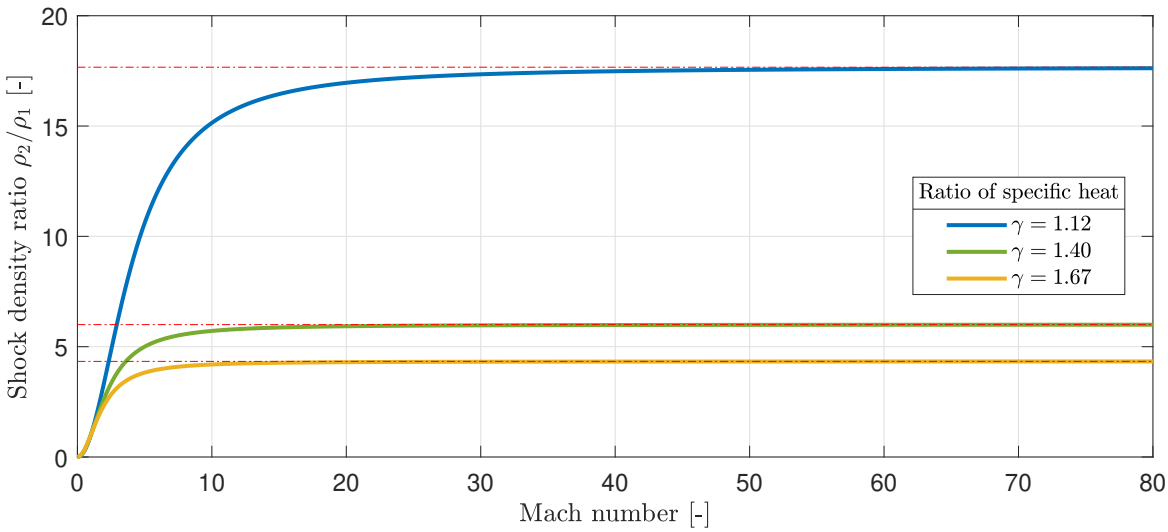

Figure 15: Value of the shock density ratio as a function of the Mach number for different ratio of specific heat and $\beta = 0$

This equation shows that the influence of the Mach number on the ratio of density can be simplified when a certain Mach number is reached. Anderson Jr (2006), Hunt and Jones (1969) and Jones and Hunt (1973) presented this behaviour as the Mach number independence

principle. The value at which this principle is applicable depends on the value of the specific heat ratio and thus of the gas considered. These references also highlighted that this principle can be assumed at lower Mach number when it is applied to a blunt body. Figure 15 proposes the variation of the shock density ratio for three different values of γ that can be attributed to CF_4 ($\gamma = 1.12$), air ($\gamma = 1.4$) and helium ($\gamma = 1.67$). The larger the specific heat ratio, the lower the Mach number requested for the assumption of this independence principle. Anderson Jr (2006), Jones and Hunt (1973) and Hunt and Jones (1969) also highlighted that this principle can be assumed at lower Mach number when it is applied to a blunt body. This statement can be observed in Fig. 13 depicting the variation of the drag coefficient as a function of the Mach number.

For Mach number higher than 10, this principle can be used for gases with specific heat ratio of 1.67. This is the case for the noble gases, such as helium or Argon. This use of the latter will be discussed by § 4.3. It proposes interesting properties due to its high specific heat ratio and is often mixed with a second heavy gas having a lower γ in order to obtain higher Mach number for the same velocity, (Chapman, 1956). Above M 22, this independence principle can be used for gases with specific heat ratio of 1.4. The error made by using the Mach number independence principle in these conditions is lower than 1%. Several gases have a specific heat ratio of 1.4, such as air, oxygen, nitrogen or hydrogen. Moreover, comparing this statement with the variation of the drag coefficient presented in Fig. 13 confirm the fact that the Mach number Independence principle can be assumed at lower Mach number for blunt bodies. The Mach number principle is more complex to reach in the case of low specific heat ratio. An example of a gas used in wind tunnel is the tetrafluoromethane, which has a γ equals to 1.12. The use of this gas is discussed by § 4.6.2. Different wind tunnels use this gas to reach higher density ratio. This is usually done in order to simulate the type of entry, such as the Aeroasist Flight Experiment (AFE) reentry vehicle, that can reach a density ratio of 18 due to the real gas effects of air. The reduction of the specific heat ratio across the shock is due to the excitation of the molecules through this shock, which is reported by Jones and Hunt (1973) to decrease this parameter. Since energy is used by the real gas effects, the temperature after shock is lower than what is proposed by the Rankine Hugoniot approximation. A better approximation to retrieve the conditions after shock over the forebody is given by the $\sin^2$ deficiency method proposed by Ashby Jr et al. (1969) and Jones and Hunt (1973).

The duplication of the density ratio ensures the measurement of the right pressure drag coefficient in inviscid conditions. Hunt and Jones (1969) highlights that, in order to simulate the entire drag coefficient over the forebody, the Reynolds number had to be matched. The reconstruction of the conditions needed to simulate the drag coefficient over the considered blunt body are then the duplication of the specific heat ratio, the Mach number, until a certain limit, and the Reynolds number. It was however presented that the contribution of the Reynolds number is lower than the Mach number at high velocities, due to the higher contribution of the pressure drag to the total drag. Moreover, Fig. 14 confirmed that the effect Reynolds number on the drag coefficient becomes lower when this adimentional number

increases. Since the specific heat ratio is the only parameter linked to the gas that is consider in this duplication, the simulation of the drag coefficient for a selected Mach and Reynolds number in a certain atmosphere does not required the use of the gas that composes this atmosphere. An alternative gas can then be used to simulate the conditions of a probe entering in a planet atmosphere as long as its specific heat ratio is matched, as well as the Mach and Reynolds numbers. This method was already used by the Ames Hypervelocity Free-Flight Aerodynamic Facility (HFFAF) wind tunnel during the aerodynamic test campaign of Galileo. Indeed, Seiff et al. (1996) presents that a part of these tests were realised using air as test gas instead of hydrogen. The selection of this gas to duplicate the Jovian atmosphere conditions comes from the different hazards linked to the use of hydrogen, which are introduced in § 4.1.4. These tests were conducted according to the work of Intrieri and Kirk (1987) who shows that this approach is pertinent. Seiff et al. (1996) also reported that the agreement between the experimental data using air as test gas and the CFD code considering the real Jovian mixture suffered from less than 1% of error in super and hypersonic regimes. The wind tunnel that provided the experimental investigations of the Galileo aerodynamic coefficients is presented in Appendix B. Figure 16 presents behaviour of the drag coefficient as a function of the Mach number using air or hydrogen/helium mixtures as test gases. The behaviour of the drag coefficient is similar when air or Jovian atmospheric mixture is used.

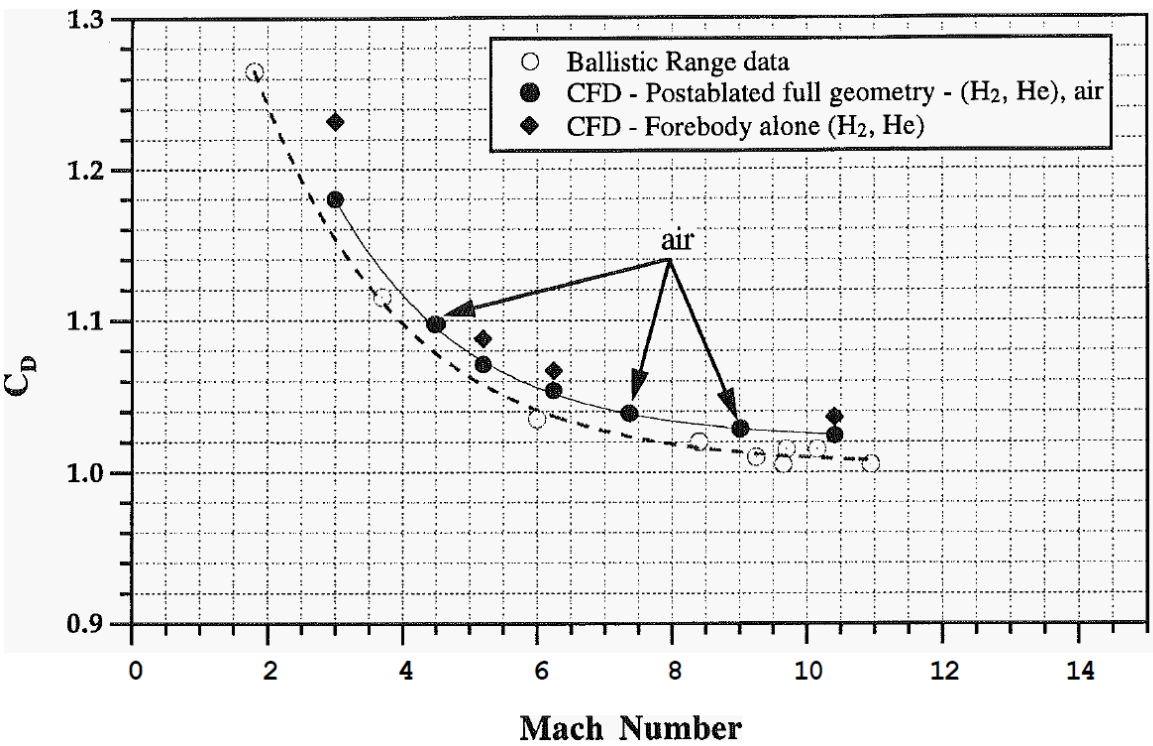

Figure 16: Drag coefficient as a function of the the Mach number for the post-ablated geometry of the Galileo probe using air and Jovian atmospheric mixtures as test gases, (Seiff et al., 1996)

The use of an alternative gas is already considered by the VKI for the simulation of the Earth reentry using only nitrogen. This method is used to avoid the dissociation and damages of the oxygen during a test done with air. The duplication of the specific heat ratio can then be made using a substitute gas that does not dissociate at the temperature and pressure reached during the test. A similar alternative is available in the case of the simulation of a dangerous gas, such as hydrogen or methane, using safer substitutes. The discussions on the use of these two gases are proposed respectively in § 4.1 and § 4.6.1.

3.4 Icy Giants mission

After the success of the Galileo and Cassini-Huygens missions, the next interest of the European and American space agencies is reported by Bavon (2019) to be the Icy Giants. Indeed, the two space agencies are currently creating a join operation to launch a mission to Uranus and Neptune. Several architectures are proposed for this mission, but it seems that at least one probe will be launched and sent inside the atmosphere of one of these planets. Two orbiter should also be sent, on each of the two planets. These orbiters should sent back measurements of several properties of these two planets and maybe their main satellites. Triton is indeed a possible extension for the mission on Neptune. If a probe mission is also launched on one or both of these planets, the probe geometry will be similar to the one sent on Jupiter or Venus, as presented by Fig. 17.

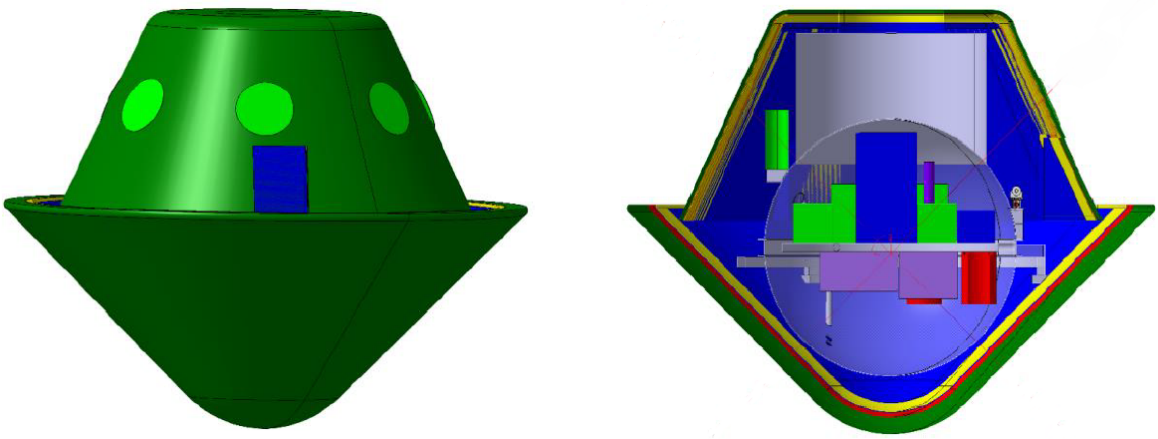

Figure 17: Scheme of the probe that will be used during the mission on Neptune, (Bavon, 2019)

This mission is proposed for several reasons:

- This class of planet is not well understood with our current observations. No model is currently consistent with all observations.
- This type of planet is extremely common in our galaxy. A better understanding of Uranus and Neptune would then offer a better characterisation of these exoplanets.

- This mission and the data collected thanks to the atmospheric probe should offer information about the formation of this type of planet.

The major objectives of this mission would then be the determination of the composition, thermal and dynamic structure of the atmosphere of these planets, as well as the determination of the abundance of heavy elements and their isotopes, (Bavon, 2019; Hofstadter et al., 2017). The different entry parameters that will be met by the probe entering Uranus or Neptune are presented in Table 2. These entry parameters are very close, even if the entry velocity is ~ 1 km/s higher in the case of Neptune.

Parameter	Uranus	Neptune
Altitude	600 km	600.133 km
Entry velocity	22.071 km/s	23.082 km/s
Flight path angle	-35°	-35.039^o
Longitude	-39.4^o E	-8.821^o E
Latitude	-26° N	-0.729^o N
Azimuth	193.4^o	84.468^o
Entry duration	6 min	6 min
Descent duration	1.5 h	1.5 h

Table 2: Entry parameters on Uranus and Neptune for the atmospheric probe, (Bavon, 2019)

The preliminary design of the atmospheric probe presented by Fig. 17 presents a mass of 342 kg, where the TPS account for 152 kg of this mass, a diameter of 1.35 m for a projected area of 1.43 m^2. The front area of this 45° cone probe is of 1.99 m^2. The drag coefficient is currently presented to be smaller than the one of Galileo, with a value of 1.07.

Thanks to the accurate measurement of the drag coefficient obtained using air as test gas during the test campaign of Galileo, the same type of measurements should be proposed with air to this probe. The von Karman Institute could then offer its expertise to the pre and post flight tests thanks to a series of simulation obtained using nitrogen as test gas. A mixture of nitrogen and helium could even increase the accuracy of these experiments. If the use of hydrogen inside the Longshot wind tunnel is approved, mixture of hydrogen and helium could be also be used. In this case, it could be an interesting exercise to compare the results obtained with the two mixtures.

3.5 Conclusions

The atmospheric entry can be made for several reasons. The measurement of the atmospheric profile of a planet in terms of temperature, pressure, density and composition is one of these applications. This experiment was carried on Venus, Jupiter and Titan, where the compositions of the atmospheres are very different. The three main gases present on the gaseous

and icy Giants are hydrogen, helium and methane. The success of the mission Galileo highlighted the possibility of the use of an alternative gas to simulate the atmospheric entry into Jupiter. Air was the test gas selected for the aerodynamic test campaign, which is pertinent due to the similar specific heat ratio of these two mixtures.

The accurate simulation of the aerodynamic coefficients of a blunt body depends on the duplication of the Mach and Reynolds number, as well as the specific heat ratio. However, the Mach number independence principle can increase the capability of a wind tunnel to measure aerodynamic coefficients above the real Mach Reynolds couple encountered during a reentry. The Reynolds number was also presented to have a limited impact on the drag coefficient when this adimensional number reaches a certain value.

The use of an alternative gas can be pertinent for three reasons. Firstly, it allows the use of a gas that does not dissociate to simulate another one that is submitted to real gas effects during the experiment. Secondly, a gas too dangerous to be used inside a wind tunnel can be replaced by a safer one. An example is provided by the use of air to simulate the hydrogen and helium atmospheric composition of Jupiter by the Ames research center. The last benefit of the use of an alternative gas comes form the use of a gas with a low specific heat ratio, such a tetrafluoromethane, to simulate the part of an entry where the real gas effect of the atmospheric gas decreases the value of this parameter.

The join mission between the NASA and the ESA could offer the von Karman Institute an opportunity to develop a series of tests in order to obtained the different drag coefficients of the probe as a function of the Mach and Reynolds numbers.

4 Implementation and verification of the equations of state

The Lagrangian one dimensional program described by § 5.4 offers several level of approximation for the driver and the driven gas. The simplest consists of using the perfect gas law and assuming an inviscid gas. However, the domain of this basic equation of state and its accuracy are unusable at the temperatures and pressures reached inside the Longshot wind tunnel during a test. More complex and accurate equations of state are then requested for the L1D simulations. This section then proposes a series of equations of state that will be used to simulate in the VKI Longshot wind tunnel the relevant environment met by a probe during its reentry. Hydrogen was presented by Table 1 as the major component of the Gaseous Giants. It will then be the first studied here. Moreover, the composition of these atmospheres shows a significant fraction of helium. This gas was already introduced by Ilich (2018) and presents a specific heat ratio higher than hydrogen or nitrogen. In order to provide accurate measurements to simulate an entry on a gaseous planet, a mixture equation is then a logical step. However, the mixture equation is obtained thanks to empirical parameters that are not available at the time of this work for the helium/hydrogen or the helium/nitrogen couple. For this reason, the equations of state for oxygen and argon will be introduced, with the objective of providing a comparison between the mixture equation and the air, one of the most studied mixture. An equation of state for air will then also be presented before the introduction of the mixture equation. Validation of the different equations of state will be done through a comparison with available data provided by the National Institute of Standards and Technology (Nist) or experimental data.

4.1 Hydrogen

Hydrogen represents more than 80% of the atmospheric composition of the different outer planets. This makes the study of this gas an important step in the study of the aerodynamic coefficients of a spacecraft going to these destinations. This gas is already used by the European magnetoplasmadynamic PWK1 arcjet at IRS, the NASA EAST shock tube or the Ames HFFAF, which is described in Appendix B, (Reynier, 2016), (Bavon, 2019) and (Dmitry V.Kotov, 2014).

4.1.1 General form of the equations of state

The von Karman Institute for Fluid Dynamics uses a form of equation of state that relies on the reduced Helmholtz energy to obtain different thermodynamic properties. Span et al. (2000), Schmidt and Wagner (1985) or Leachman et al. (2009) presented this method as the sum of a perfect gas contribution (α^0) and a residual contribution (α^r), presenting the correction brought when considering a real gas. The density and the temperature are coupled with the critical density and temperature in order to have a purely dimensionless equation of the form

$$\alpha(\delta, \tau) = \alpha^0(\delta, \tau) + \alpha^r(\delta, \tau) \tag{8}$$

where $\delta = \rho/\rho_c$ is the reduced density and $\tau = T_c/T$ is the reduced temperature. The subscript "c" presents the critical values.

Depending on the gas considered, the form of the perfect and residual contributions varies, but these expressions can be derived according to the reduced density or temperature and combined to obtain different thermodynamic parameters. The equations of state for nitrogen and carbon dioxide currently used by the von Karman Institute are already expressed by this type of equation, (Grossir, 2015), (Ilich et al., 2019). The thermodynamic parameters that are the specific internal energy u, the specific enthalpy h, the specific entropy s, the speed of sound w and the two heat capacities computed c_p and c_v using these two gases are obtained thanks to the relations Eq. 9 to Eq. 14.

$$u = RT\tau \left[\left(\frac{\partial \alpha^0}{\partial \tau} \right)_\delta + \left(\frac{\partial \alpha^r}{\partial \tau} \right)_\delta \right] \tag{9}$$

$$h = RT \left(\tau \left[\left(\frac{\partial \alpha^0}{\partial \tau} \right)_\delta + \left(\frac{\partial \alpha^r}{\partial \tau} \right)_\delta \right] + \delta \left(\frac{\partial \alpha^0}{\partial \delta} \right)_\tau + 1 \right) \tag{10}$$

$$s = R \left(\tau \left[\left(\frac{\partial \alpha^0}{\partial \tau} \right)_\delta + \left(\frac{\partial \alpha^r}{\partial \tau} \right)_\delta \right] - \alpha^0 - \alpha^r \right) \tag{11}$$

$$w = \sqrt{\frac{RT}{M_w} \left(1 + 2\delta \left(\frac{\partial \alpha^r}{\partial \delta} \right)_\tau + \delta^2 \left(\frac{\partial^2 \alpha^r}{\partial \delta^2} \right)_\tau - \frac{\left[1 + \delta \left(\frac{\partial \alpha^r}{\partial \delta} \right)_\tau - \tau\delta \left(\frac{\partial^2 \alpha^r}{\partial \delta \, \partial \tau} \right) \right]^2}{\tau^2 \left[\left(\frac{\partial^2 \alpha^0}{\partial \tau^2} \right)_\delta + \left(\frac{\partial^2 \alpha^r}{\partial \tau^2} \right)_\delta \right]} \right)} \tag{12}$$

$$c_v = -R\tau^2 \left[\left(\frac{\partial^2 \alpha^0}{\partial \tau^2} \right)_\delta + \left(\frac{\partial^2 \alpha^r}{\partial \tau^2} \right)_\delta \right] \tag{13}$$

$$c_p = c_v + R \frac{\left[1 + \delta \left(\frac{\partial \alpha^r}{\partial \delta} \right)_\tau - \delta\tau \left(\frac{\partial^2 \alpha^r}{\partial \delta \, \partial \tau} \right) \right]}{\left[1 + 2\delta \left(\frac{\partial \alpha^r}{\partial \delta} \right)_\tau - \delta^2 \left(\frac{\partial^2 \alpha^r}{\partial \delta^2} \right)_\tau \right]} \tag{14}$$

4.1.2 Specific form of the hydrogen

The equation of state for normal, para and ortho hydrogen proposed by Leachman et al. (2009) is computed in the same way than for the nitrogen or the carbon dioxide currently studied by the VKI. The perfect gas contribution of the reduced Helmholtz energy for hydrogen is presented by

$$\alpha^0 = \ln \delta + 1.5 \ln \tau + a_1 + a_2 \tau + \sum_{k=3}^{N} a_k \ln \left[1 - e^{b_k \tau} \right] \tag{15}$$

where the value of N depends on the type of hydrogen concerned. In the case of the normal hydrogen, N is equal to 7. This number reaches 9 while considering parahydrogen and is reduced to 6 for orthohydrogen. The normal hydrogen is defined here as a mixture of 75% orthohydrogen and 25% parahydrogen at room temperature. It is known that this balance depends on the temperature. Indeed, at very low temperature (of the order of 20K), this

proportion becomes largely in favour of the parahydrogen (97.5%), since this form has a lower energy level than orthohydrogen. However, this high ratio in favour of the parahydrogen quickly disappears when the temperature increases. Above the temperature of 300K, the 3 for 1 ratio in favour of the orthohydrogen is kept constant, according to Leachman et al. (2009) and Tikhonov and Volkov (2002). Even if temperature has a strong impact on the composition of the hydrogen considered, the normal hydrogen is the only one considered here, since the time requested for a modification of the proportion takes several days to change significantly. The duration of the Longshot experiment being of the order of 100 ms, considering a constant composition is a reasonable assumption. The different values of the a_k and b_k parameters used in Eq. 15 are presented in Tab. 3. These values depend on the type of hydrogen considered. Leachman et al. (2009) presented the corresponding coefficients for pure para and orthohydrogen.

k	a_k	b_k
1	-1.4579856475	-
2	1.888076782	-
5	1.616	-16.0205159149
4	-0.4117	-22.6580178006
5	-0.792	-60.0090511389
6	0.758	-74.9434303817
7	1.217	-206.9392065168

Table 3: Values of the a_k and b_k parameters used in Eq. 15 for normal hydrogen, (Leachman et al., 2009)

The residual term of the reduced Helmholtz energy is presented by

$$\alpha^r = \sum_{i=1}^{l} N_i \delta^{d_i} \tau^{t_i} + \sum_{i=l+1}^{m} N_i \delta^{d_i} \tau^{t_i} e^{-\delta^{p_i}} + \sum_{i=m+1}^{n} N_i \delta^{d_i} \tau^{t_i} e^{\left[\phi_i(\delta - D_i)^2 + \beta_i(\tau - \gamma_i)^2\right]}. \tag{16}$$

In this equation, the second term is present to aid in liquid and critical region property calculations. The last term contains a Gaussian bell-shaped term that serves to improve the modelling of the critical region. In the case of the normal hydrogen, the values of l, m and n were set respectively to 7, 9 and 14 by Leachman et al. (2009). The different values of the parameters present in Eq. 16 are given in Table 4. Thanks to the two contributions of the total Helmholtz energy presented by Eq. 15 and Eq. 16, Eq. 8 can be computed. Since the latter is one of the four fundamental equations of thermodynamics, the different other properties can be calculated using the relations proposed by Eq. 9 to Eq. 14.

i	N_i	d_i	t_i	p_i	ϕ_i	D_i	β_i	γ_i
1	-6.9364300	1	0.6844	0	-	-	-	-
2	0.01	4	1	0	-	-	-	-
3	2.1101	1	0.989	0	-	-	-	-
4	4.52059	1	0.489	0	-	-	-	-
5	0.732564	2	0.803	0	-	-	-	-
6	-1.34086	2	1.1444	0	-	-	-	-
7	0.130985	3	1.409	0	-	-	-	-
8	-0.777414	1	1.754	1	-	-	-	-
9	0.351944	3	1.311	1	-	-	-	-
10	-0.0211716	2	4.187	0	-1.685	1.506	-0.171	0.7164
11	0.0226312	1	5.646	0	-0.489	0.156	-0.2245	1.3444
12	0.032187	3	0.791	0	-0.103	1.736	-0.1304	1.4517
13	-0.0231752	1	7.249	0	-2.506	0.67	-0.2785	0.7204
14	0.05573460	1	2.986	0	-0.3967	1.662	-0.3967	1.5445

Table 4: Parameters of the equation of state for normal molecular hydrogen presented by Eq. 16, (Leachman et al., 2009)

The values of the critical temperature and density are needed for the computation of the reduced temprature and density used in this Helmholtz formulation. These values were also proposed by Leachman et al. (2009) with their new equation of state. These values were then set to $T_c = 33.145$ K and $\rho_c = 15.508$ mol/dm^3 respectively. It must be highlight that the critical density of normal hydrogen had never been measured. The value presented here was borrowed from the reference and was based on approximation from saturation data. Another useful parameter of the normal hydrogen is the molar mass, taken to be 2.01588 g/mol from the National Institute of Standards and Technology website[7]. The different thermodynamic parameters need the computation of the different first and second derivatives of α^0 and α^r with respect to δ and τ. They are rewritten in Appendix. A.1.

The next step is the introduction of the different thermodynamic parameters in the Lagrangian 1D code. To achieve this goal, the different expressions depicted by Eq. 15 to Eq. 16, as well as the derivatives presented in Appendix. A.1 and the parameters of Table 3 and Table 4 were transposed into a *Matlab* code. The latter uses the temperature and either the pressure or the density as inputs. In both cases, the missing density or pressure are computed before solving the thermodynamic relations. The outputs of this program are then the pressure, the temperature, the density and the different thermodynamic parameters presented. If the pressure was not an input, its value is obtained thanks to the relation

$$p = \rho RT \left[1 + \delta \left(\frac{\partial \alpha^r}{\partial \delta} \right)_\tau \right] \tag{17}$$

[7]NIST website of the normal dihydrogen: URL

again proposed by Leachman et al. (2009). The same method is used for the different gases presented here and is based on the existing test gases already used in the VKI Longshot. If an equation of state is not available in the reduced Helmholtz energy formulation, it is possible to obtain this expression by integrating the expression of the pressure proposed by Eq. 17 and combine it with the expression of the ideal gas heat capacity, (Lemmon and Tillner-Roth, 1999). However, a large part of the existing equations of state are provided using the reduced Helmholtz energy formulation.

4.1.3 Verification of the equation of state

The accuracy of the equation of state of normal hydrogen used here is tested in this section by comparing it to the data provided by the Nist in its program *NIST Mini-refprop* that provides a database for several gases, among which most of those that will be tested in this work. The choice of this method for the test of the accuracy of the different equations of state comes from the temperature range available in this database, often greater than those considered in the different articles. Indeed, the temperature range presented by Leachman et al. (2009) covers the temperatures from approximately 14 K to 33K, while the Nist can reach temperature up to 1500 K. Due to the real gas effects of the hydrogen that will be discussed in § 4.1.4, the database provided by the Nist does not contain the thermodynamic properties of normal hydrogen at temperature higher than 1500 K. The relative error presented by Fig. 18 and Fig. 19 were calculated using the following equation

$$Error = 100 \times \frac{X_{NIST} - X_{EoS}}{X_{NIST}} \tag{18}$$

The relative error computed at 10^5 Pa and 10^7 Pa is very low in this temperature range. This shows that the equation of state proposed by Leachman et al. (2009) offers accurate results in a large range of temperatures. This conclusion was already proposed by the reference, but only for temperatures up to 1000 K. The relative error on these thermodynamic parameters could explain the validation of the extrapolation of the results to higher temperatures. In § 5.3, the introduction of the normal hydrogen into the Longshot and the simulation of this gas during a test is presented. Leachman et al. (2009) presents that the accuracy of the different thermodynamic parameters are very low, in the order of those observed in Fig. 18.

Fig. 20 to Fig. 24 present the different thermodynamic parameters of hydrogen at a pressure of 10^7 Pa and a temperature extrapolated to 2600 K, the order of the maximum temperature measured during the simulation of the Lagrangian 1D program. McCarty (1981) proposed several values of the thermodynamic properties that are presented in the following figures. Using these data as references, the relative error on the entropy, enthalpy, internal energy , speed of sound, c_v and c_p can be computed. They are respectively of 0.28%, 0.985%, 1.19%, 0.496%, 8.95% and 10.29% at 2600 K. The relative error on most of these parameters are low, but both c_p and c_v suffer of a large difference with the reference. However, the error on

their ratio is only of 1.49%. In both cases, the heat capacities underestimate the reference values. The error measured on these parameters begins to increase at 2000 K, where the error is 0.5%, to reach 1.8% at 2200 K and 4.5 % at 2400 K. A special attention should then be given on these parameters when the equation of state is used at high temperature.

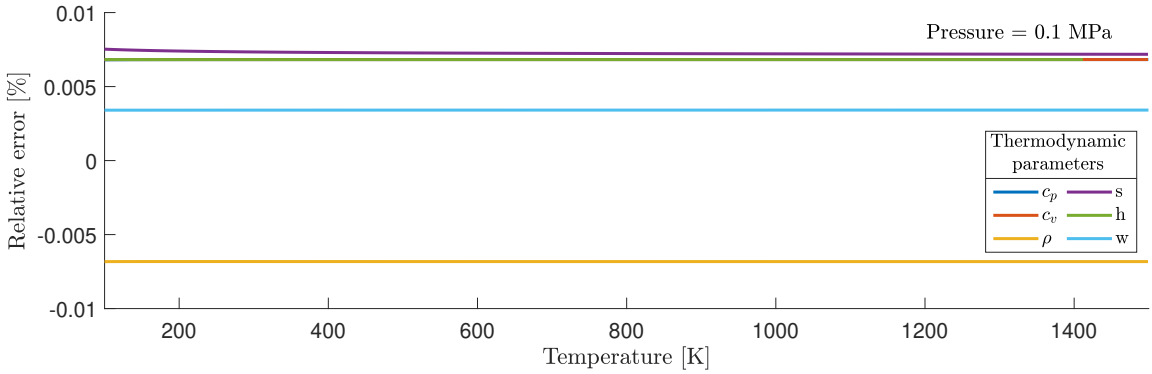

Figure 18: Relative error on the thermodynamic parameters of molecular hydrogen for a pressure of 0.1 MPa and a temperature range from 100 to 1500 K

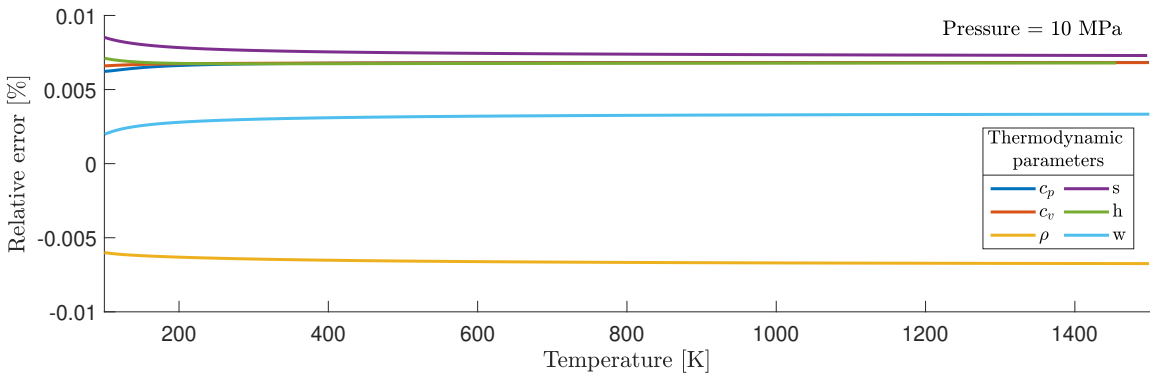

Figure 19: Relative error on the thermodynamic parameters of molecular hydrogen for a pressure of 10 MPa and a temperature range from 100 to 1500 K

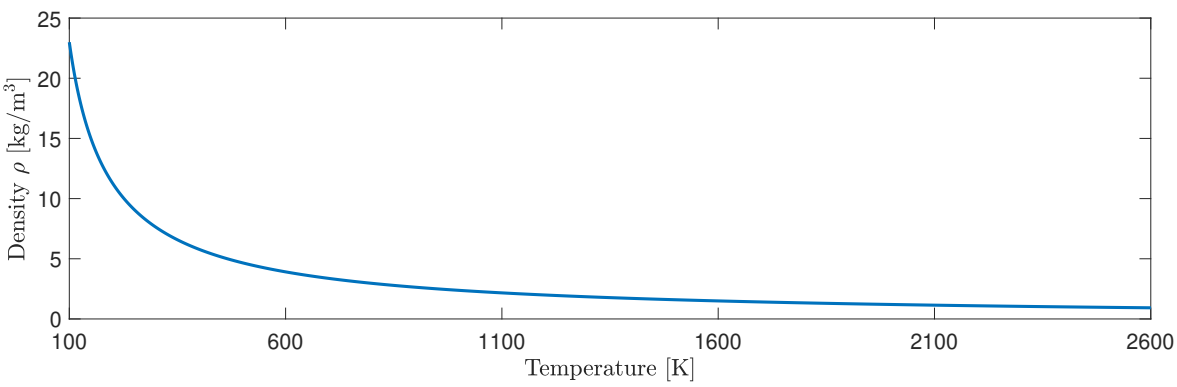

Figure 20: Density of normal hydrogen at 10^7 Pa from 100 to 2600 K

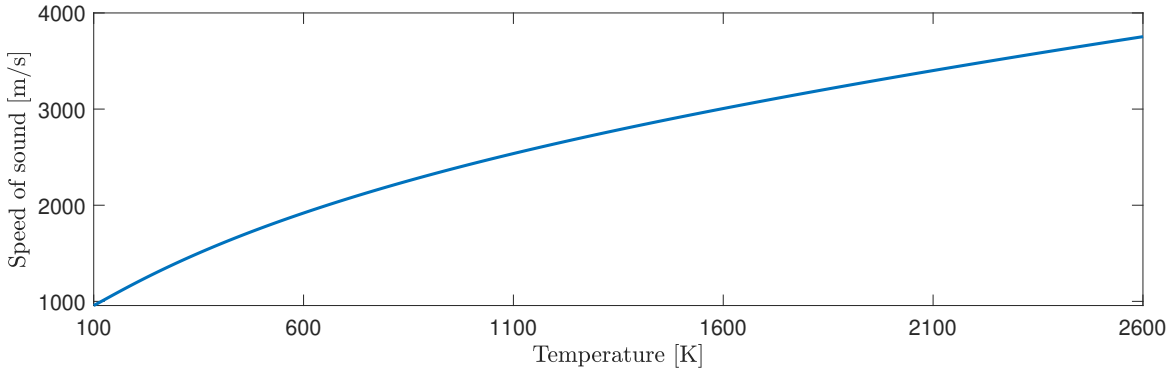

Figure 21: Speed of sound in normal hydrogen at 10^7 Pa from 100 to 2600 K

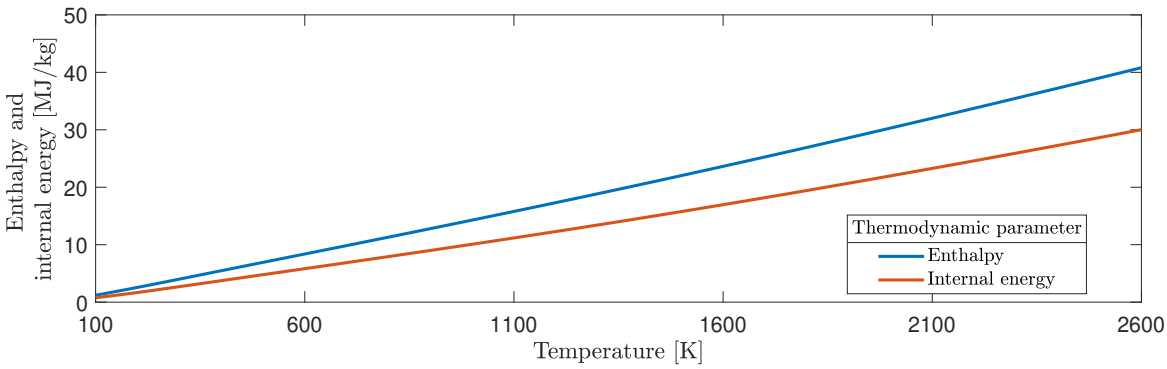

Figure 22: Enthalpy and internal energy of normal hydrogen at 10^7 Pa from 100 to 2600 K

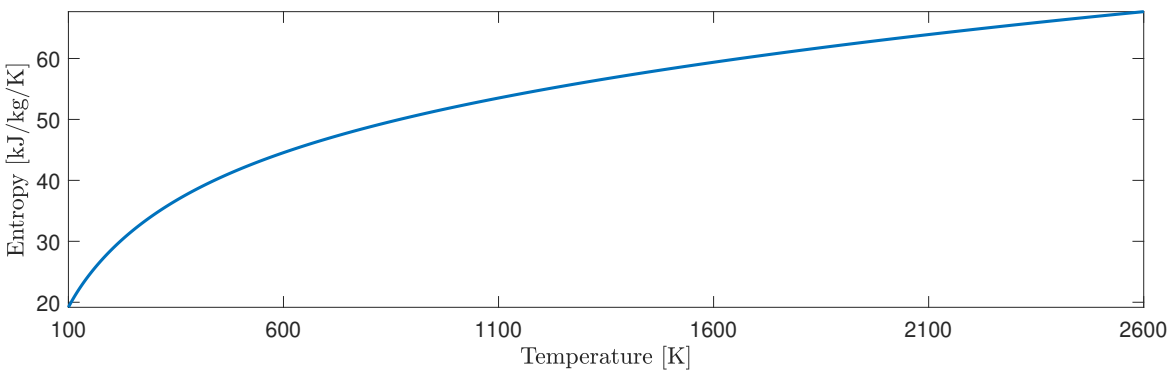

Figure 23: Entropy of normal hydrogen at 10^7 Pa from 100 to 2600 K

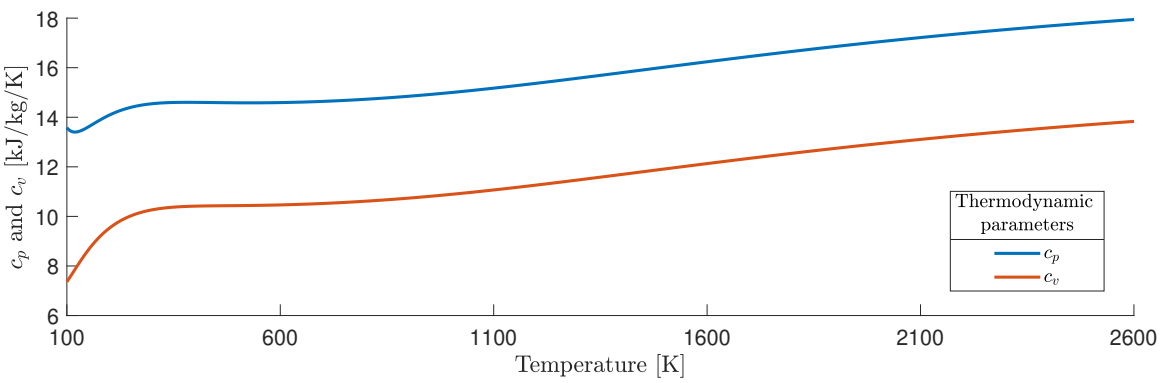

Figure 24: c_p and c_v of normal hydrogen at 10^7 Pa from 100 to 2600 K

4.1.4 Safety aspects and advice for Longshot use

Normal hydrogen is a gas well known for its use in the launcher propulsion. This highlights several of the safety aspects of the molecule. McCarty (1981), Najjar (2013) and Molkov (2012) exposed several safety warnings concerning the use of hydrogen.

The following discussions will be based on the normal hydrogen alone, since it is the type of molecule found in normal conditions. It was already mentioned that this composition is found at room temperature and is not significantly modified when the temperature is quickly altered. This is noticed due to several differences, however low, in different properties of the gas.

Flammability and detonability limits

When the use of hydrogen is considered, flammability and detonation become the highest concerns for the different possible applications. The flammability limits of hydrogen in contact with air are larger than for most of the conventional fuels. At room temperature and in air, the lower flammability limit (LFL) is 4 % in volume of hydrogen, while the upper limit (UFL) is 75 %. This flammability limit is far larger than with methane or gasoline, that are respectively from 5.3 % to 15 % and from 1 % to 7.6 %, (McCarty, 1981). The lower and upper limits are functions of both the temperature and the pressure. Molkov (2012) presented the decrease of the LFL to be a linear function of the temperature. This lower limit decreases from 4% at 293.15 K to 1.5 when the temperature is increased by 400 K. In the same range of temperature, the upper flammability limit increases from 75% to 87%. No data were found about the flammability limits at higher temperature. The modification of these limits with pressure is proposed by Fig. 25. This modification in the different flammability limits is however lower than the contribution of the temperature. These flammability limits are also functions of the direction of propagation. Indeed, the flammability limits are both lower when the flame propagates horizontally than vertically. This is mainly due to the buoyancy of the

gas in air. This buoyancy and high diffusivity of the gas offer a high level of safety, since the concentration of hydrogen in air quickly decreases under the flammability limit. However, in confined environment, detectors will be necessary in order to alert to operators of a possible leak.

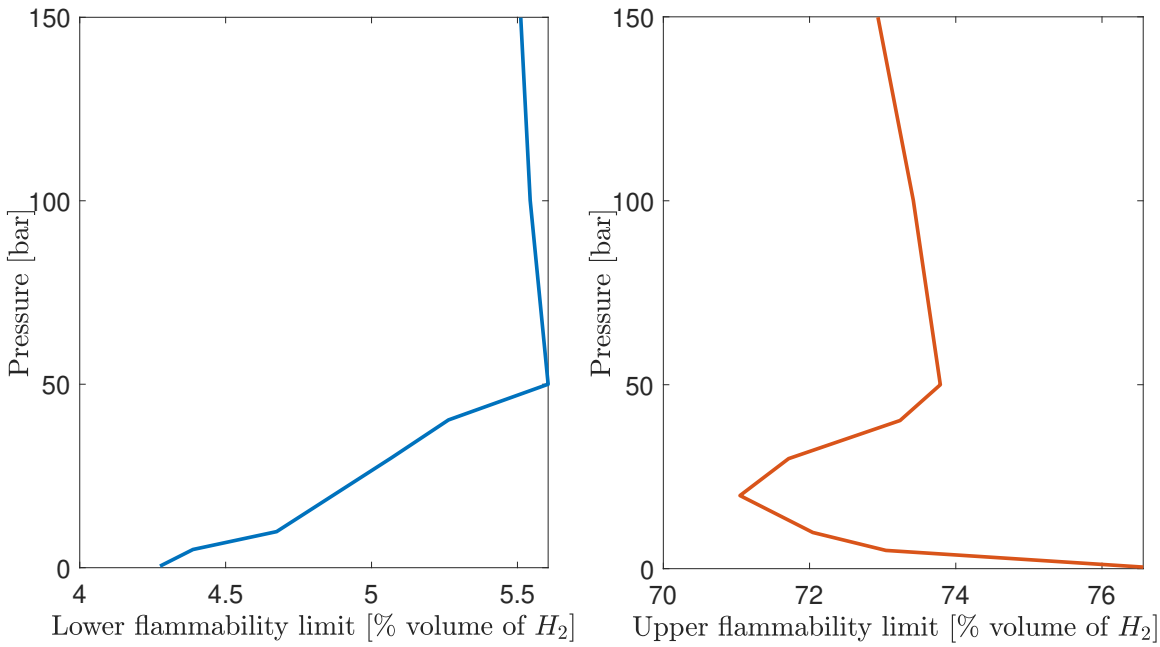

(a) LFL (b) UFL

Figure 25: Evolution of the flammability limits of molecular hydrogen, expressed in % of volume in air, with respect to the pressure, (Molkov, 2012)

At ambient temperature, the reaction between oxygen and hydrogen is very slow. However, the presence of a catalyst or a spark in the flammability region accelerates explosively the reaction, (Molkov, 2012). In this region, the ignition of the air and hydrogen mixture starts if the temperature of auto-ignition of hydrogen is reached. This temperature is also reported to have a large range and was observed either at 793 K and 1023 K, but it is usually taken to be 858.15 K. This temperature is higher than methane or gasoline and was experimented by Cain (1997) to be independent of the pressure. The risk of flammability of hydrogen could also come from its low ignition energy in air, 0.02 mJ, which is lower than the typical energy delivered by an electrical, striking or electrostatic spark (10 mJ).

In case of a leak, either in the reservoir or in the working area, a spark could ignite the air hydrogen mixture and form an invisible flame with a temperature of 2318 K, (McCarty, 1981). In case of H_2 fire, the supply must be shut off before any attempt to extinguish the fire because of the risks of re-ignition and explosions, (Molkov, 2012). The leak rate is of the order of 10 times higher than nitrogen and 50 times higher than water. The detection of a leak is usually not possible for the operator, since the gas is colourless, odourless and

tasteless. Special hydrogen detectors must then be added to the test area, as well as fire detectors. Infrared cameras could also detect the invisible hydrogen fires.

Molkov (2012) described detonation as the worst case scenario. It proposed a conservative detonability range of 11% to 70% in air. The International Association for Hydrogen Safety (HySafe) proposes a similar range, but highlights that this depends on the size of the system. In pure hydrogen, the upper range can even reach 90%. Lind (1975) reported that, when a leak appears on a tank, the possible explosion would only liberate 0.1 to 10 % of its thermal energy, but less than 1% in most of the cases. However, Ordin (1997) highlights that, in case of an uncontrollable leak, especially in confined area, the area should be evacuated in a 152 m radius to offer an acceptable level of safety in case of an explosion. This type of leak cannot be quenched by the operators, because of the high risk of explosion due to the low ignition energy.

Both the detonation or the ignition are low in probability inside the Longshot wind tunnel due to the lack of a significant quantity of air during a test. However, these two phenomena have to be considered seriously during the storage and the filling phase of the gas. The disposal of the gas once the test is completed should also be done with care.

Health hazards

The most important aspect of the safety review is dedicated to the safety of the operators. Molkov (2012) and Ordin (1997) presented a safety review dedicated to this subject. It reported that hydrogen is classified as an asphyxiant. It is not carcinogen or toxic, does not cause mutagenicity or embryotoxicity. Moreover, exposure of skin or eyes to this gas does not cause adverse effects. As mentioned above, the main risk of this gas is its flammability. Nevertheless, in case of a massive leak and inhalation of hydrogen in a confined area, the deficit of oxygen and the introduction of hydrogen would result in a flammable mixture inside the body. The symptoms of the ingestion of this gas are related to the lack of oxygen and would include:

- headaches
- dizziness
- drowsiness and unconsciousness
- nausea
- vomiting
- depression
- blue colour skin

The first symptoms to appear are the decreased ability to perform tasks and headaches when the oxygen concentration decreases down to the range of 15 to 19%. These symptoms appear first and with a higher intensity on a person with heart, lung or circulatory problems. In case of a suspicion of inhalation of hydrogen, the victims must be evacuated and keep under surveillance in fresh air. If breathing is difficult, the victim should receive oxygen, but caution is to be observed due to the explosive mixture hydrogen and oxygen create. Artificial respiration must be applied if the victim is not able to breath by herself or himself. In the most serious cases, if the concentration of oxygen decreases under 8%, the victim must be treated under 4 minutes to ensure a high chance of recovery. Below 6 minutes, the recovery chances drop to 50 %. There is no chance of recovery after 8 minutes. If the concentration of oxygen further decreases to 4%, the victim falls in coma in less than 40 seconds. When a leak or dysfunction is suspected, the test section must be ventilated to decrease the concentration of hydrogen below the flammability limit as soon as possible. This should prevent the ignition of the mixture due to a spark.

The flame of hydrogen being invisible and reaching a temperature of 2318 K, a victim can suffer from a burn if contact. This type of event could occur because of a leak either in the storage tank or in the test section. In the case of a use in the Longshot wind tunnel, a special attention should be given during the filling of the driven tube and the disposal of the test gas after the run. If the storage of hydrogen in a liquid state is proposed, the low temperature of the hydrogen could result in frostbite.

Effects on materials

Ordin (1997) and Oriani (1978) presented reviews of the effect of hydrogen on materials. Metals with a face-centred cubic structure, such as martensitic stainless steel are satisfactory to be used with hydrogen at ambient temperature. However, significant deteriorations of mechanical properties of metals are known when they are used with this gas. This is known as hydrogen embrittlement, (Ordin, 1997). This effect depends on several variables, such as the temperature and pressure of the gas, its purity and concentration, the exposure time, ... In the case of the VKI Longshot, several main types of embrittlement can be highlighted, (Ordin, 1997)

- In case of a plastic deformation, *environmental hydrogen embrittlement* had been noticed in metals. This creates a loss of ductility. The cracks start at the surface.
- Depending on the pressure, temperature, purity, ... of the hydrogen, the gas is absorbed by the metal. This modifies its structural lattice, leading to premature failures. Since the cracks start internally, the failure can arrive with little or no warning. This is know as *internal embrittlement*.
- At high temperature, the absorbed hydrogen can combine with the carbon of steel to form methane. The resulting hybrid composition of the wind tunnel bore could then be more brittle. This third type of embrittlement is known as the *reaction embrittlement*.

Depending on the type of steel used, the embrittlement differs in intensity. The stainless steel 310, 316 and A286 are not expected to suffer from a noticeable embrittlement, while others, such as 18Ni-250 Maraging steel, 410 stainless steel or 1042 steel experience extreme decreases of their mechanical properties. The effects of environmental and internal embrittlement are maximum between 200 and 300 K, while the reaction embrittlement occurs at higher temperature. During the operation in the Longshot wind tunnel, the two first embrittlements are expected to occur during the loading of the driven tube and the time it remains in this tube before the test. Reaction embrittlement effects should be kept under surveillance in the reservoir, where the temperature is at its highest. This area is especially vulnerable to catastrophic failure due to the high pressure and temperature noticed in this location.

The embrittlement of steel can lead to a decrease of the lifespan of the wind tunnel, but several options exist to decrease the effects of the embrittlement or the risks of failure and severe damages.

- The severity of embrittlement depends on the purity of the gas. The addition of impurity to the gas would reduce them.
- Aluminium is used to eliminate embrittlement because of its minimal susceptibility. It is one of the rare metals to have such a property. A layer of this metal could protect the steel structure of the wind tunnel.

Gardiner Jr and Kistiakowsky (1961), Moore and Unterwald (1964) andJansen et al. (1989) studied the dissociation of the molecular hydrogen. It appears that the molecule starts its dissociation at a temperature of 1200 K, but this real gas phenomenon continues above the temperature of 2500 K. Lockwood et al. (1964) event shows that the fraction of dissociated hydrogen at 2380 K is of 87.5%. Atomic hydrogen attacks the steel by diffusing into its crystal lattice in a similar way than previously proposed. When the temperature increases above 2000 K, the formation of acetylene begins, using the carbon taken from the bore steel. The molar fraction of this compound should be very limited due to the low duration of the test. However, this gas is reported to have an explosivity range between 2 and 100% in contact with air, with an auto ignition temperature of 578.15 K, according to the French National Institute for Research and Safety (INRS), (Jargot et al., 2019). This gas is also reported to explode even without the presence of oxygen, especially when the temperature or the pressure increases, notably above 200 kPa. The ignition energy of this gas is the lowest recorded, $17\mu J$. If the hydrogen is used as a test gas in the Longshot wind tunnel, the quantity of acetylene produced should be sufficiently low to be ignored. However, the use of other gases, such as methane that will be discussed in § 4.6.1, must take this threat into account. Another phenomenon that must be taken into account during in the reservoir is the recombination of molecular hydrogen. Indeed, the energy delivered by this recombination creates an intense heat usually used by welding tools.

4.2 Oxygen

Oxygen is the second most important gas in the Earth atmosphere. However, due to its low temperature of dissociation, the use of this gas inside the Longhsot wind tunnel was proved to create significant damages to the reservoir. Indeed, the recombination of atomic oxygen with the steel bore of the wind tunnel increases significantly its rate of oxidation. Replacement of the reservoir and the valve system is then necessary after each test. Molecular oxygen was never used alone in the Longshot wind tunnel, but Grossir (2015) described a test where air was used in the driven tube. The damages noticed in the different parts of the Longshot where attributed to the dissociation of oxygen.

If air is a test gas used by several hypersonic facilities, such as the former IUSTI TCM2 in Marseilles or the NASA EAST shock tube, the use of oxygen as test gas was only reported in a few wind tunnel, such as the HIEST shock tunnel of the JAXA, where the dissociation of the molecule is studied, (Reynier, 2016). The implementation of oxygen proposed in this section has then not the objective of proposing the use of this gas in the VKI Longshot. Nevertheless, the mixture equation proposed by §. 4.5 will use this gas in order to compare the results of this equation with the well known mixture that is air.

4.2.1 Equation of state

The equation of state used in this work was presented by Schmidt and Wagner (1985). It follows the general construction of the total Helmholtz energy proposed by Eq. 8. The perfect gas contribution of the Helmholtz equation was obtained thanks to the integration of the ideal gas heat capacity of the molecule and can be expressed by

$$\begin{aligned}\alpha^0(\delta,\tau) = &\ln\delta + k_1\tau^{1.5} + k_2\tau^{-2} + k_3\ln\tau + k_4\tau + k_5\ln\left(e^{k_7\tau}-1\right)\\ &+ k_6\ln\left(1+\frac{2}{3}e^{-k_8\tau}\right) + k_9 + \frac{h^{id}(\tau)}{RT} - \frac{s^{id}(\tau,\delta)}{R}\end{aligned} \tag{19}$$

where the different value of the k_i are presented by Table 5. Schmidt and Wagner (1985) presented these coefficients to be valid from 30 to 3000 K. The critical density and temperature of oxygen were borrowed from this reference and confirmed by the Nist. They are respectively $\delta_c = 13.6298 mol/dm^3 = 436.14 kg/m^3$ and $T_c = 154.581 K$.

i	k_i	i	k_i	i	k_i
1	$-7.40775 \cdot 10^{-4}$	4	-21.4487	7	14.5066
2	$-6.6493 \cdot 10^{-5}$	5	1.01258	8	74.9148
3	2.50042	6	-0.944365	9	4.14817

Table 5: Coefficients k_i used in Eq. 19, the perfect gas contribution of the Helmholtz energy for oxygen, (Schmidt and Wagner, 1985)

Schmidt and Wagner (1985) also proposed the expression of $h^{id}(\tau)$ and $s^{id}(\tau, \delta)$ to be chosen arbitrarily. This reference proposed these two functions to be equal to zero. However, the latter could have an effect on the computation of the internal energy, the enthalpy, the entropy and the two heat constants, as presented by Eq. 9 to Eq. 14. A comparison between the data provided by the NIST and those computed using the approach proposed by Schmidt and Wagner (1985) was carried in order to determine a form for $h^{id}(\tau)$ and $s^{id}(\tau, \delta)$. The relative difference obtained by comparing the computed value with the reference of the NIST is very low in the case of the isochoric and isobaric heat capacities. The variations of the internal energy, enthalpy and entropy with respect to the temperature have the same slope if obtained with the equation of state of with the NIST data. However, these two sets of data differ of a constant. This difference is due to the reference taken by the two approaches. The data obtained from the NIST takes 0 K as reference, while Schmidt and Wagner (1985) uses a higher temperature, 298.15 K. Since the reference temperature used by the VKI to model nitrogen and carbon dioxide is the same than the NIST, the two different terms h^{id} and s^{id} are here different from Schmidt and Wagner (1985).

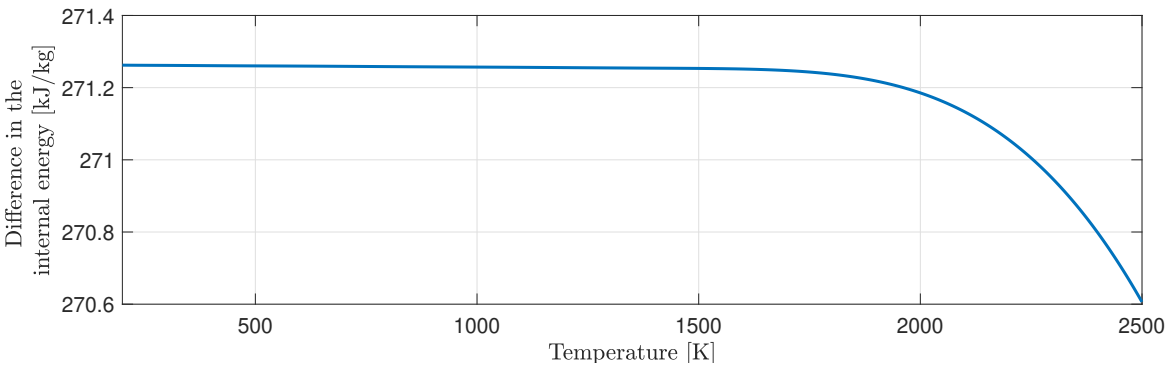

Figure 26: Absolute difference in the internal energy computed by the equation of state and the data from the Nist for different temperatures and at a pressure of 10^7 Pa

In order to obtain the expressions of h^{id} and s^{id} the absolute difference between the internal energy calculated by the equation of state and the data provided by the NIST is computed at different temperatures and pressures. This interval is presented by Fig. 26 in the case of the internal energy at a pressure of 10 MPa. The maximum, minimum and mean of this difference, as well as the case of a pressure 100 times lower, is presented by Table 6.

Pressure [Pa]	Minimum difference	Mean Difference	Maximum difference
10^5	$2.7060 \cdot 10^5$	$2.7119 \cdot 10^5$	$2.7126 \cdot 10^5$
10^7	$2.7061 \cdot 10^5$	$2.7119 \cdot 10^5$	$2.7126 \cdot 10^5$

Table 6: Maximum, minimum and mean absolute differences in the internal energy computed by the equation of state and the data from the Nist at pressures of 10^5 and 10^7 Pa and on the temperature range of 100 to 2500 K

The difference between the computed data and those obtained from the Nist database is roughly constant between 200 K and 1800 K, before decreasing when the temperature rises. The addition of a constant is then used to modify the value of the internal energy. Since the reduced density does not have a significant impact on the difference, the form of the first derivatives of h^{id} and s^{id} are assumed to be respectively $2.7119 \cdot 10^5/(rT_c)$ and 0. The effect of the change of reference in the relative error on the internal energy and the enthalpy are presented in § 4.2.2.

The same method was applied on the entropy for the same reason than for the internal energy. The absolute difference between the Nist database and the results of the equation of state are presented in Table 7. Once again, the effect of the pressure is negligible and the addition of a constant to change the reference temperature is used. The computation of this constant was made after the introduction of the first correction obtained with the internal energy.

Pressure [Pa]	Minimum difference	Mean Difference	Maximum difference
10^5	$4.8980 \cdot 10^3$	$4.8983 \cdot 10^3$	$4.8983 \cdot 10^3$
10^7	$4.8981 \cdot 10^3$	$4.8983 \cdot 10^3$	$4.8983 \cdot 10^3$

Table 7: Maximum, minimum and mean absolute differences in the entropy computed by the equation of state and the data from the Nist at pressures of 10^5 and 10^7 Pa and on the temperature range of 250 to 2500 K

i	n_i	d_i	t_i	i	n_i	d_i	t_i
1	0.3983768749	1	0	17	$-9.067701064 \cdot 10^{-2}$	2	5.5
2	-1.846157454	1	1.5	18	$-3.540084206 \cdot 10^{-2}$	3	3
3	0.4183473197	1	2.5	19	$-3.623278059 \cdot 10^{-2}$	3	7
4	$2.370620711 \cdot 10^{-2}$	2	-0.5	20	$1.327699290 \cdot 10^{-2}$	5	6
5	$9.771730573 \cdot 10^{-2}$	2	1.5	21	$-3.254111865 \cdot 10^{-4}$	6	8.5
6	$3.017891294 \cdot 10^{-2}$	2	2	22	$-8.313582932 \cdot 10^{-3}$	7	4
7	$2.273353212 \cdot 10^{-2}$	3	0	23	$2.124570559 \cdot 10^{-3}$	8	6.5
8	$1.357254086 \cdot 10^{-2}$	3	1	24	$-8.325206232 \cdot 10^{-4}$	10	5.5
9	$-4.052698943 \cdot 10^{-2}$	3	2.5	25	$-2.626173276 \cdot 10^{-5}$	2	22
10	$5.454628515 \cdot 10^{-4}$	6	0	26	$2.599581482 \cdot 10^{-3}$	3	11
11	$5.113182277 \cdot 10^{-4}$	7	2	27	$9.984649663 \cdot 10^{-3}$	3	18
12	$2.953466883 \cdot 10^{-7}$	7	5	28	$2.199923153 \cdot 10^{-3}$	4	11
13	$-8.687645072 \cdot 10^{-5}$	8	2	29	$-2.591350486 \cdot 10^{-2}$	4	23
14	-2.127082589	1	5	30	-0.1259630848	5	17
15	$8.735941958 \cdot 10^{-2}$	1	6	31	0.1478355637	5	18
16	1.275509190	2	3.5	32	$-1.011251078 \cdot 10^{-2}$	5	23

Table 8: n_i, d_i and t_i parameters used in Eq. 20, the residual part of the oxygen equation of state,(Schmidt and Wagner, 1985)

The second part of the equation, dedicated to the residual contribution takes the form presented by Eq. 20. Schmidt and Wagner (1985) presented it as the most efficient combination of a bank of terms obtained by experience. In order to fulfil the accuracy requirement on the critical regions, a minimum number of 32 terms was selected and are divided into 13 polynomials, 11 Benedict-Webb-Rubin (BWR) terms and 8 "e^4" terms. The equation was designed in order to cover the temperature range from the oxygen triple point at 54K up to 400K and pressures up to 81.8 MPa. The possible application of this equation for higher temperature will be discussed below, by § 4.2.2. The second part of the oxygen equation of state is then

$$\alpha^r = \sum_{i=1}^{13} n_i \delta^{d_i} \tau^{t_i} + e^{-\delta^2} \sum_{i=14}^{24} n_i \delta^{d_i} \tau^{t_i} + e^{-\delta^4} \sum_{i=25}^{32} n_i \delta^{d_i} \tau^{t_i} \tag{20}$$

where the different coefficients are available in Table 8.

4.2.2 Verification of the equation of state

In order to test the accuracy of the equation of state used in this work, the results obtained thanks to this equation are compared to the database provided by the NIST. Several experimental data are also available and could have been considered, but the range of temperature and pressure they cover are usually restricted. The different thermodynamic parameters presented by Eq. 9 to Eq. 14 have been compared from 100 to 2500 K and at the pressure of 0.1 MPa. The resulting relative error is presented by Fig. 27. This relative error is computed in the same way than in the case of hydrogen by taking the values from the Nist database as references. Fig. 28 presents the same study in the case of a higher pressure (10 MPa). However, the temperature range is smaller in this case, since the relative error at high pressure and low temperature rises quickly.

The relative error on the different parameters are very low at both pressure for the temperature range tested. In the case where the pressure is equal to 0.1 MPa, the accuracy of the results is very good, under 0.1% for most of the temperature range. It should however be noticed that the relative error on c_v and c_p increases when the temperature is higher than 1500 K. Nevertheless, at "low" pressure, the equation of state provides accurate results far over the limit of its application. The extrapolation of the latter to higher temperature can then be validated. The same conclusions can be made when the pressure is higher. Indeed, the behaviour of most of the thermodynamic properties is the same than in the case of low pressure. As an example, the relative error on c_p and c_v at 2500 K are the same, respectively -0.179% and -0.2281%, at both pressure. A special attention has to be given to the speed of sound and c_p. These two thermodynamic parameters suffer a noticeable error at low temperature and high pressure. This could be due to the form of the term $\alpha^r_{\delta\tau}$, only used for the computation of these two parameters. This second derivative of the residual contribution of the Helmholtz energy could suffer some trouble in the simulation of the phase of the oxygen at this type of temperature and pressure. However, this type of conditions are not reached in

the Longshot wind tunnel and will not be considered as a major drawback in the validation of the mixture equation.

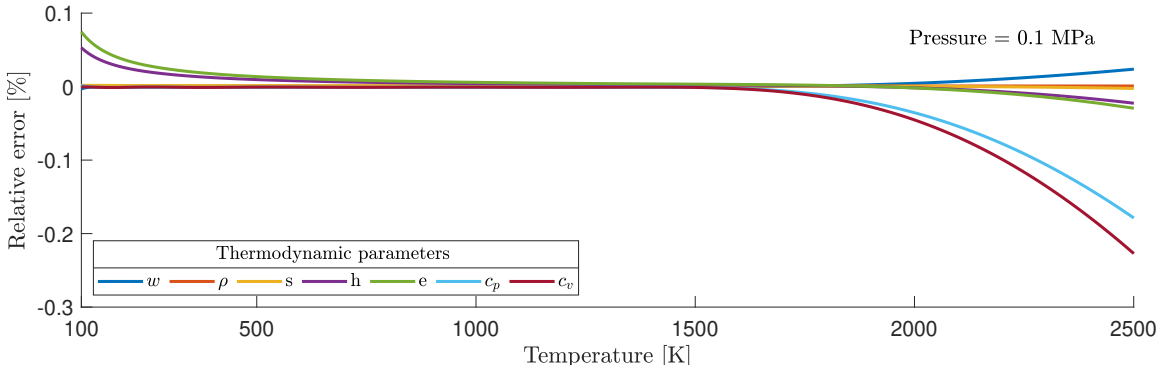

Figure 27: Relative error between the thermodynamic parameters of molecular oxygen computed with the equation of state and the data from the Nist database (taken as reference). The temperature range is between 100 K and 2500 K, the pressure is 0.1 MPa

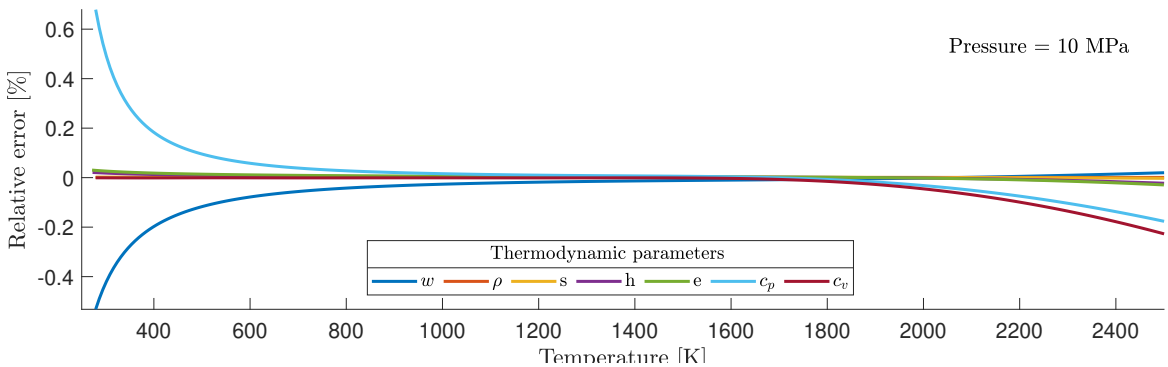

Figure 28: Relative error between the thermodynamic parameters of molecular oxygen computed with the equation of state and the data from the Nist database (taken as reference). The temperature range is between 250 K and 2500 K, the pressure is 10 MPa

4.3 Argon

The third component of the air mixture considered in this study is Argon. This gas was used in the former French IUSTI TCM2 wind tunnel, in the Russian TSAGI IT-2 hot shot or the American GASL HYPULSE facility, which are all wind tunnels that have the objective of studying the aerodynamic characteristics of blunt vehicle during reentry, (Reynier, 2016). According to Chapman (1956), the use of heavy gas to simulate air is possible, but most of the possible gases are unusable, due to their toxicity, their chemical activity or their specific heat ratio too different from the air. It proposed the use of a mixture of a heavy monoatomic gas and a heavy polyatomic gas. The interest of noble gases, such as Argon, Xenon or Krypton can then be explained by the will of simulating air thanks to an alternative mixture. Another reason for the use of this type of mixture is the lower speed of sound in the heavier molecules and atoms. At the same velocity, this type of gas could offer a higher Mach number. When the same initial conditions are used during a simulation carried with air or this mixture, the Reynolds number obtained was reported higher with this second gas.

4.3.1 Equation of state

Tegeler et al. (1999) proposed an equation of state based on the Helmholtz energy to describe this gas. This equation, primarily developed for temperature up to 700K and pressure of 1 GPa presents acceptable levels of accuracy for higher temperature. Using once again the sum of the ideal gas Helmholtz energy α^0 and its residual part α^r, Argon's behaviour can be predicted by

$$\alpha^0 = \ln\delta + a_1^0 + a_2^0\tau + 1.5\ln\tau \tag{21}$$

where $a_1^0 = 8.31666243$ and $a_2^0 = -4.94651164$. The value of the critical temperature T_c is here considered as 150.687K and the critical density ρ_c is taken as $13.4074 mol/dm^3$,(Tegeler et al., 1999). Just as in the case of the oxygen, the reference temperature used by this reference is not the same than Nist. A correction is proposed by the modification of a_1^0 and a_2^0 using the same method than for oxygen. Since Stewart and Jacobsen (1989) also proposes an equation of state and uses the same reference temperature than the VKI, the new constants will be based on this reference. The additional term, added to the expression of α^0 is then -96.958869170091788. The effect of this additional term will be presented by § 4.3.2.

The residual contribution of the Helmholtz energy equation is given by

$$\alpha^r = \sum_{i=1}^{12} n_i\delta^{d_i}\tau^{t_i} + \sum_{i=13}^{37} n_i\delta^{d_i}\tau^{t_i}e^{-\delta^{c_i}} + \sum_{i=38}^{41} n_i\delta^{d_i}\tau^{t_i}e^{-\eta_i(\delta-\varepsilon_i)^2-\beta_i(\tau-\gamma_i)^2} \tag{22}$$

where the different terms were determined by nonlinear regression analysis, as reported by Tegeler et al. (1999). These coefficients and exponents are presented in Table 9.

i	n_i	d_i	t_i	c_i	η_i	β_i	γ_i	ε_i
1	$8.872230499 \cdot 10^{-2}$	1	0	0	0	0	0	0
2	0.70514805167298	1	0.25	0	0	0	0	0
3	-1.682011565409	1	1	0	0	0	0	0
4	-0.14909014431486	1	2.75	0	0	0	0	0
5	-0.1202480460094	1	4	0	0	0	0	0
6	-0.12164978798599	2	0	0	0	0	0	0
7	0.40035933626752	2	0.25	0	0	0	0	0
8	-0.27136062699129	2	0.75	0	0	0	0	0
9	0.24211924579645	2	2.75	0	0	0	0	0
10	$0.5788958318557 \cdot 10^{-2}$	3	0	0	0	0	0	0
11	$-4.1097335615341 \cdot 10^{-2}$	3	2	0	0	0	0	0
12	$2.4710761541614 \cdot 10^{-2}$	4	0.75	0	0	0	0	0
13	-0.32181391750702	1	3	1	0	0	0	0
14	0.33230017695794	1	3.5	1	0	0	0	0
15	$0.31019986287345 \cdot 10^{-1}$	3	1	1	0	0	0	0
16	$-0.30777086002437 \cdot 10^{-1}$	4	2	1	0	0	0	0
17	$0.93891137419581 \cdot 10^{-1}$	4	4	1	0	0	0	0
18	$-0.90643210682031 \cdot 10^{-1}$	5	3	1	0	0	0	0
19	$-0.45778349276654 \cdot 10^{-3}$	7	0	1	0	0	0	0
20	$-0.82659729025197 \cdot 10^{-4}$	10	0.5	1	0	0	0	0
21	$0.13013415603147 \cdot 10^{-3}$	10	1	1	0	0	0	0
22	$-0.11397840001996 \cdot 10^{-1}$	2	1	2	0	0	0	0
23	$-0.24455169960535 \cdot 10^{-1}$	2	7	2	0	0	0	0
24	$-0.64324067175955 \cdot 10^{-1}$	4	5	2	0	0	0	0
25	$0.58889471093674 \cdot 10^{-1}$	4	6	2	0	0	0	0
26	$-0.64933552112965 \cdot 10^{-3}$	8	6	2	0	0	0	0
27	$-0.13889862158435 \cdot 10^{-1}$	3	10	3	0	0	0	0
28	0.40489839296910	5	13	3	0	0	0	0
29	-0.38612519594749	5	14	3	0	0	0	0
30	-0.18817142332233	6	11	3	0	0	0	0
31	0.15977647596482	6	14	3	0	0	0	0
32	$0.53985518513856 \cdot 10^{-1}$	7	8	3	0	0	0	0
33	$-0.28953417958014 \cdot 10^{-1}$	7	14	3	0	0	0	0
34	$-0.13025413381384 \cdot 10^{-1}$	8	6	3	0	0	0	0
35	$0.28948696775778 \cdot 10^{-2}$	9	7	3	0	0	0	0
36	$-0.22647134304796 \cdot 10^{-2}$	5	24	4	0	0	0	0
37	$0.17616456196368 \cdot 10^{-2}$	6	22	4	0	0	0	0
38	$0.58552454482774 \cdot 10^{-2}$	2	3	0	20	250	1.11	1
39	-0.69251908270028	1	1	0	20	375	1.14	1
40	1.5315490030516	2	0	0	20	300	1.17	1
41	$-2.7380447449783 \cdot 10^{-3}$	3	0	0	20	225	1.11	1

Table 9: Coefficients and exponents used by Eq. 22

4.3.2 Verification of the equation of state

Due to the availability of the experimental data offered by Tegeler et al. (1999) between 80 K and 700 K and Stewart and Jacobsen (1989) between 100 and 1200 K, these two references will be used to estimate the accuracy of the equation of state for Argon. These data are used as reference in order to compute the relative error on the different thermodynamic properties. Tegeler et al. (1999) highlighted that its equation of state offers accurate results in the temperature range from the melting line to 700 K for pressures up to 1000 MPa. Fig. 29 presented the relative error on the different thermodynamic properties at the pressure of 0.1 MPa and between 85 and 1200 K. Unfortunately, no other experimental data had been found to continue this comparison further.

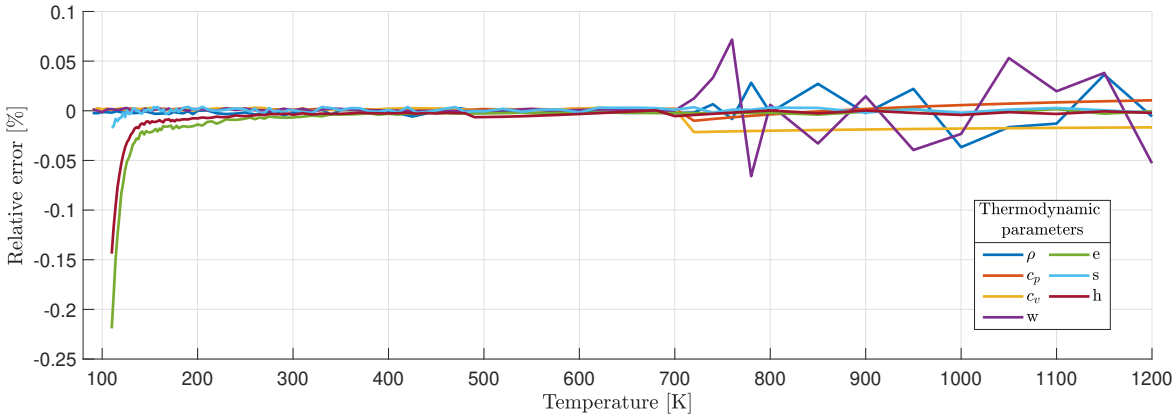

Figure 29: Relative error on the different thermodynamic properties of Argon at a pressure of 0.1 MPa, (Tegeler et al., 1999) and (Stewart and Jacobsen, 1989)

The relative error on the different thermodynamic parameters presented by Fig. 29 was obtained by using the database from Tegeler et al. (1999) from the melting line to 700 K and Stewart and Jacobsen (1989) for the data between 720 and 1200 K. At the pressure of 0.1 MPa, the relative error is acceptable on a wide range of temperature. The behaviour of the relative error curves above 700 K can be explained by the quality of the data provided by Stewart and Jacobsen (1989) and the unit transformations that had to be performed to used them. However, the relative error is low for most of the temperature range. Tegeler et al. (1999) concluded that its equation of state can be used to extrapolate data up to 17000 K and 50 GPa with a "reasonable accuracy". Additional experimental data will be required to obtain a quantitative projection of this error. Then, the projection of the density, speed of sound and specific heat ratio proposed by Fig. 30, Fig. 31 and Fig. 32 respectively only consider the database proposed by Tegeler et al. (1999).

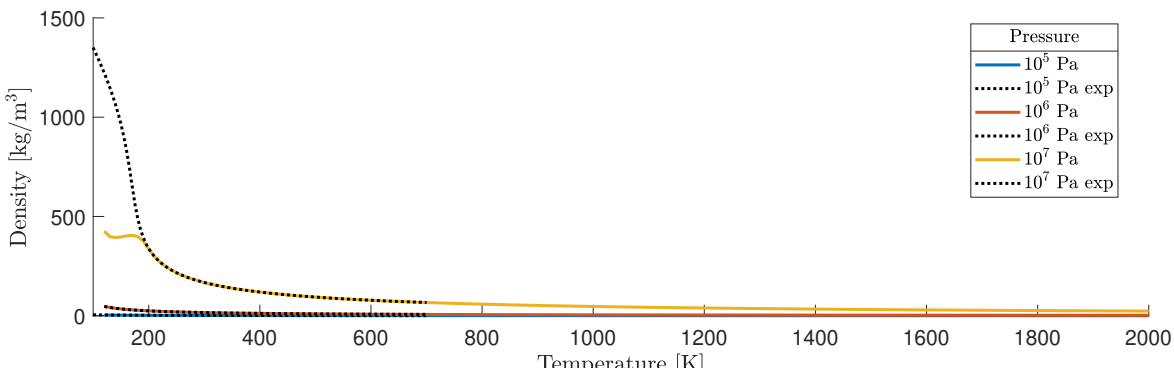

Figure 30: Projection of the density above the temperature limit proposed by Tegeler et al. (1999) at different pressures

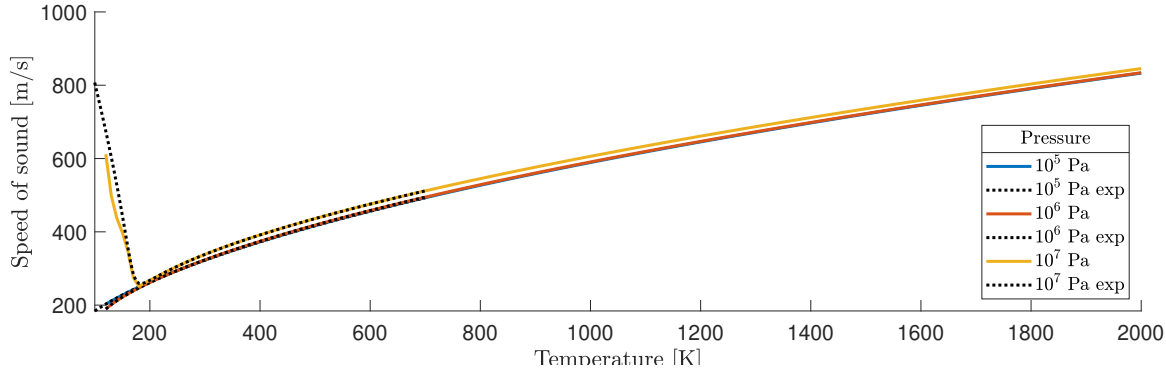

Figure 31: Projection of the speed of sound above the temperature limit proposed by Tegeler et al. (1999) at different pressures

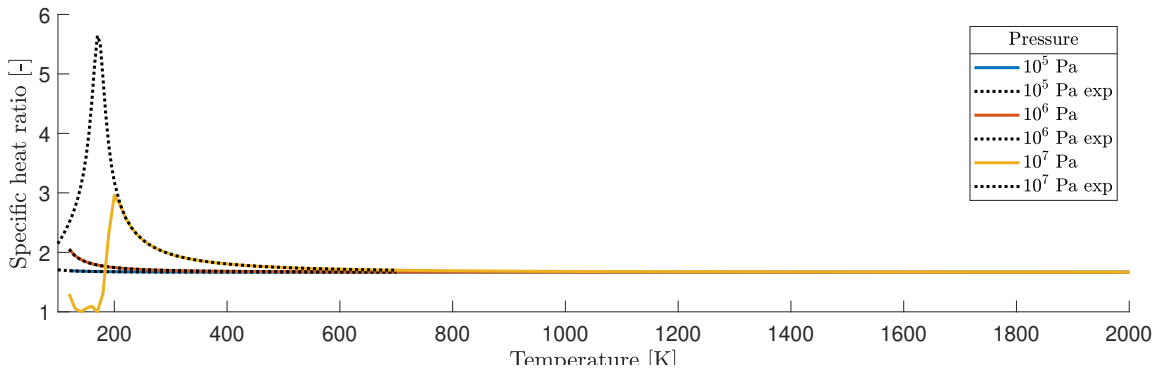

Figure 32: Projection of the specific heat ratio above the temperature limit proposed by Tegeler et al. (1999) at different pressures

The behaviour of these three thermodynamic parameters is pertinent in most of the temperature range. However, in the high density region, where p=10 MPa and the temperature is below 200 K, the equation of state provides completely useless data. The problem was noticed

by Tegeler et al. (1999). The reference also provides some reservations about the validity of derived properties, such as the speed of sound or the specific heat ratio. Nevertheless, the different projections of these thermodynamic properties and the relative error study proposed above tends to show that these parameters could offer a satisfactory accuracy. Moreover, since the objective of this equation of state is its inclusion in the air mixture, with a low molar ratio in this mixture, the accuracy provided by this equation of state is considered pertinent for this application.

4.4 Air

When the simulation of the atmospheric entry into the Earth atmosphere is matter of interest, the use of air as a test gas seems the best choice. However, the use of this mixture is not always possible due to the real gas effects of oxygen. Indeed, a severe oxidation is reported by Grossir (2015) when the test 1190 was run with air instead of nitrogen. The specific heat ratio of the nitrogen being equal to the one of the air, the former is used by the von Karman Institute to simulate the Earth reentry. Several wind tunnels, such as the German DLR HEG shock-tunnel, the Russian MIPT VUT-1 shock-tube or the NASA EAST shock tube use air as test gas, (Reynier, 2016). The latter used air to simulate both the Earth reentry and the Jovian reentry in order to obtained the different aerodynamic coefficients of the Galileo probe during its test campaign, (Dmitry V.Kotov, 2014) and (Seiff et al., 1996). The equation of state presented by Lemmon et al. (2000) is introduced in this section, before a test of its accuracy.

4.4.1 Equation of state for air

Lemmon et al. (2000) proposed an equation of state with the same Helmholtz energy formulation than the previous gases. The maximum temperature proposed by this equation of state is 2000K and the maximum pressure is 2MPa. The conditions that would have been obtained in the vki Longshot if air was used as a test gas would then have been well approximated by this equation. As usual, the Helmholtz equation of state is composed of two contributions. The first one, linked to the perfect gas contribution, is expressed by

$$\begin{aligned}\alpha^0 = &\ln\delta + \sum_{i=1}^{5} N_i\tau^{i-4} + N_6\tau^{1.5} + N_7\ln\tau + N_8\ln\left[1-\exp\left(-N_{11}\tau\right)\right] \\ &+ N_9\ln\left[1-\exp\left(-N_{12}\tau\right)\right] + N_{10}\ln\left[2/3+\exp\left(N_{13}\tau\right)\right]\end{aligned} \tag{23}$$

where the different N_i are presented in Table. 10.

i	N_i	i	N_i
1	$6.057194 \cdot 10^{-8}$	8	0.791309509
2	$-2.10274769 \cdot 10^{-5}$	9	2.12236768
3	-1.58860716·10−4	10	-0.197938904
4	-13.841928076	11	25.36365
5	17.275266575	12	16.90741
6	-1.9536342·10−4	13	87.31279
7	2.490888032	-	-

Table 10: N_i parameters used in Eq. 23,(Lemmon et al., 2000)

The residual part of the equation for air is

$$\alpha^r(\delta,\tau) = \sum_{k=1}^{10} N_k \delta^{i_k} \tau^{j_k} + \sum_{k=11}^{19} N_k \delta^{i_k} \tau^{j_k} \exp\left(-\delta^{l_k}\right) \tag{24}$$

where the different parameters used are proposed in Table 11.

k	N_k	i_k	j_K	l_k	k	N_k	i_k	j_K	l_k
1	0.118160747229	1	0	0	11	-0.101365037912	1	1.60	1
2	0.713116392079	1	0.33	0	12	-0.173813690970	3	0.80	1
3	-1.618241920670	1	1.01	0	13	-0.0472103183731	5	0.95	1
4	0.0714140178971	2	0	0	14	-0.0122523554253	6	1.25	1
5	-0.0865421396646	3	0	0	15	-0.146629609713	1	3.6	2
6	0.134211176704	3	0.15	0	16	-0.0316055879821	3	6	2
7	0.0112626704218	4	0	0	17	0.000233594806142	11	3.25	2
8	-0.0420533228842	4	0.20	0	18	0.0148287891978	1	3.5	3
9	0.0349008431982	4	0.35	0	19	-0.00928782884667	3	15	3
10	0.000164957183186	6	1.35	0	-	-	-	-	-

Table 11: N_k, i_k, j_k and l_k parameters used in Eq. 24, (Lemmon et al., 2000)

4.4.2 Verification of the equation of state

The validation of the equation of state for air can be made thanks to the data provided by the Nist or to the experimental measurements provided by Lemmon et al. (2000). These data being equally pertinent and since the equation of state used is considered by the Nist as the state-of-the-art, the experimental data are here used as reference for the different computations of the relative errors on the thermodynamic properties. A comparison between the experimental data provided by Lemmon et al. (2000) and those from the Nist was carried, but no significant difference had been noticed. The relative difference between these experimental data and those obtained with the equation of state is presented by

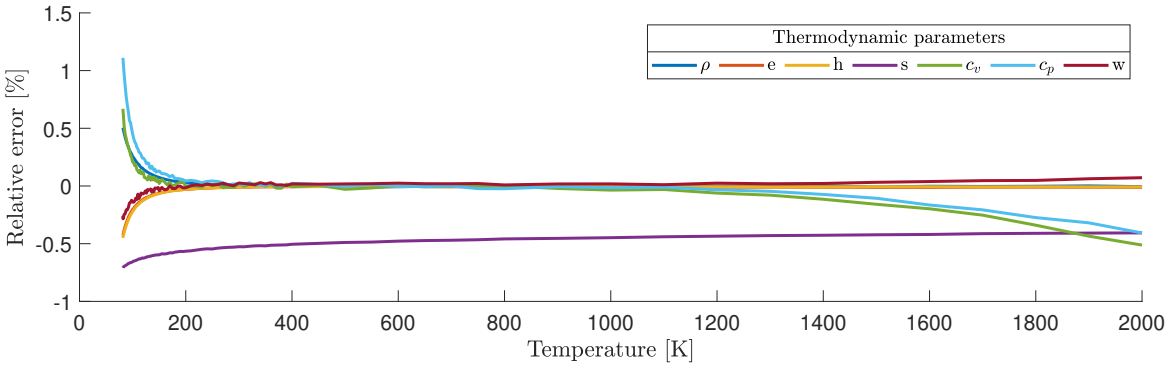

Figure 33: Relative difference between the thermodynamic data obtained by the equation of state for air and the experimental data provided by Lemmon et al. (2000), that are used as reference. The pressure is of 1 atmosphere

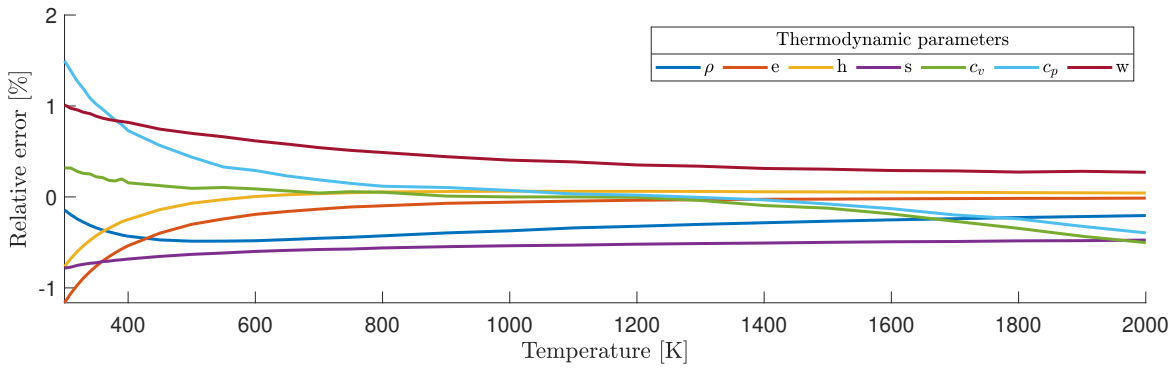

Figure 34: Relative difference between the thermodynamic data obtained by the equation of state for air and the experimental data provided by Lemmon et al. (2000), that are used as reference. The pressure is of 10 MPa

The relative errors due to the equation of state for air are low for most of the temperature range at a pressure of 1 atmosphere. At very low temperature, this equation of state provides data with a higher error than between 200 and 1200 K, where the approximation is very good. The entropy has however a constant error that could be linked to a small difference in the reference temperature. This error is however low enough and it can be considered that the approximation offered by the equation of state is accurate enough at low pressure. When the pressure is increased up to 10 MPa, the error on the different thermodynamic parameters increase on several of the properties. The error on the entropy is roughly unchanged, as well as those on the enthalpy and the heat constants. However, the errors on the density and the speed of sound are greatly affected by this increase of pressure. Moreover, under the temperature of 400K, the relative error on most of the parameters becomes very high, sometimes higher than 10% under 300K. Low temperature at high pressure being not likely in the Longshot wind tunnel, these errors should not be a problem.

Even if the relative error increases with the pressure, the equation of state for air proposed by Lemmon et al. (2000) can be considered as accurate enough for most of the temperature and pressure range. The equation of state for mixture discussed by § 4.5 will be compared to the equation of state proposed here.

4.5 Mixture equation

The composition of the gaseous planets presented in § 3 highlighted the need of a mixing equation to simulate their atmosphere. Indeed, as previously presented, the measurement of the aerodynamic coefficients is linked to the density ratio through shock, and then to the composition of the considered gas(es). The ratio of specific heat must be respected in order to obtain accurate measurements of the model drag coefficient. This section will first introduce the mixing rule selected here, as well as several others that could have been considered. The objective of the introduction of this mixture equation is then the simulation of mixture, such as those of the giant planet atmosphere, where the specific heat ratio is mostly influenced by the presence of hydrogen ($\gamma = 1.405$) and helium ($\gamma = 1.667$). The equation being dependent of empirical data that are not available at the present time for this mixture, the validation of the equation of state is made through the use of a well known mixture, air. A second mixture, composed of various concentrations of oxygen and nitrogen will also be compared to the reference Nist database.

4.5.1 Mixing rules

Several equations of state were developed to express the thermodynamic properties of several mixtures. De Hemptinne and Ledanois (2012) presents several possibilities, such as the modification of the use of "regular" higher order equation of state. It proposes to take advantage of the Van der Waals, the Soave-Redlich-Kwong or the Peng-Robinson equations of state. However, the expression of the different parameters used in these equations are modified to take into account the different coupling terms. These three equations are proposed by eq. 25, Eq. 26 and Eq. 27 respectively.

$$P = \frac{RT}{v-b} - \frac{a}{v^2} \tag{25}$$

$$P = \frac{RT}{v-b} - \frac{a_c\alpha(T)}{v(v+b)} \tag{26}$$

$$P = \frac{RT}{v-b} - \frac{a_c\alpha(T)}{v^2+2bv-b^2} \tag{27}$$

In these three equations, a is the cohesion function and b is the covolume parameter. The expression of the former depends on the model chosen for pure substances, while the latter can be declined into several approximations. They can take the simple form of a mean or a product, using the values of the pure substances. In a similar way, the a parameter of a mixture can be obtained as a function of the corresponding values of a pure substances. However, the combination of these cohesion functions depends on empirical measurements. Hudson and McCoubrey (1960), Coutinho et al. (2000) or Twu et al. (1994) presented different methods to simulate these empirical parameters. However, a better choice for the estimation of the empirical parameters could be the approximation proposed by Vitu et al. (2006), which has application in mixtures containing, among others, carbon dioxide or nitrogen. These elements being currently extensively used by the VKI Longshot, the approximation proposed by "PPR78" model could have been a reasonable choice for the present application. It can be noticed that most of these equations and mixtures models were developed for the fossil fuel industry and are then more accurate for these types of mixtures.

The mixture model presented here was introduced by Lemmon (1997), Lemmon et al. (2000) and Estela-Uribe (2006). However, the formulation of the second reference, judged more adapted to the current methodology of the L1d code, is the only one that is presented here. Moreover, this reference also provided the air equation of state discussed by § 4.4. The approach used by this formulation is based on the construction of the expression of the reduced Helmholtz energy by the use of a contribution of the ideal gas mixture, the residual gas mixture and the excess contribution, linked to the mixture interactions. Mathematically, the three contributions can be expressed as

$$\alpha_{mix} = \alpha^0 + \alpha^r + \alpha^E, \tag{28}$$

where the ideal gas contribution can be expressed by

$$\alpha^0 = \sum_{i=1}^{N} x_i \left(\alpha_i^0(\rho, T) + \ln x_i\right), \tag{29}$$

where x_i is the concentration (expressed in molar fraction) of the pure component i in the mixture of N components. Notice that this ideal contribution depends of the density and the temperature of the mixture. The critical temperature and pressure will then be different for each component of this final mixture. The two other terms do not consider the same approach and can be expressed by

$$\alpha^r = \sum_{i=1}^{N} x_i \alpha_i^r(\delta, \tau) \tag{30}$$

and

$$\alpha^E = \left(\sum_{i=1}^{N-1} \sum_{j=i+1}^{N} x_i x_j F_{ij}\right) \cdot \left(-0.00195245\delta^2\tau^{-1.4} + 0.00871334\delta^2\tau^{1.5}\right) \tag{31}$$

where Lemmon et al. (2000) reported that the exponents and coefficients were obtained from non linear regression of experimental mixture data. The reduce density and temperature used in Eq. 30 and Eq. 31 are the same for every gases. These two variables are computed as

$$\delta = \rho/\rho_{red} \qquad \tau = T_{red}/T$$

where

$$\rho_{red} = \left(\sum_{i=1}^{N} \frac{x_i}{\rho_{ci}} + \sum_{i=1}^{N-1} \sum_{j=i+1}^{N} x_i x_j \xi_{ij} \right)^{-1} \tag{32}$$

$$T_{red} = \sum_{i=1}^{N} x_i T_{ci} + \sum_{i=1}^{N-1} \sum_{j=i+1}^{N} x_i x_j \zeta_{ij} \tag{33}$$

The values of ζ_{ij} and ξ_{ij} are presented by Table 12, as well as the constant F_{ij} for the binary mixture that are nitrogen + oxygen, nitrogen + argon and oxygen + argon. These parameters were obtained through experiments and are not yet available for the mixture of hydrogen and helium or nitrogen and helium that is the main interest here. However, the ratio of specific heat of the noble gas being of approximately 1.67, a first guess could be the use of the coupling constant of the nitrogen/argon mixture for the nitrogen (or hydrogen)/helium mixture considered.

Mixture	F_{ij}	ζ_{ij} (K)	ξ_{ij} (dm^3/mol)
$N_2 + Ar$	1.121527	-1.237713	-7.6031·10^{-4}
$N_2 + O_2$	1	-0.856350	$-4.1847 \cdot 10^{-4}$
$O_2 + Ar$	0.597203	-2.115126	$4.1232 \cdot 10^{-4}$

Table 12: Parameters of the mixture model used in Eq. 31, Eq. 32 and Eq. 33, (Lemmon et al., 2000)

The composition of air was precisely proposed by several references. The composition that will be used here was proposed by Lemmon et al. (2000) to be a simple mixture of three components that are nitrogen, oxygen and argon. Table 13. Other elements, such carbon dioxide or trace elements will be neglected here. Indeed, the concentration of these elements in air is negligible compared to the one of the three main elements[8]

Component	Molar fraction
N_2	0.7812
O_2	0.2096
Ar	0.0092

Table 13: Composition of air used in the simple air reconstruction using the mixture equation, (Lemmon et al., 2000)

[8]Notice that the difference between the air composition of Table 1 and Table 13 can be explained by the fact that the trace elements are neglected. Table 13 can however be seen as a reasonable approximation

4.5.2 Validation of the mixing equation

There are several advantages of the mixture equation of state proposed by Lemmon et al. (2000). The first one is its Helmholtz energy form, already used by the von Karman Institute for several studies with nitrogen, carbon dioxide or helium. Then, the number of empirical data needed is lower than in the equations of state used by the petroleum industry. Moreover, the accuracy of the results depends on the accuracy of the different equations of state used for the pure gases involved. However, the accuracy of the equation of state have to be tested, due to the importance of the specific heat ratio in the simulation of reliable drag coefficients highlighted in § 3.3. Unfortunately, the empirical data needed for the computation of mixtures of hydrogen (or nitrogen) and helium are not available. The validation campaign of the mixing equation of state will then be made thanks to the simulation of the properties of air. This mixture is here simplified and uses the equation of state presented by Schmidt and Wagner (1985) for oxygen, Tegeler et al. (1999) for argon and Span et al. (2000) for nitrogen. These different equations of state were either presented in their dedicated section or are already used by the von Karman Institute. In the case of the nitrogen equation of state, the validation of its accuracy was already discussed and will not be exposed here.

The first gas tested with the mixture gas is then the simplified three components air with the compositions proposed by Table 13. The thermodynamic properties obtained thanks to the mixing equation of state is compared to those provided by the Nist, which serve as reference for the computation of the relative errors presented by Fig. 35 at a pressure of 0.1 MPa and by Fig. 36 when the pressure is increased up to 10 MPa.

The different thermodynamic properties obtained thanks to the mixture equation are close to the values provided by the Nist. Except for the c_p and c_v, these errors are lower than 1% for both pressures. A larger error can be noticed on the two heat capacities. Nevertheless, the specific heat ratio is well represented by the mixture equation. This equation of state can then be considered as accurate for this particular composition. It is however important to ensure that the results for different composition are also accurately computed by this mixing rule. A mixture composed of nitrogen and oxygen is then tested here. This new mixture has a molar fraction of oxygen and nitrogen different than in air. The composition uses a volume ratio of 50% oxygen and 50% nitrogen. The relative errors obtained with this gas at 0.1 and 10 MPa are both represented by Fig. 37 and Fig. 38. The second mixture tested is also composed of nitrogen and oxygen, but the molar ratio of oxygen is here elevated up to 75%. The relative errors on the thermodynamic properties of this mixture are presented by Fig. 39 and Fig. 40 at the same pressures than for the first mixture. In both cases, the references are the data provided by *miniREFPROP*, the Nist database.

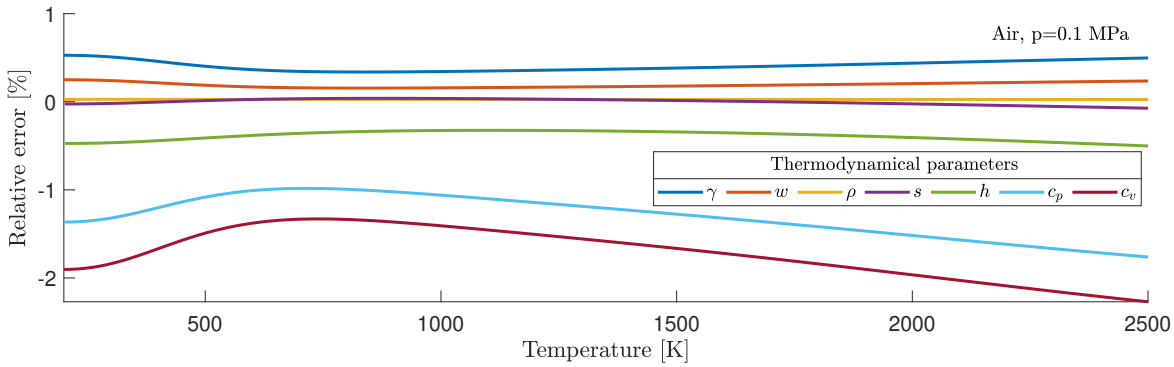

Figure 35: Relative errors on different thermodynamic parameters between the results obtained with the mixture equation of state and the data of the Nist, taken as references. The mixture considered is depicted by Table 13 and the pressure is 0.1 MPa

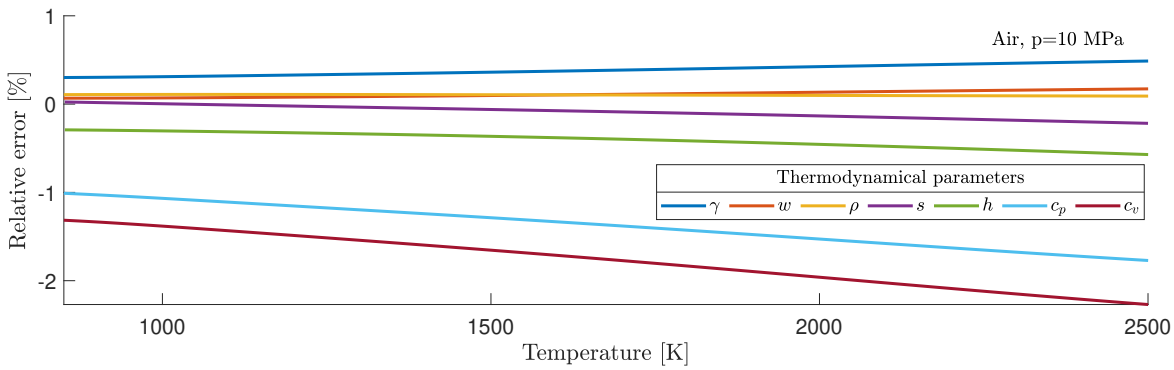

Figure 36: Relative errors on different thermodynamic parameters between the results obtained with the mixture equation of state and the data of the Nist, taken as references. The mixture considered is depicted by Table 13 and the pressure is 10 MPa

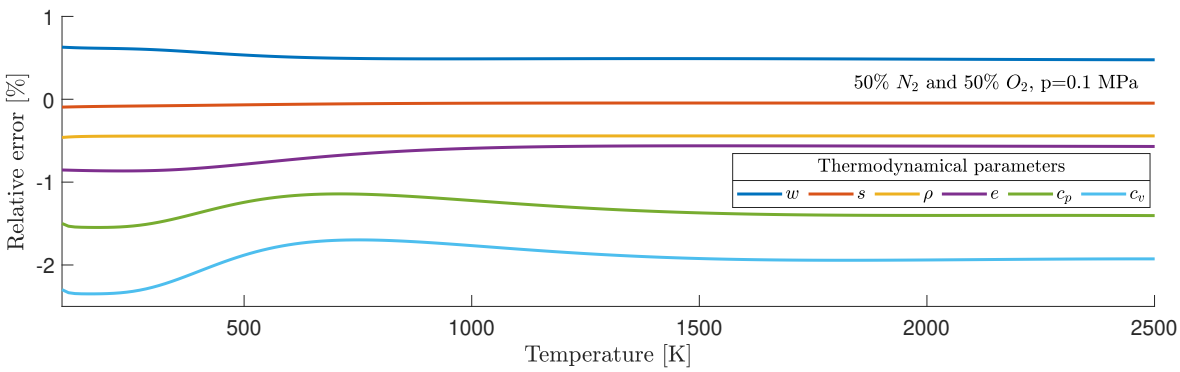

Figure 37: Relative errors on different thermodynamic parameters between the results obtained with the mixture equation of state and the data of the Nist taken as references. The mixture is composed of 50% oxygen and 50% nitrogen at a pressure of 0.1 MPa

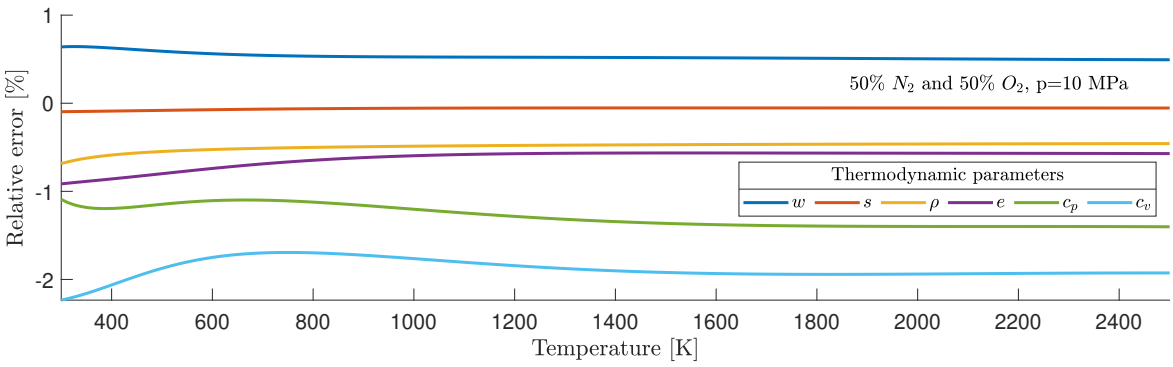

Figure 38: Relative errors on different thermodynamic parameters between the results obtained with the mixture equation of state and the data of the Nist taken as references. The mixture is composed of 50% oxygen and 50% nitrogen at a pressure of 10 MPa

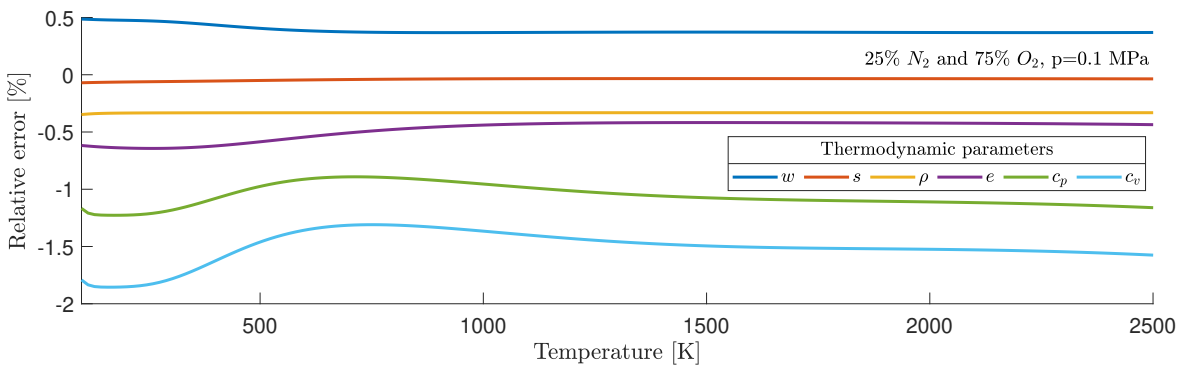

Figure 39: Relative errors on different thermodynamic parameters between the results obtained with the mixture equation of state and the data of the Nist taken as references. The mixture is composed of 75% oxygen and 25% nitrogen at a pressure of 0.1 MPa

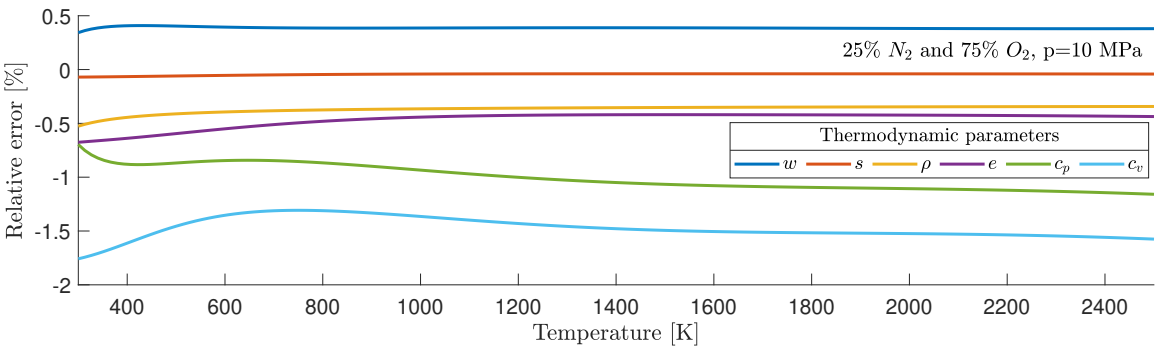

Figure 40: Relative errors on different thermodynamic parameters between the results obtained with the mixture equation of state and the data of the Nist taken as references. The mixture is composed of 75% oxygen and 25% nitrogen at a pressure of 10 MPa

The relative errors measured on the different thermodynamic parameters are lower than 1% for both pressure and composition, except for the two heat capacities that suffer of a higher relative error. This type of error is comparable to the one obtained when air was the gas tested. When the pressure is of 0.1 MPa, the lower temperature shown on these error graphs is 100 K, but is 250 K when the pressure is taken at 10 MPa. At this pressure, the relative error on the heat capacities below this temperature quickly increases. This equation of state should then not be used at very high density. It can be noticed that the relative error on the different parameters is lower in the case of mixtures that are not equal in molar ratio. This can be linked to the coupling terms that decrease the accuracy of the equation due to the low number of empirical parameters.

Thanks to the consideration of the different mixture that are air, 50% O_2 + 50% N_2 and 75% O_2 + 25% N_2, the accuracy of the mixing equation of state can be validated. While the errors on the two heat capacities are the highest, reaching about 2%, the errors made on the speed of sound, density, entropy, enthalpy and specific heat ratio are always lower than 1%. The error also increases when the volume ratio of the components of this binary mixture are close, mainly due to the coupling terms.

4.6 Other gases

Several other gases are used in different wind tunnels around the world. Methane served as test gas in the former French IUSTI TCM2 to simulate reentries on Titan. It is used by the Australian X2 super-orbital expansion tube in a mixture representing the atmosphere on Titan to investigate on the radiation during reentry on this satellite. Tetrafluoromethane (CF_4) is currently used by the German HTG HHG Ludwieg tube. This gas is not present in significant concentration in the different atmospheres of the different planets of the solar system, but it is used to take advantage of its low specific heat ratio to reach higher density ratio. The Russian TSAGI UT-1M uses freon as test gas to take advantage of the low specific heat ratio of the gas. However, this gas is forbidden in Belgium due to its environmental impact. Methane and CF_4 are introduced in this section for a possible application inside the Longshot wind tunnel.

4.6.1 Methane

Methane is presented in § 3 as the second most present gas in the atmosphere of Titan. An equation of state of the same Helmholtz energy formulation that the previous ones is proposed by Setzmann and Wagner (1991). The ideal gas part has the form

$$\alpha^0 = \ln\delta + a_1 + a_2 + a_3 \ln\tau + \sum_{i=4}^{8} a_i \ln\left(1 - e^{-\theta_i^c \tau}\right) \tag{34}$$

and the residual contribution is

$$\sum_{i=1}^{13} n_i \delta^{d_i} \tau^{t_i} + \sum_{i=14}^{36} n_i \delta^{d_i} \tau^{t_i} + \sum_{i=37}^{40} n_i \delta^{d_i} \tau^{t_i} e^{-\alpha_i(\delta-\Delta_i)^2-\beta_i(\tau-\gamma_i)^2}. \tag{35}$$

The different parameters used in these two equations are presented in Setzmann and Wagner (1991). It uses the critical temperature $T_c = 190.564$ K and the critical density $\delta_c = 162.66$ kg/m^3. The reference proposed this form of equation of state for a temperature up to 625 K and 1000 MPa. Fig. 41 presents the relative error on the different thermodynamic properties of methane. The reference used in these relative error computations are the data provided by the Nist. Unfortunately, above 914 K, the equation of state becomes useless due to the dissociation of the molecule.

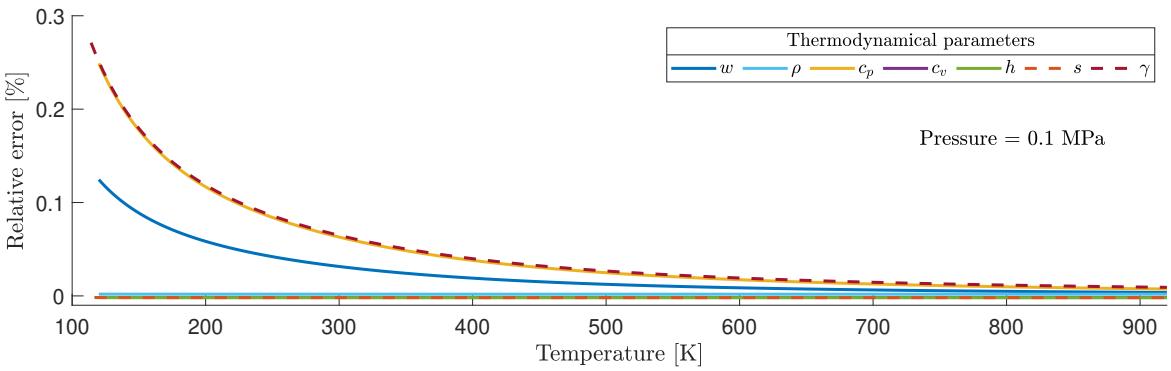

Figure 41: Relative error between the thermodynamic properties of methane computed with the equation of state and the data from the Nist, taken as reference

The errors on the different parameters shown in Fig. 41 are very low, especially when the temperature increases. The reference also ensures that the equation of state provide accurate data for higher pressure and in the superfluid area. Above the temperature of 500 K, the dissociation of the methane in molecular hydrogen and black carbon begins, (Gutsol et al., 2011) and (Weimer et al., 2001). This dissociation is shown in Fig. 42.

The first dissociation of methane at 500 K is followed by a second dissociation of the molecular hydrogen into atomic hydrogen. If this gas is selected for applications in the Longshot wind tunnel, the creation and dissociation of hydrogen should be kept under surveillance due to the different embrittlement problems discussed in § 4.1.4. Moreover, when the temperature increases above 2000 K, the formation of acetylene is noticeable. The French National Institute for Research and Safety (INRS) classes this compound as extremely inflammable and dangerous at high temperature. Most of the security concerns about this gas were given in § 4.1.4. In the case of the use of methane in the VKI Longshot, the effects of this gas would be higher than when hydrogen is considered, due to the presence of carbon in the mixture. The typical temperature and pressure reached in the reservoir being of 2600 K and 35 MPa, the detonation of this gas is unavoidable. Even if the mass fraction of this gas is reported

to be low at ambient pressure, the increase of the latter should lead to a higher amount of acetylene in the reservoir than presented in Fig. 42. The detonation of this gas could exceed the structural limits of the reservoir, damaging it, and propagate the deflagration into the test section.

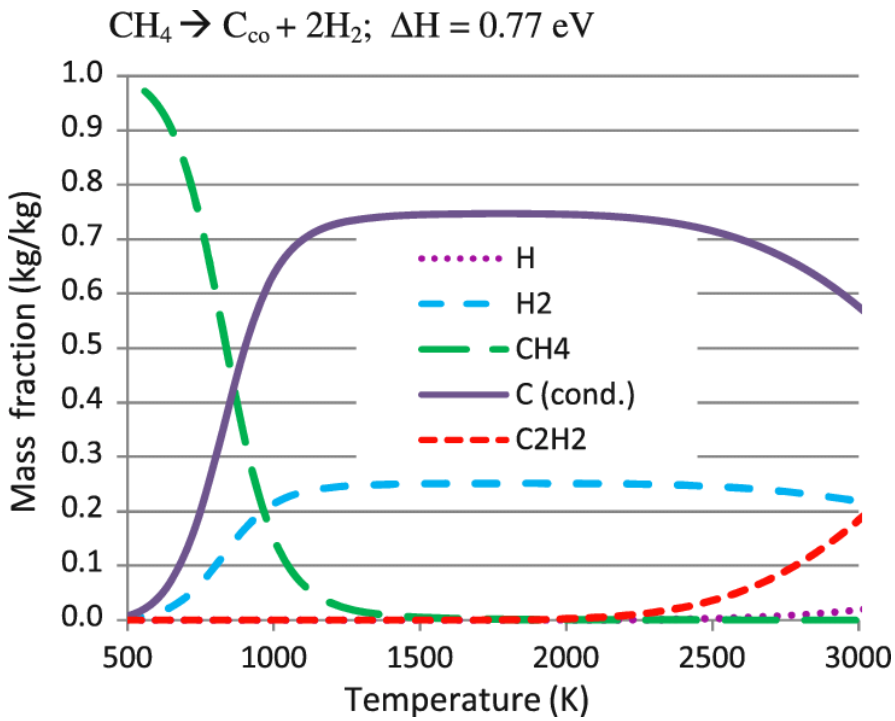

Figure 42: Mass fraction of the compound of methane after dissociation at temperature up to 3000 K at ambiant pressure, (Gutsol et al., 2011)

4.6.2 Tetrafluoromethane

The tetrafluoromethane (CF_4) is mainly used because of its low specific heat ratio. Bertin et al. (1992) presents this application in the Langley 20-inch Mach 6 CF4 tunnel at a maximal temperature of 850 K and 17.24 MPa. With these conditions, a density ratio of 12 had been reached, which is the double of the one reached using air or nitrogen. The theoretical limit of the density ratio that can be obtained using this gas is 18. However the Mach number independence principle presented in § 3.3 and Fig. 15 is not reached until a high Mach number. Indeed, this independence principle can be considered with an error lower than 1% when $M \geq 41$. This type of value is currently impossible to reach with the Longshot wind tunnel. However, the density ratio reached at Mach 14 is 16.28, and can be increased up to 16.96 if the mach number is 20. These conditions could be interesting for the VKI, since the maximum density ratio during the reentry of vehicles such as the Aeroassist Flight Experiment (AFE) is 18, according to Bertin et al. (1992). Hunt and Jones (1969) exposes that the density ratio during reentry can even reach 20 due to the real gas effects and the chemical dissociation after the shock. However, due to environmental hazard of this gas, its use could be restricted

in Belgium. Indeed, the IPCC classify the green house effect of this gas as 6500 times higher than carbon dioxide.

No equation of state in the form of the Helmholtz energy had been found for this gas. However, if the use of this gas is validated by the von Karman Institute, the expression could be obtained by using the equation for pressure proposed by Hunt and Jones (1969), which is expressed by

$$\begin{aligned} p =& \frac{RT}{V-b} + \frac{A_2 + B_2T + C_2e^{-KT}}{(V-b)^2} + \frac{A_3 + B_3T + C_3e^{-KT}}{(V-b)^3} + \frac{A_4 + B_4T}{(V-b)^4} \\ &+ \frac{A_5 + B_5T + C_5e^{-KT}}{(V-b)^5} + (A_6 + B_6T)\, e^{\alpha V} \end{aligned} \tag{36}$$

and the expression of the constant volume heat capacity

$$c_v = a_4 + b_4T + c_4T^2 + d_4T^3 - JTK^2e^{-KT}\frac{c_2}{v-b} + \frac{c_3}{2(v-b)^2} + \frac{c_5}{4(v-b)^4}. \tag{37}$$

The different values of the parameters used in Eq. 36 and Eq. 37 are available in Hunt and Jones (1969) for a temperature range from 100 K to 1390 K. A second version of the expression of c_v is proposed by Hwang and Martin (1964), but for a smaller temperature range (140 to 620 K), as

$$c_v = 0.00375 + 102.9T^{-2} + 5.7887 \cdot 10^{-4}T - 3.7829 \cdot 10^{-7}T^2 \tag{38}$$

Notice that these coefficients are proposed for a heat capacity expressed in *cal/kg/K*.

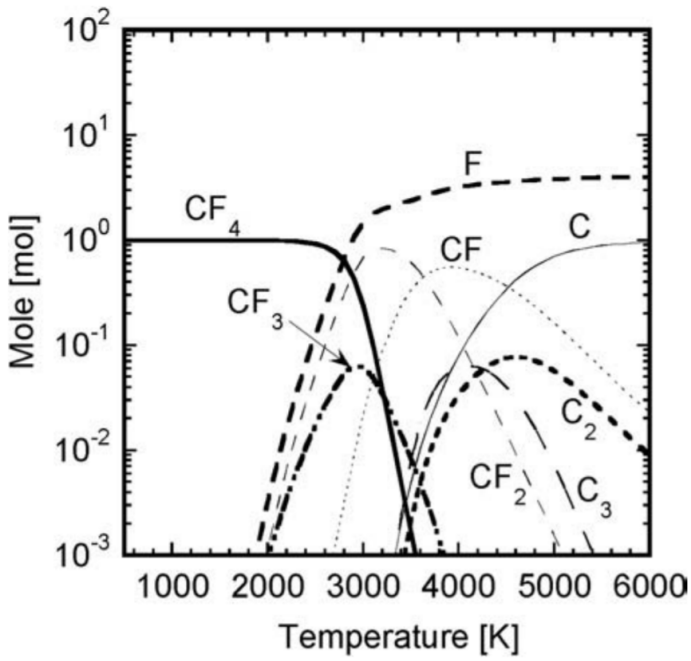

Figure 43: Dissociation of CF_4 at ambient pressure, (Saito et al., 2009)

The dissociation of CF_4 was studied by Saito et al. (2009) and is presented by Fig. 43 at a pressure of 1 atmosphere. This dissociation is very low under the temperature of 2400 K, which tends to enable its use inside the VKI Longshot. The health hazard of this gas is low. The safety data sheet P-4665 provided by *Praxair* shows that this gas has no explosive or flammability characteristics and is only considered as an asphyxiant gas. Moreover, the contact with this gas is not harmful to the skin. However, in case of contact with the eyes, they must be washed with water during 15 minutes minimum and medical attention should be provided as soon as possible.

4.7 Summary

The general form of the equations of state using the Helmholtz energy formulation had been introduced. It consists of the sum of a real gas contribution and the addition of a residue that models the real gas effects. Thanks to this type of equation, the different thermodynamic parameters can be retrieved. This methodology was then first applied to Hydrogen, oxygen, argon, air and methane. In all the case, the resulting thermodynamic properties were compared to reference values coming from the Nist or experimental data. It was concluded that these equations of state offer a interesting level of accuracy in most of the temperature and pressure range. A special attention should however be given in the high pressure and low temperature conditions, where the accuracy of the results decreases rapidly. A first proposition of the use of tetrafluoromethane was also given, but no Helmholtz equation of state formulation had been found. This gas could however be interesting due to its possibilities of measuring higher density ratio than those obtained with more conventional gases.

Several safety warning were given concerning the possible use of hydrogen for experimental purposes in the Longshot wind tunnel. This gas is not consider as more dangerous than any other fuel. It is consider as a simple asphyxiant, but its higher safety risks comes from its possibility of ignition or detonation. This gas has indeed large flammability and detonation ranges in air. If the auto-ignition of the air hydrogen mixture is high, its ignition energy is lower than the energy delivered by an electrostatic spark. Moreover, a moderate and high temperature, several embrittlement process occurs when hydrogen is used with certain types of steels. Another safety hazard that was highlighted was the possible production of acetylene, a violent explosive. However, this risk is limited but could be significant when using methane as test gas.

An equation of state based on the Helmholtz energy was also proposed for mixtures of gases. The different thermodynamic properties obtained using this mixture equation were compared to the reference data proposed by the Nist for the well known mixture that is air. A binary mixture of oxygen and nitrogen was also tested with different molar concentrations, in order to validate the approach of this equation. It appeared that the error obtained with this mixture equation is lower than 1% for most of the thermodynamic parameters. However, this error is higher for the two heat capacities, which are between 1 and 2.5%. The

error was also found lower when the concentration in a component is higher than the other. Nevertheless, the increase of the error when the molar concentrations are equivalent is low. The mixture equation presented here uses several empirical parameters. These parameters should be measured during a series of tests if the gases used in the simulated mixture are not oxygen, nitrogen or argon.

5 On the use of the Lagrangian 1d program

The phenomena inside the Longshot are modelled by a Lagrangian quasi one dimensional code. This section aims to introduce this code, initially developed by the Queensland University. The computations are also checked as a function of the number of cells in a grid convergence study. The latter is mainly focused on the maximum pressure and temperature encountered in the reservoir, as well as the maximum position and velocity of the piston. The behaviour of the hydrogen during a simulation in this code is then obtained using several approximations on the nature of the gas. The perfect gas law is the first approximation proposed for the simulation of the behaviour of this gas. The results obtained are then compared to those computed with the more advance equation of state. In both case the gas is tested in inviscid and viscous conditions. The results obtained by considering the equation of state proposed by Leachman et al. (2009) in viscous case are then compared to those simulated with nitrogen as test gas, using the same initial conditions. A sensitivity analysis is finally presented.

5.1 Introduction to the Lagrangian 1d code

Over the years, the compression process of the VKI Longshot had been improved, starting from the method of characteristics to Lagrange-Euler solvers by way of analytical solution. The method of characteristics, initially used by Vasiliu and Humphrey, and described by Grossir and Ilich (2018), was the first method used to analyse the Longshot compression process. An unsteady, one dimensional, inviscid and ideal flow was then assumed. The complex flow inside the valves was assumed to be quasi-steady and a correction for chambrage was applied. The results of this method gave a first coarse approximation of the experimental data, mainly due to the inviscid assumption and the negligence of the real gas effects.

An analytical approach was developed at the von Karman Institute to enhance the accuracy and the quality of the simulations. The motion of the piston and the final conditions are based on the second law of Newton and the theoretical expression of the pressure in front and behind the piston. The real gas effects are here considered thanks to the use of variable specific heats and Van der Waals equations of state. The three main assumptions are a negligible bore friction (between the piston and the bore of the driven tube), negligible losses in the check valves and an isentropic real-gas compression process after the first shock reflection. Moreover, a chambrage correction has to be applied on the piston velocity. More elaborate equations of state were also implemented to increase the accuracy of the numerical approximation. This method was concluded to be in good accord with the experimental results, (Grossir and Ilich, 2018).

The currently method used to model the compression process in the Longshot was created and presented by Jacobs (1994). It is described by Grossir and Ilich (2018) as a "*numerical approach based on a quasi-one-dimensional Lagrangian description of the gas dynamics coupled with engineering correlations for viscous effects and point-mass dynamics for piston motion*". One advantage of this Lagrangian-Eulerian solver is that the chambrage correction factor has no longer to be applied, as the variation of the cross section is directly taken into account. Two geometries are currently used in the L1d codes to model the VKI Longshot:

- The first one consider a simplified geometry, where the complex set of check valves is neglected. The geometry, called "E" is used to perform the initial computations, i.e. to select the appropriate physical models (equation of state, viscous effect,...) that will describe the compression process before reaching the valves.
- The second geometry, called "F" takes the valves system into account. These valves are represented by tubes with cross sections and volumes equivalent to the real assembly. This approximation is only used once the physical process is validated thanks to the simulations run on the geometry E.

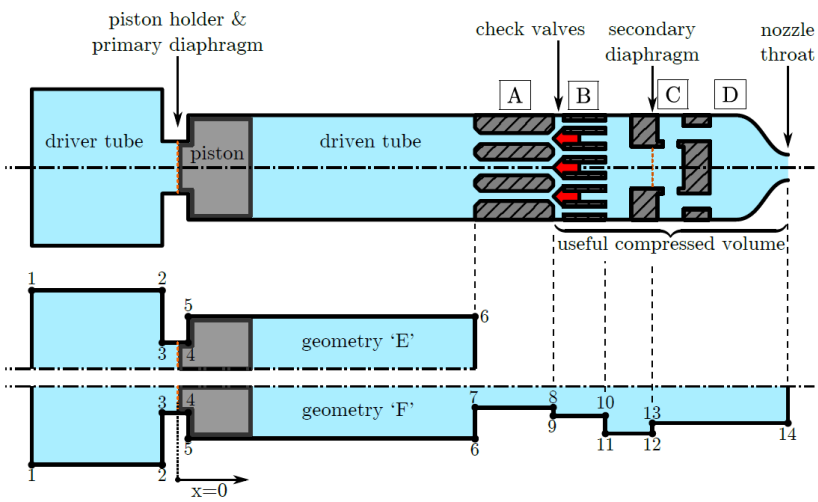

Figure 44: Real (on the top) and simplified geometry "E" and "F" of the Longshot used in the L1d, (Grossir and Ilich, 2018)

Different levels of approximation are offered by the L1d program. Indeed, the operator has the possibility of selecting the gas considered in the driver and the driven tube, the equation of state used to describe the behaviour of these gases and to take into account or not the viscosity of these gases. The driver gas is currently always chosen to be nitrogen, while the gas in the driven tube can be selected more freely. The two gases that are currently used are the nitrogen and the carbon dioxide. Helium was also considered and used for a series of tests.

The typical output graph that can be obtained with the quasi 1d Lagrangian code depicts the position of the piston, the pressure and the shock wave. Examples of such graphs are presented by Fig. 45 for nitrogen and carbon dioxide. These graphs present several "events", such as the passage of the shock wave, its reflection or the passage of the piston. Other output can be obtained at different positions that represent the location of the pressure tabs inside the wind tunnel. Six of these discrete positions are inside the driver tube, while nine more are inside the driven tube. The last position in the driven tube, named hx15, represents the conditions in the reservoir. The maximum temperature and pressure encountered in the system are expected to be found there during the simulation. These pressure tabs are also used to notice the passage of the shock wave and the piston. Other tabs are available when the geometry F is used.

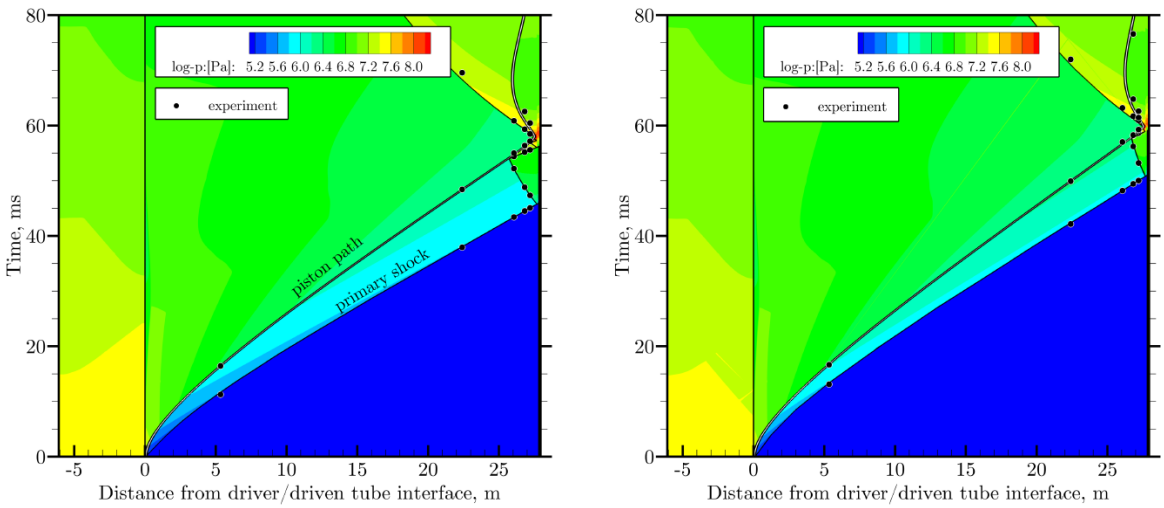

Figure 45: Space-time diagram, obtained with L1d code and experimental data for nitrogen (left) and carbon dioxide (right), (Ilich et al., 2019)

Before the test, the experimental initial temperatures in both the driver and the driven tube are measured by K thermocouple (Chromel-Alumel), while the initial pressures are obtained thanks to several gauges. When the test begins, 8 ports of instrumentation measure the pressure along the driven tube. The instruments used here are a set of different Kistler piezoelectric pressure transducer. More information about the measurement techniques used inside the Longshot are reported by Ilich (July 2017). Characteristic events are detected by these pressure sensors and are presented in Fig. 45 by the series of discrete points. The motion of the piston and the primary shock are well represented by the numerical simulation. However, the accuracy of the numerical simulation decreases after the rebound of the piston. The approach presented by the 1d Lagrangian code seems then to be justified.

The integration scheme of the Lagrangian 1 dimensional code can be selected by the operator. Indeed, the order of integration of both the space and time discretisation can be chosen. In the frame of this work, both integration orders were set to 2. The operator can select

the number of cells in front and behind the piston. This selection, linked to the convergence study, is discussed in the following section. The time step cannot be modified directly by the operator. The selection of the appropriate time step is done automatically by the program to respect to maximum value of the Courant Friedrichs Lewy (CFL) number chosen by the operator. This adimentional number had to be small enough to comply with the rupture of the diaphragm and was then set to 0.25.

5.2 Convergence study

In order to ensure a satisfactory level of accuracy when a discretisation process is involved, a convergence study is necessary and is the subject of this section.

The L1d program described above was first used considering the geometry E, the perfect gas equation and carbon dioxide as test gas inside the driven tube. This choice was made in order to speed up the computation process by neglecting either the complex valve system, the real gas phenomena and the viscous effects. These contributions are obviously taken into account in the more advanced studies that will follow further in this report. Both the spatial discretisation and the time step between two measurements were investigated. The L1d program allows the user to choose the number of cells behind and in front of the piston. This number was set to 2000 cells behind this piston and was not increased or investigated further, since this region is not critical and the gas conditions are not submitted to changes of the same magnitude than in front of the piston. This second region was then submitted to a higher level of attention. The output are saved every 0.1 ms during most of the simulation and every 10 ns when the piston is close to the reservoir.

The convergence study applied on the region in front of the piston is focused on the four parameters that are the pressure and the temperature at the position hx15 as well as the position and the velocity of the piston across time. The criterion selected to consider that the different parameters have converged are a relative difference smaller than 0.2%. These relative errors are computed using the simulation with the highest number of cells as reference. In this case, the simulation using 4500 cells is considered as the reference.

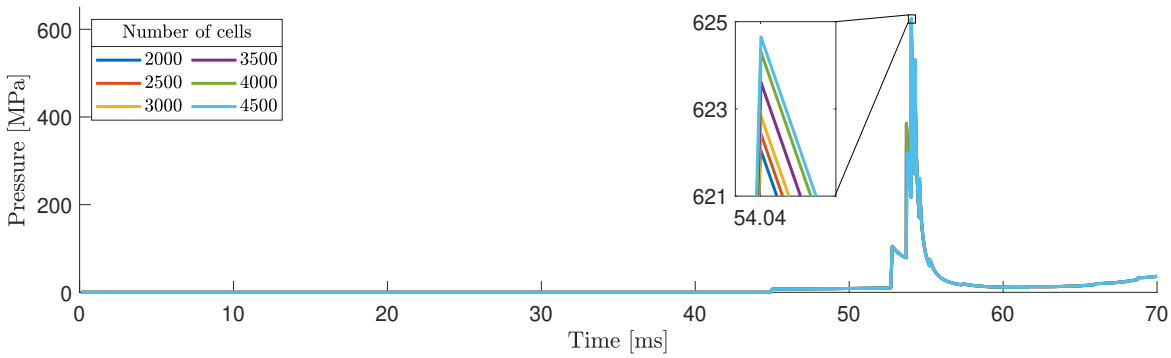

Figure 46: Evolution of the pressure measured at the hx15 station using several number of cells in front of the piston and 2000 cells behind the piston

Fig. 46 and Fig. 47 present the evolution of the pressure and temperature at position hx15 using different number of cells. The first figure shows that the maximum pressure increases with the number of cells. This increase is however small, especially between the three higher cells numbers. The effect of the increase of the number of cells on the maximum temperature is more chaotic, since the increase of the number of cells does not lead to a convergence in the final value. The variation of temperature is nevertheless low, of the order of 5 K. Fig. 48 presents the relative difference obtained by varying the number of cells and using the case of 4500 cells as reference. This graph shows that the maximum values of the position and the velocity are quickly obtained and the convergence on these two values is then validated. The relative error on the pressure decreases to a converged value. This error is lower than 0.2% when the number of cells reaches 3500. The maximum temperature fluctuates around a specific value, the relative error is then impacted by this behaviour. However, the relative error on this parameter remains low. Due to the high computation time that a higher number of cells would require and low relative error already obtained with the number of cells already computed, no additional tests were run with a finer space discretisation.

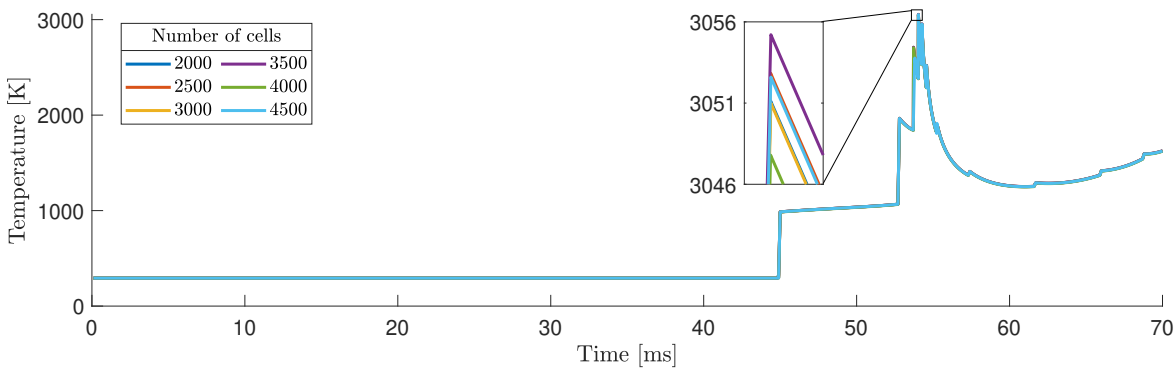

Figure 47: Evolution of the temperature measured at the hx15 station using several number of cells in front of the piston and 2000 cells behind the piston

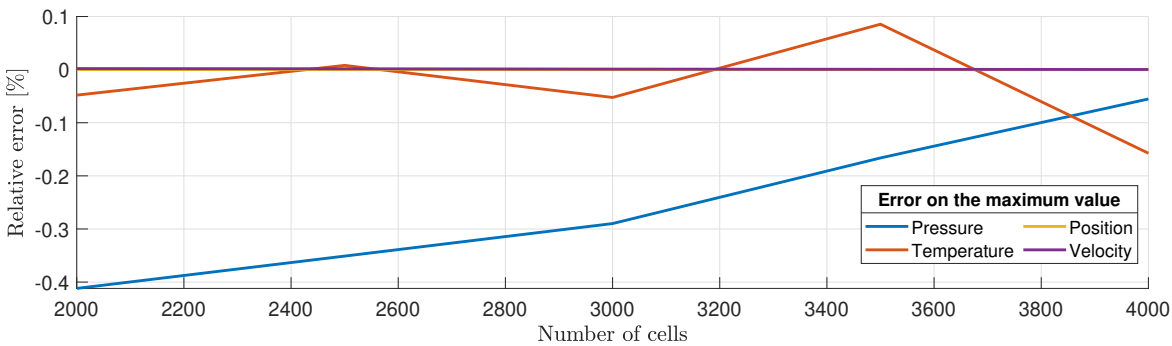

Figure 48: Relative errors on the maximal values of the temperature and pressure measured at the hx15 position, as well as the maximum velocity and position reached by the piston. The references are the results obtained when using 4500 cells

The difference of pressure, temperature, position and velocity used in Fig. 48 are presented by Table. 14. Both the relative and absolute errors, computed using the data obtained with 4500 cells as reference, are presented in this table. For the following computations, the number of cells used is set to 3500, since the convergence criterion is fulfilled with this amount of cells and the absolute error on the temperature is low. This convergence study was quickly performed on the different tests run using hydrogen as test gas in order to validate the results obtained.

Number of cells		2000	2500	3000	3500	4000
Pressure	Absolute [MPa]	-2.573	-2.1929	-1.8104	-1.0386	-0.3451
	Relative [%]	-0.4119	-0.3511	-0.2898	-0.1663	-0.0552
Temperature	Absolute [K]	-1.466	0.244	-1.599	2.611	-4.804
	Relative [%]	-0.048	0.008	-0.0524	0.0855	-0.1574
Position	Absolute [m]	$2 \cdot 10^{-5}$	10^{-5}	0	0	0
	Relative [%]	$7.27 \cdot 10^{-5}$	$3.63 \cdot 10^{-5}$	0	0	0
Velocity	Absolute [m/s]	0.0126	0.0104	0.0064	0.004	0.0016
	Relative [%]	0.002	0.0016	0.001	0.0006	0.0003

Table 14: Comparison of the relative and absolute error made on the maximum values of different parameters by using 2000, 2500, 3000 or 3500 cells with comparison to the results obtained with 4500 cells

5.3 Introduction of the hydrogen

The Lagrangian one dimensional code offers the operator the opportunity of selecting the gas and the initial conditions in both tubes, as well as the mass of the piston. This section presents the effects of different approximations on the nature of the gases considered and presents the type of results that can be offered for hydrogen. A sensitivity analysis is also proposed.

5.3.1 Approximations on the gases used

The introduction of hydrogen inside the VKI Longshot could offer the opportunity to simulate the environment of the Gaseous and Icy Giants with the gas that composes the majority of their atmospheres. A first approximation of this environment can be offered by the use of the perfect gas law to simulate hydrogen. This case was investigated both in the inviscid and viscous case. The same computation was performed using the real gas equations presented in § 4.1. The initial conditions used for these simulations are presented in Table 15.

	Driver tube	Driven tube
Gas	Nitrogen	Hydrogen
Initial pressure [MPa]	34.5	0.1441
Initial temperature [K]	300	293
Number of cells	2000	3500
Mass of the piston [kg]	1.59	

Table 15: Initial conditions in the driver and driven tube used for the different simulations with hydrogen

The position of the piston across time and the measurement of the pressure at the position hx15, i.e. inside the reservoir, are presented respectively by Fig. 49 and Fig. 50 for the different approximations made on the gases involved. Notice that the driver gas is considered inviscid when the hydrogen of the driven gas is submitted to the same assumption.

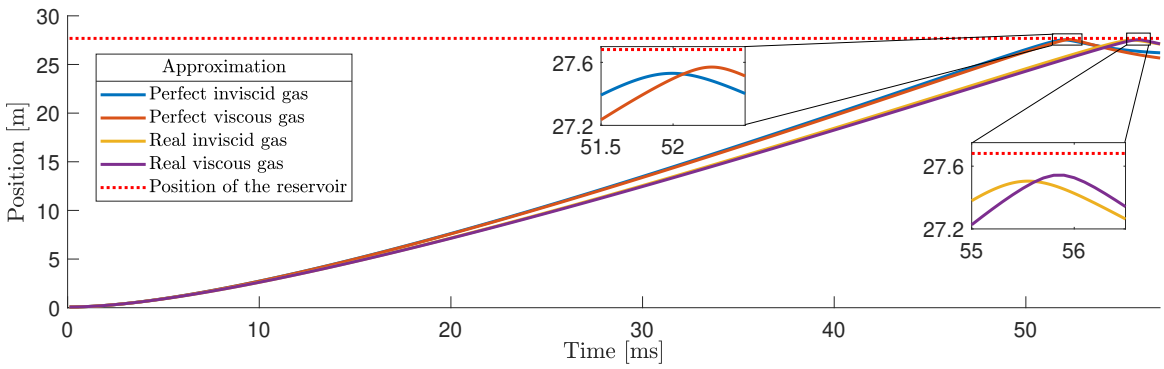

Figure 49: Position of the piston across time for different approximations on the test gas using 3500 cells in the driven section, 2000 in the driver section and the initial conditions presented in Table 15

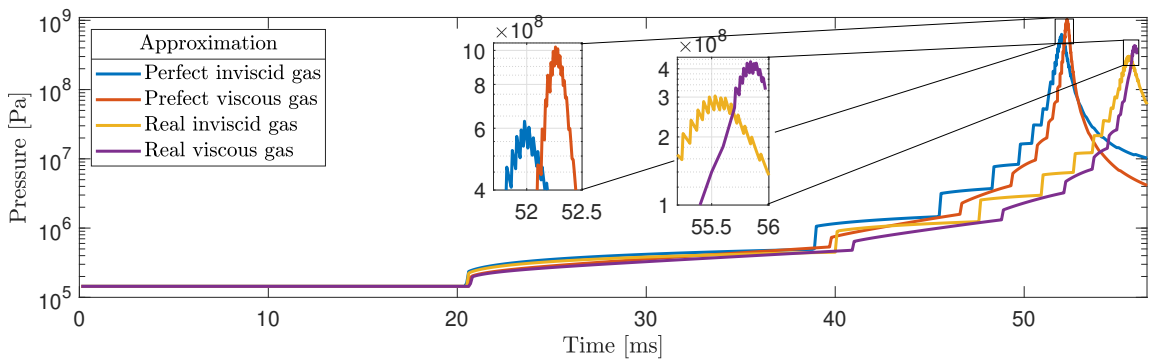

Figure 50: Pressure in the reservoir (position hx15) across time for different approximations on the test gas using 3500 cells in the driven section, 2000 in the driver section and the initial conditions presented in Table 15

Approximation		Inviscid perfect gas	Viscous perfect gas	Inviscid real gas	Viscous real gas
Pressure	Value [MPa]	628.246	1022.754	303.58	430
	Relative difference [%]	-46.08	-137.8	29.4	-
Temperature	Value [K]	3451.5	3894.4	2581.7	2619.29
	Relative difference [%]	-31.77	-48.68	1.43	-
Position	Value [m]	27.53	27.57	27.5	27.54
	Relative difference [%]	0.043	-0.1	0.14	-

Table 16: Maximum pressure, temperature and position obtained with the different approximations on the driver and driven gases

The behaviour of the curves presented by Fig. 49 and Fig. 50 shows similar qualitative behaviours, offering the same number of shocks and similar increase of the pressure. However, these similarities vanish when the maximum values of the pressure and temperature are compared. Indeed, Table 16 shows these maximum values and the relative difference between these maximum values and those obtained by considering the gases as real and viscous. The difference is very large, particularly for the maximum pressure. The perfect gas equation overestimates both the pressure and the temperature in the reservoir. This leads to an overestimation of the maximum deceleration, which reaches $2.88 \cdot 10^6$ m/s^2 in the viscous perfect gas case and about $1.82 \cdot 10^6$ m/s^2 for the real viscous case. The maximum acceleration of the piston is however very close in all cases. This maximum acceleration is logically observed at the beginning of the simulation, when the piston is released after the rupture of the first diaphragm. At this moment, the acceleration reaches $9.49 \cdot 10^4$ m/s^2. The high difference between the results obtained with the perfect gas equation of state and the one presented by (Leachman et al., 2009) highlight the inadequacy of the use of the simple perfect gas law for this application.

5.3.2 Results and discussions

The conditions in the reservoir are not those met in the test section. Nevertheless, computing then is reported by (Ilich, July 2017) as a way to ensure the repeatability of the tests, to validate the equations of state and the numerical simulation used, and to ensure that the structural limits of the reservoir are not reached during the test. Since the simulations presented here use the initial conditions usually considered for simulations of nitrogen, a comparison between the results of the simulation using hydrogen and the simulation using nitrogen is made. In both cases, the initial conditions are the same and were depicted by Table 15.

Several pressure tabs are placed in the driver and in the driven tube. (Ilich, July 2017) reported their positions, which are exposed in Table 17 and depicted in Fig. 51. These stations are usually used for the measurement of the pressure as well as the passage of the shock wave

and the piston. These data are then compared with those obtained during the experiment in order to validate the simulation.

Station	Distance from the 1st diaphragm [m]
hx7	5.3363
hx8	9.6035
hx9	13.8707
hx10	18.1379
hx11	22.4051
hx12	26.0627
hx13	26.8247
hx14	27.2057
hx15	27.6762

Table 17: Position of the different measurement positions in the driven tube, (Ilich, July 2017)

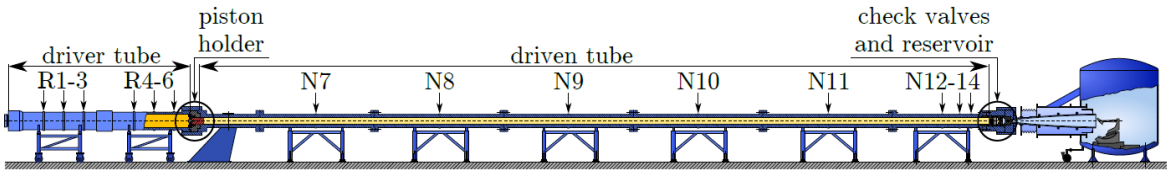

Figure 51: Available measurement positions in the driver and in the driven tubes

The different pressure measured at the different stations are shown in Fig. 52 to Fig. 60. These figures presents the pressure when hydrogen or nitrogen are used as test gas, but they also shows the passage of the shock wave (when there is a sudden elevation of the pressure), the passage of the piston (when the pressure drops to 0) and, in Fig. 59, the rebound of the piston. Due to the higher speed of sound in hydrogen, the shock propagates faster in this medium than in nitrogen. This leads to a higher number of reflections. Indeed, taking the case of the position hx14, depicted by Fig. 59, at least 12 passages of the shock are measured by the station when hydrogen is the driven gas, while only 3 are obtained for nitrogen. The compression due to these shocks is however smaller in the case of hydrogen. This combination of faster shock resulting in smaller compression of the driven gas leads to a situation where the pressure in front of the piston is higher in the case of the hydrogen than in the case of nitrogen. This situation remains true until the first passage of the shock in nitrogen. At this moment, the pressure is higher in the case of nitrogen. The successive shock passages in the hydrogen will then increase the pressure to a higher level than in nitrogen. Behind the piston, the pressure is higher when nitrogen is used. The acceleration of the piston, and then its velocity, are linked to the pressure in front of and behind the piston. This velocity profile is depicted by Fig. 61. During the first 10 ms, the velocities in both gas are very similar. Then, due to the higher pressure difference on either side of the piston when the driven gas is hydrogen, the velocity of the piston becomes higher for hydrogen. The maximum velocity, as well as the maximum pressure and temperature, and the critical accelerations reached during

the simulations in both gases are presented by Table. 18. This higher velocity leads to the maximum position of the piston to be reached sooner than when hydrogen is used. However, both the positions and the velocities proposed for the two gases by Fig. 61 and Fig. 62 are similar for the two gases.

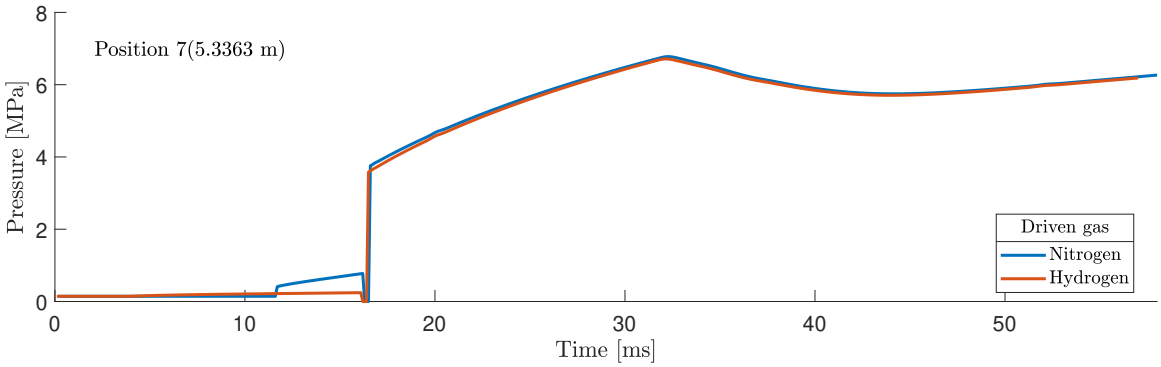

Figure 52: Pressure measured at the position hx7

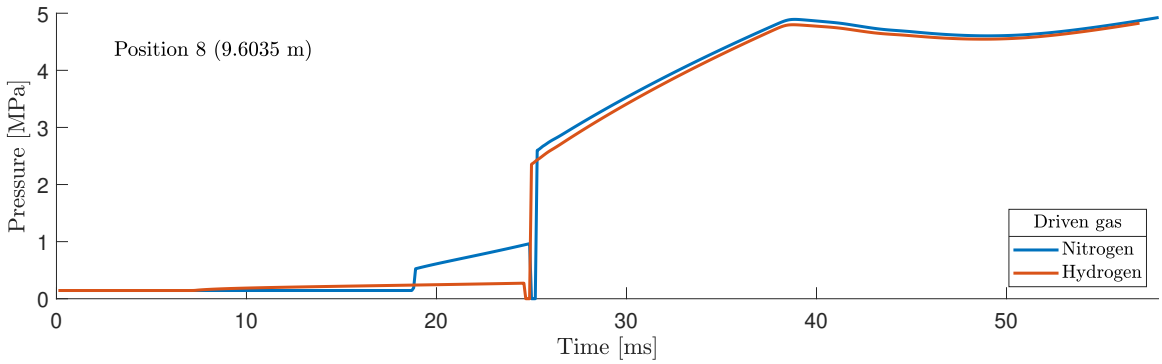

Figure 53: Pressure measured at the position hx8

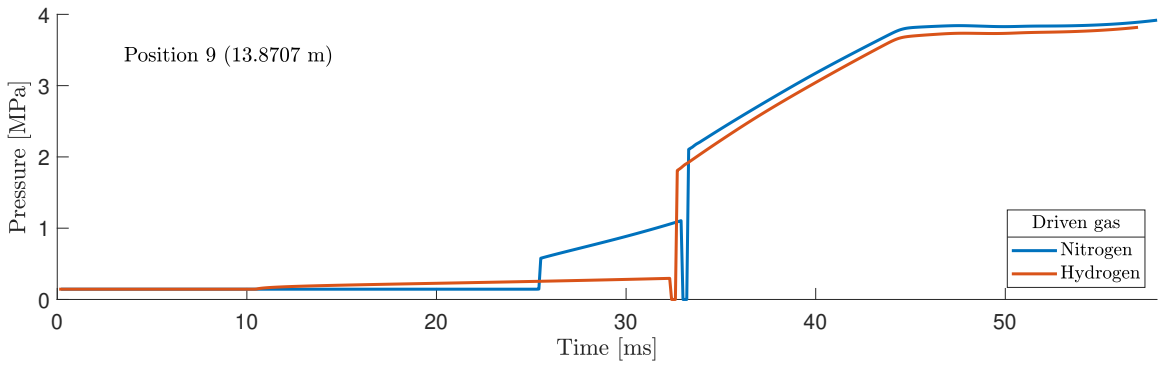

Figure 54: Pressure measured at the position hx9

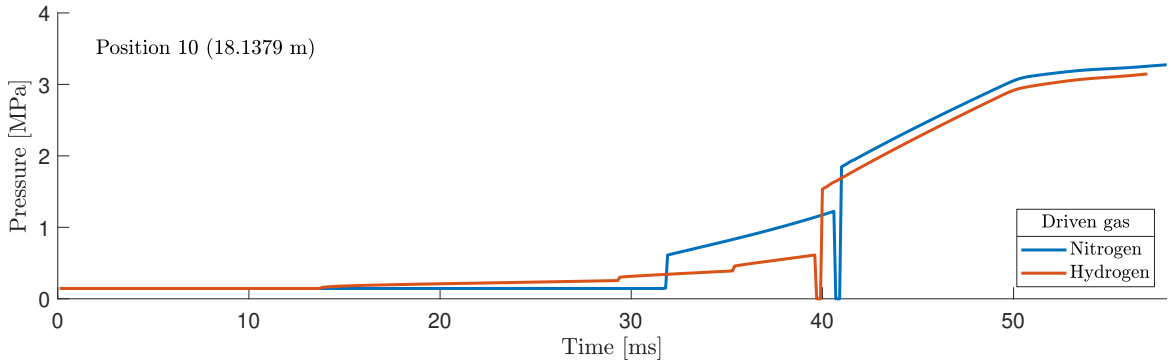

Figure 55: Pressure measured at the position hx10

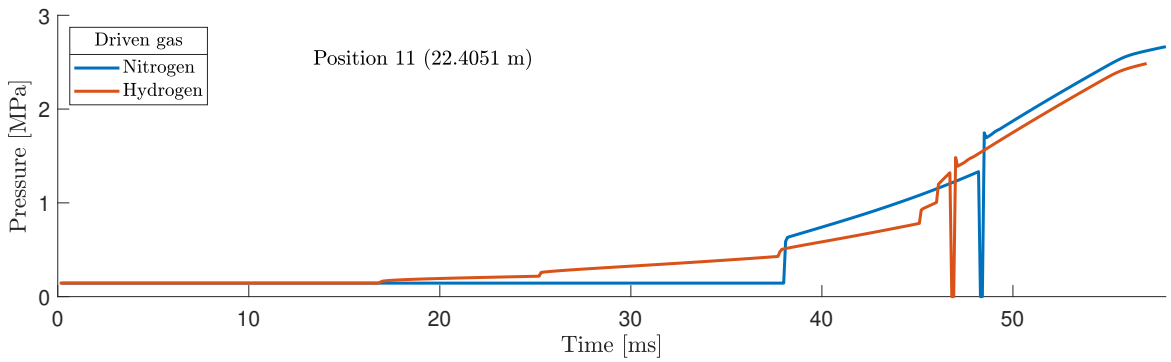

Figure 56: Pressure measured at the position hx11

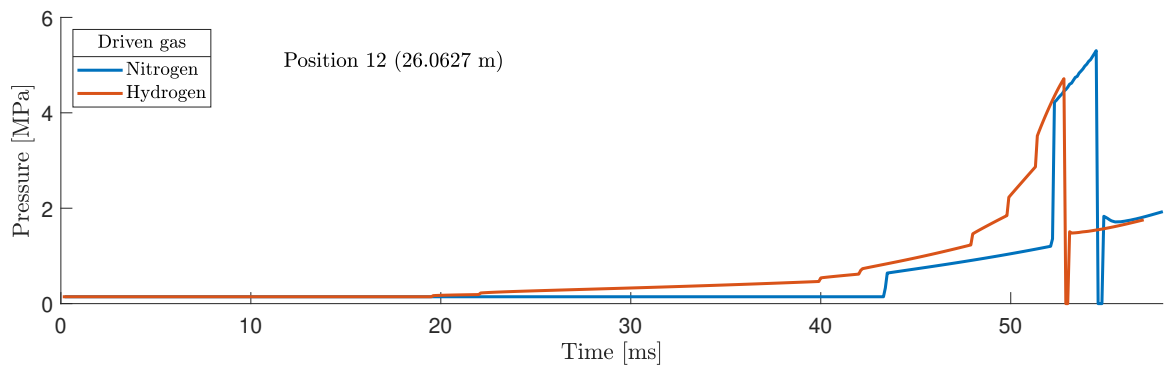

Figure 57: Pressure measured at the position hx12

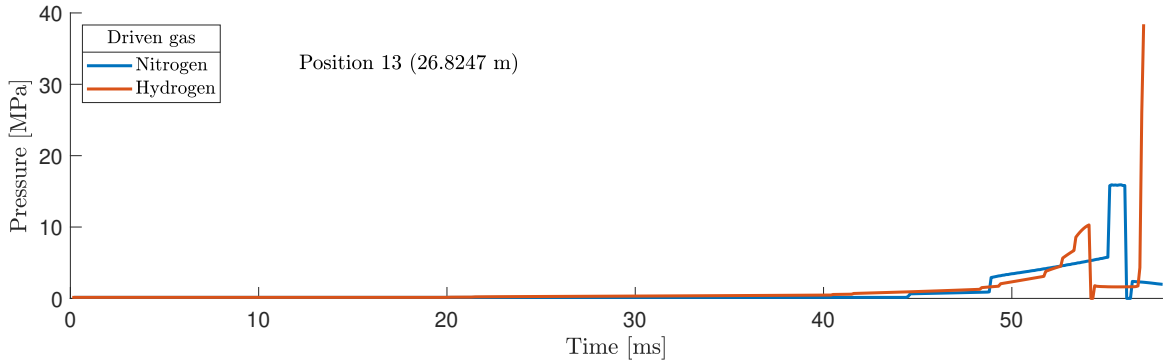

Figure 58: Pressure measured at the position hx13

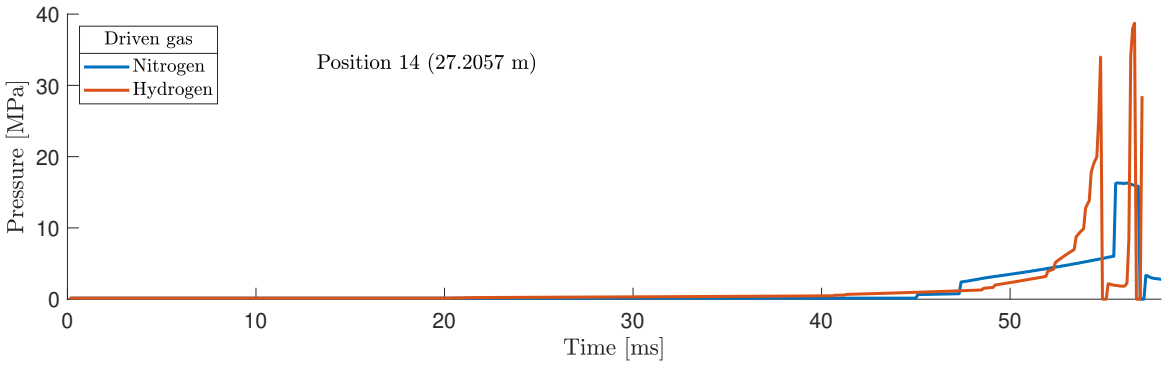

Figure 59: Pressure measured at the position hx14

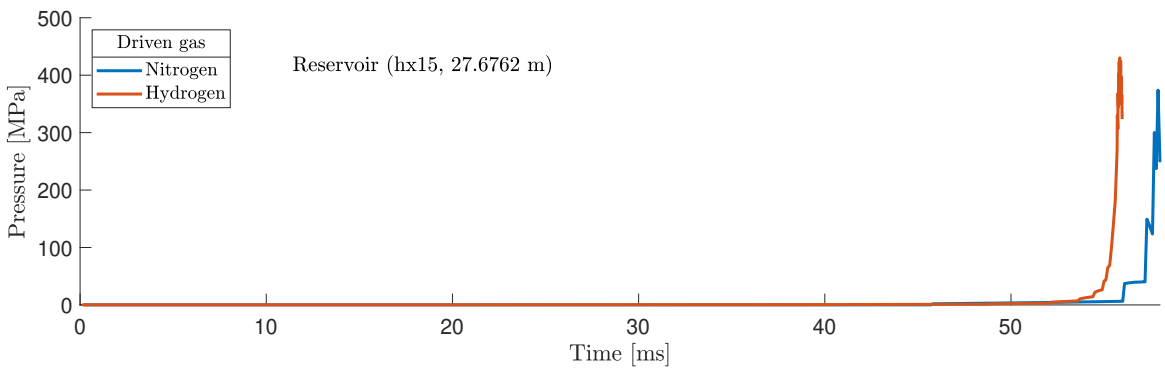

Figure 60: Pressure measured at the position hx15

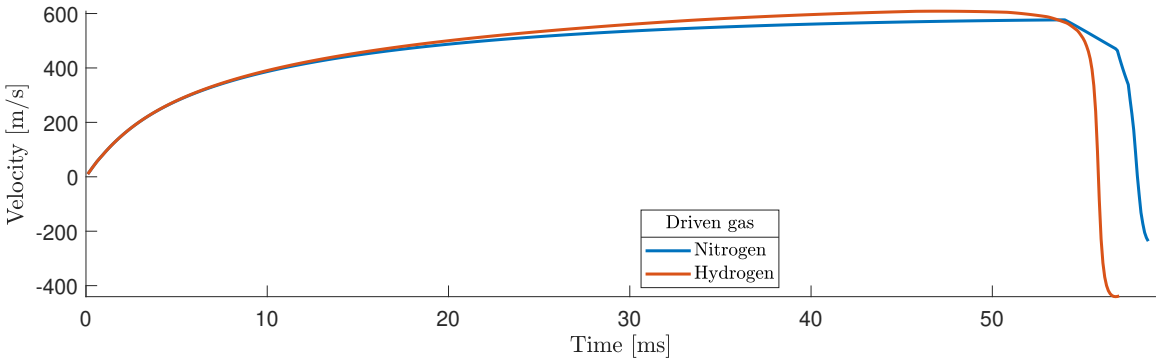

Figure 61: Velocity of the piston across time, simulated in the L1d program with hydrogen and nitrogen as test gas and using 3500 cells in front of the piston

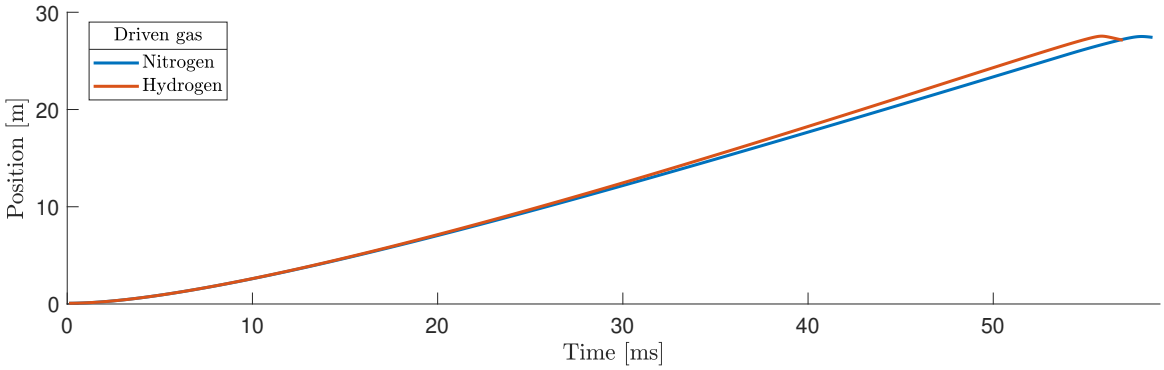

Figure 62: Position of the piston across time, simulated in the L1d program with hydrogen and nitrogen as test gas and using 3500 cells in front of the piston

Table 18 shows several critical parameters of the simulation using both gases. The maximum temperature and pressure reached in the reservoir are higher in the case of hydrogen. The temperature is more than 300 K higher in the case of hydrogen, while the pressure is also increased by 56 MPa. The initial conditions presented by Table 15 being designed for the use of nitrogen, the fact that the maximum pressure is above the structural limit of the reservoir is not problematic. It must be noticed however that these initial conditions could not be used to perform experiments on hydrogen. Moreover, due to the temperature reached during the test, the chemical embrittlement and the dissociation of hydrogen presented by the safety review of § 4.1.4 will occur. The creation of acetylene exposed in the same section is also likely to be noticed, even with a low quantity. The effect of a modification of the initial parameter is the object of the following section. As expected from the graphs presented above, the maximum velocities and initial accelerations are similar in both cases. However, the maximal deceleration (minimal acceleration) of the piston using hydrogen as test gas is about two times higher than when nitrogen is used in the driven tube. This high deceleration can be explained by the high pressure in the reservoir and the lower pressure behind the piston shown by the different pressure stations. The minimum distances between the piston and the reservoir are comparable, even if this distance is smaller in the case of the hydrogen.

Gas	Nitrogen	Hydrogen
Maximum temperature [K]	2297.7	2619.3
Maximum pressure [MPa]	374	430
Maximum velocity [m/s]	576.8	608.5
Maximum acceleration [m/s^2]	95058.8	95310.7
Minimum acceleration [m/s^2]	-9.99·10^5	-1.8·10^6
Minimum distance to the reservoir [m]	0.168	0.139

Table 18: Critical parameters obtained during the simulation of the compression process of the Longshot wind tunnel, using nitrogen and hydrogen as test gases and 3500 cells in the driven tube

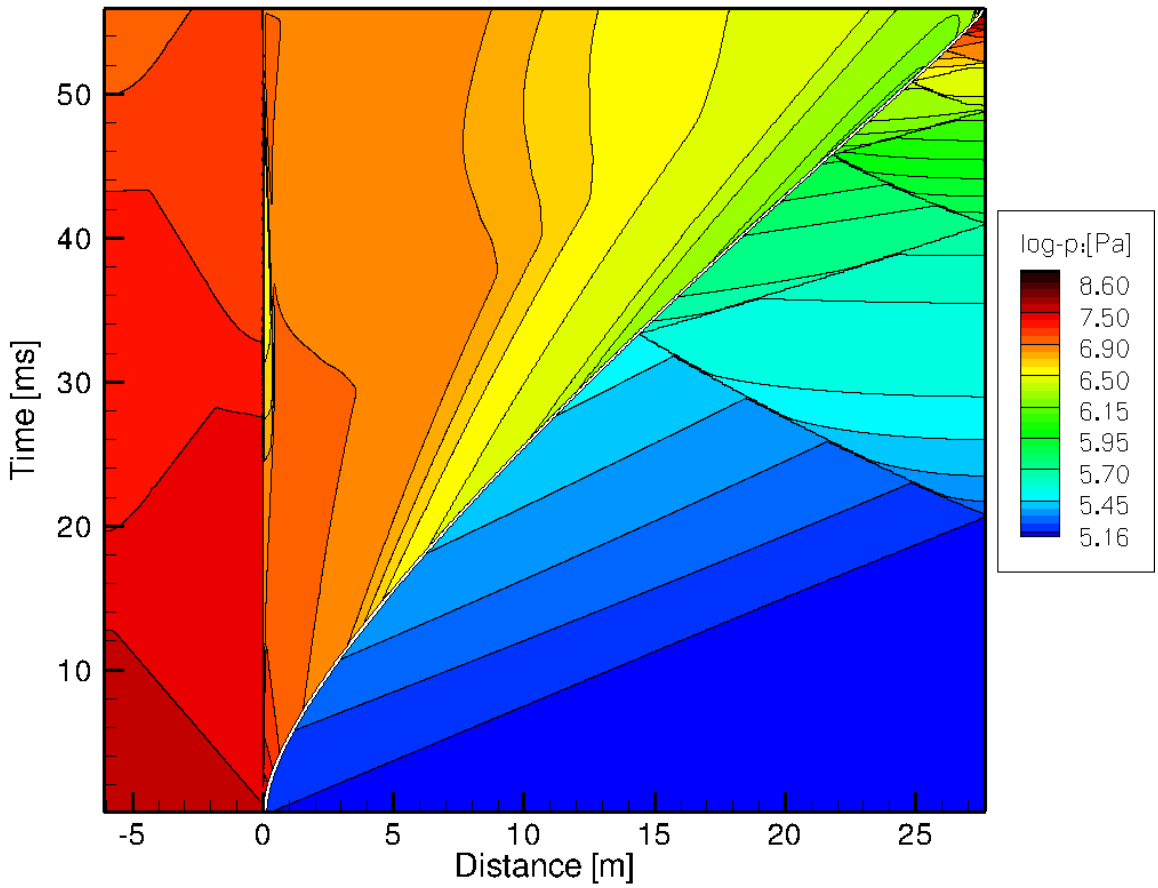

Figure 63: x-t diagram of hydrogen obtained using 2000 cells in the driver tube, 3500 cells in the driven tube and the initial conditions presented by Table 15

A typical representation of the pressure and piston's position output used by the von Karman Institute is the x-t diagram presented by Fig. 63. The primary shock and its reflections are also visible on this graph. The velocity of this first shock is approximately 1333 m/s. The velocity of the shock after its first reflection decreases to 1047 m/s. The velocity of this shock will then increase after its second reflection, this velocity always being larger when the shock goes from the piston to the reservoir than in the other direction. This multiple "weak" shock behaviour is not met when nitrogen or carbon dioxide is used as test gas, as it was presented by Fig. 45.

The temperature and pressure profiles obtained using nitrogen are different than those computed with hydrogen as test gas. For the same initial conditions, higher maximum temperature and pressure are measured with this second gas, as well as a higher piston velocity or deceleration. These initial conditions are not usable for nitrogen, since the maximum pressure reached using hydrogen would be higher than the structural limit of the reservoir. If hydrogen is selected for a series of test inside the Longshot wind tunnel, a modification of these initial conditions will be required. A first possibility would be the reduction of the mass of the piston, which could lead to a lower pressure and temperature inside the reservoir. These modifications of the initial conditions should then be investigated in a more advanced study.

5.3.3 Effect of a modification of the initial parameters

In order to check the stability of the results obtained thanks to the Lagrangian one dimensional simulation, a sensitivity analysis is performed by modifying the initial temperature and pressure of both the driver and the driven tube. The effect of the modification of the mass of the piston is also investigated. Each of these parameters are decreased by 1%. The pressure and temperature modifications in front of the piston are then measured and compared to the values obtained with the non modified initial conditions presented by Table 15. In order to be more representative of the situation, the relative differences presented in Table 19 were calculated by checking the modification of the temperature and pressure profiles in front of the piston in the station hx12, hx13, hx14 and hx15. The mean of the relative differences between these profiles and those obtained with the non modified conditions were then used to obtained the relative difference presented in this table. Notice that these relative differences are given in absolute value.

Modified parameter	Modification of the temperature	Modification of the pressure
Driven pressure	0.110 %	1.41 %
Driven temperature	1.028 %	0.183 %
Driver pressure	0.183 %	0.817 %
Driver temperature	0.650 %	0.184 %
Mass of the piston	0.334 %	1.26 %

Table 19: Mean relative difference between the temperature and pressures measured after the decrease of the initial conditions by 1% and those obtained with the initial conditions presented by Table 15. The reference used for these relative difference is the simulation with the non modified initial parameters

Thanks to the relative differences presented by Table 19, it becomes clear that a modification of the initial parameters of the simulation does not lead to a unexpected modification of the temperature and pressure profile. When the pressure in the driver and the driven tube are modified, the modification of the pressure in front of the piston is modified with the same order of magnitude. A modification of the temperature profile is also noticed, but this change is lower than the one of the pressure. Similarly, a modification of the initial temperature in the different tubes results in an alteration of the temperature in front of the piston with the same order of magnitude, while a smaller modification of the pressure is observed. It can also be noticed that the modification of an initial conditions in the driven tube leads to higher modifications of the temperature and pressure profiles than the same modification applied in the driver tube. Indeed, decreasing the initial pressure in the driver tube by 1% is translated by a modification of 0.817% of the pressure profile in the driven tube, while the same modification applied in the driven tube leads to an alteration of 1.41% of this pressure profile. In both case, a similar relative change is observed in the parameter not directly modified. A reduction of the mass of the piston leads to a similar reduction of the pressure profile, and a smaller decrease of the temperature profile. A larger modification of the mass of the piston was also simulated. This modification of mass (10%) led to a significant decrease of the maximum pressure (about 20%) and a smaller decrease of temperature of the order of 6%. The design of new initial conditions should then be investigated for the following simulations using hydrogen.

The different modifications of the initial parameters of the simulation all lead to the same type of difference in the temperature and pressure profiles. As expected, the modification of the pressure profile is higher when the initial pressure is altered. The same behaviour is observed with the temperature. The Lagrangian one dimensional code offers then stable results when used with hydrogen.

5.4 Conclusions

The Lagrangian one dimensional program used by the von Karman Institute to simulate the conditions that would occur during a experiment in the Longshot wind tunnel was created in the 90's and replaced the analytical approach previously used by the VKI. This program has the advantage of providing accurate results for simulations using nitrogen, carbon dioxide and helium. A convergence study was carried using the carbon dioxide as test gas, since its behaviour in this type of simulation is well known by the von Karman Institute. This convergence study was carried with the will of approximating the maximum temperature and pressure with a relative error lower than 0.2%. This led to the selection of 3500 cells to model the driven tube in front of the piston. The number of cells used in the driver tube was set to 2000, since this section of the wind tunnel is less critical and the modification of the number of cells used in this area does not lead to significant improvement of the temperature, pressure, velocity and position profiles.

Several simulations were performed in the L1d program using different approximation of the gas, a CFL of 0.25 and 3500 cells inside the driven tube. The perfect gas law and the more advanced equation of state proposed by Leachman et al. (2009) were both used in these simulations, either in inviscid and viscous situations, and their results were compared. It appeared that the perfect gas law overestimated the maximum temperature and pressure met inside the reservoir. This difference was event more significant when the gas viscosity had been taken into account. Considering hydrogen as a perfect gas inside the wind tunnel would then lead to conditions very different than those obtained by using the real gas equation of state. The inviscid assumption have also led to high relative error on the computation of the pressure and temperature profile, especially on the former.

Using the real gas equation of state presented by Leachman et al. (2009) and validated in § 5.3, the pressure profiles at the different pressure tab positions, as well as the position and velocity of the piston across time were studied and compared to the case where the driven gas is nitrogen. It appeared that the primary shock inside the wind tunnel is faster in the case of hydrogen, but offers lower compression than when nitrogen is used. This series of faster shocks had a smaller impact on the velocity of the piston in the case of hydrogen. This led to a faster piston but also to a maximum deceleration almost two times bigger than when nitrogen is used. The maximum pressure and temperature reached inside the reservoir were then found higher when hydrogen was used, however, these higher maximum temperature and pressure can be explained by the initial conditions that are not appropriated to the use of hydrogen. Despite the higher deceleration of the piston, the minimum distance between the end of the reservoir and the piston is lower when hydrogen is present in the driven tube. This distance is however comparable to the one obtained with nitrogen. The need of the design of several initial conditions for the use of nitrogen inside the Longshot and the L1D.

A sensitivity analysis was then applied by modifying the pressure and the temperature inside the driver and the driven tubes, as well as the mass of the piston. These initial parameters were modified one by one by 1% and the effect on the temperature and pressure profiles were investigated. It appeared that these modification in the initial conditions led to a relative difference of the results of the same order. The simulation using hydrogen is then concluded stable. The reduction of the mass of the piston by 10% decreased the maximum temperature and pressure respectively by 6 and 20 %.

6 Conclusions and propositions of future investigations

6.1 Conclusions

The density ratio through shock can be duplicated by the use of a gas that has the same specific heat ratio than the gas met in the real conditions of an atmospheric reentry. The duplication of the Mach number is necessary, until it reaches the type of value that allows the application of the Mach number independence principle. The duplication of the Reynolds number leads to the complete simulation of the total drag coefficient in the relevant viscous conditions. The specific heat ratio is then highlighted as one of the most important parameters to duplicate the atmospheric entry conditions, along with the Mach and Reynolds numbers. Since the Gaseous and Icy Giants atmospheres are composed of large concentrations of hydrogen and helium, the duplication of the conditions encountered during an atmospheric entry on these planets could be made using an another gas. The latter must however have the same specific heat ratio than hydrogen, which is the case for nitrogen or air. This second gas was indeed used to perform the test campaign for Galileo. Hydrogen can however be modelled inside the Lagrangian 1D program that simulates the Longshot wind tunnel. The equation of state of this gas offers indeed accurate results in a large temperature range. The major safety hazards of hydrogen are its risks of ignition or explosion, as well as the structural embrittlement noticed in several materials. Health hazard are limited to the usual recommendations considered for asphyxiant gases.

The mixture equation offers several possibilities of improvement of the simulation capabilities of the Longshot wind tunnel. The empirical parameters used by this equation must however be obtained by a series of experiments. Methane should not be used inside the Longshot, due to its low dissociation temperature that would lead to the formation of black carbon and hydrogen, with the possibility of creating a highly explosive gas inside the reservoir. Moreover, the dissociation of this gas also lead to the formation of hydrogen, either molecular or atomic, with the same concerns than previously presented. Tetrafluoromethane could be used in the Longshot wind tunnel, but an equation of state for this gas must be derived in terms of reduced Helmholtz energy in order to be used in the L1d. The use of this gas can however be compromised due to the interdiction of several refrigerants because of environmental hazard.

A series of simulations on the L1D program shows that the behaviour of hydrogen differs from nitrogen one in several ways. First, the shock wave in front of the piston is faster in the case of hydrogen, but the compression due to this wave is far smaller than using nitrogen. The final conditions in terms of temperature and pressure are also higher in the case of hydrogen. If hydrogen is selected as a test gas inside the Longshot wind tunnel, the design of initial conditions will then have to be carried. A first proposition on the decrease of the mass of the piston is introduced. The sensitivity analysis of the L1D highlighted the stability of the results to small modifications of the initial conditions.

6.2 Propositions of future investigations

This work offers several possibilities of improvement to the Longshot simulation capabilities. A series of topics could however be studied:

- If hydrogen is used inside the wind tunnel, an advanced study of the effects of this gas on the driven tube and the test section should be performed. Protection systems could then be developed to limit the damages in these areas. The possibility of an aluminium coating was presented, but simulations should be performed to ensure the effectiveness of this type of protection. Moreover, a series of hydrogen detectors should be installed to notice the possible leaks of hydrogen inside the laboratory.
- New initial conditions, more suitable for the use of hydrogen, should be designed, since those used during the L1D simulation proposed here were not adapted to the structural limits of the reservoir. A first possibility linked to the reduction of the mass of the piston was proposed, but an advanced study of the different initial conditions that could be used to obtained the desired Mach and Reynolds conditions should also be done.
- If the use of argon and CF_4 are investigated using L1D program, the insertion of an equation of state for the latter and an advance study of the accuracy of this equation for Argon at higher temperatures should be considered. The equation of state used in this work is sufficient for the validation of the mixture equation, but the lack of experimental data above 1200 K does not allow the validation of this equation of state at higher temperatures or for higher concentrations.
- The mixing rule presented here depends on several empirical parameters that are not available yet for several interesting mixtures such as nitrogen + helium or hydrogen + helium. Other mixtures, such as argon + CF_4 could also be considered to take advantage of the high mass and low specific heat ratio of the latter.
- It was reported that the relative error on the mixture equation can be linked to the the accuracy of the measurements of the different coupling parameters used by the equation. If a mixture containing oxygen should not be used inside the VKI Longshot, a mixture of nitrogen and argon could be used to precise these coupling parameters.

A Derivatives of the equations of states

A.1 Hydrogen equation of states

The different equations used to determine the thermodynamic properties of the hydrogen depicted by Eq. 9 to Eq. 14 need the definition of several derivatives of α^0 and α^r with respect to δ and/or τ.

First and second derivatives of α^0

$$\frac{\partial \alpha^0}{\partial \tau} = 1.5 \cdot \tau^{-1} + a_2 + \sum_{k=3}^{N} a_k b_k \frac{1}{1 - e^{-b_k \tau}} \tag{39}$$

$$\frac{\partial^2 \alpha^0}{\partial \tau^2} = -1.5 \cdot \tau^{-2} - \sum_{k=3}^{N} a_k b_k^2 \frac{e^{-b_k \tau}}{\left(1 - e^{-b_k \tau}\right)^2} \tag{40}$$

First derivatives of α^r

$$\begin{aligned}\frac{\partial \alpha^r}{\partial \tau} =& \sum_{i=1}^{l} N_i \delta^{d_i} t_i \tau^{t_i - 1} + \sum_{i=l+1}^{m} N_i \delta^{d_i} t_i \tau^{t_i - 1} e^{-\delta^{p_i}} \\ &+ \sum_{i=m+1}^{n} N_i \delta^{d_i} \left(t_i \tau^{t_i - 1} + 2\beta_i \tau^{t_i} (\tau - \gamma_i)\right) e^{\left[\phi_i (\delta - D_i)^2 + \beta_i (\tau - \gamma_i)^2\right]}\end{aligned} \tag{41}$$

$$\begin{aligned}\frac{\partial \alpha^r}{\partial \delta} =& \sum_{i=1}^{l} N_i d_i \delta^{d_i - 1} \tau^{t_i} + \sum_{i=l+1}^{m} N_i \tau^{t_i} \left(d_i \delta^{d_i - 1} - p_i \delta^{d_i}\right) e^{-\delta^{p_i}} \\ &+ \sum_{i=m+1}^{n} N_i \tau^{t_i} (d_i \delta^{d_i - 1} + 2\phi_i \delta^{d_i} (\delta - D_i)) e^{\left[\phi_i (\delta - D_i)^2 + \beta_i (\tau - \gamma_i)^2\right]}\end{aligned} \tag{42}$$

Second derivatives of α^r

$$\begin{aligned}\frac{\partial^2 \alpha^r}{\partial \tau^2} =& \sum_{i=1}^{l} N_i \delta^{d_i} t_i (t_i - 1) \tau^{t_i - 2} + \sum_{i=l+1}^{m} N_i \delta^{d_i} t_i (t_i - 1) \tau^{t_i - 2} e^{-\delta^{p_i}} \\ &+ \sum_{i=m+1}^{n} N_i \delta^{d_i} \big(4\beta_i^2 \tau^{t_i + 2} - 8\beta_i^2 \gamma_i \tau^{t_i + 1} + 2\beta_i (2t_i + 2\beta_i \gamma_i^2 + 1) \tau^{t_i} \\ &- 4\beta_i t_i \gamma_i \tau^{t_i - 1} + t_i (t_i - 1) \tau^{t_i - 2}\big) e^{\left[\phi_i (\delta - D_i)^2 + \beta_i (\tau - \gamma_i)^2\right]}\end{aligned} \tag{43}$$

$$\begin{aligned}\frac{\partial^2\alpha^r}{\partial\delta^2} =& \sum_{i=1}^{l} N_i\tau^{t_i}d_i(d_i-1)\delta^{d_i-2}+ \\ & \sum_{i=l+1}^{m} N_i\tau^{t_i}\Big(d_i(d_i-1)\delta^{d_i-2}-2p_id_i\delta^{d_i-1}+p_i^2\delta^{d_i}\Big)e^{-\delta^{p_i}}+ \\ & \sum_{i=m+1}^{n} N_i\tau^{t_i}\Big(4\phi_i^2\delta^{d_i+2}-8\phi_i^2D_i\delta^{d_i+1}+2\phi_i(2d_i+2\phi_iD_i^2+1)\delta^{d_i} \\ & \quad -4\phi_iD_id_i\delta^{d_i-1}+d_i(d_i-1)\delta^{d_i-2}\Big)e^{\left[\phi_i(\delta-D_i)^2+\beta_i(\tau-\gamma_i)^2\right]}\end{aligned} \tag{44}$$

$$\begin{aligned}\frac{\partial^2\alpha^r}{\partial\delta\ \partial\tau} =& \sum_{i=1}^{l} N_id_it_i\delta^{d_i-1}\tau^{t_i-1}+\sum_{i=l+1}^{m} N_it_i\left(d_i\delta^{d_i-1}-p_i\delta^{d_i}\right)\tau^{t_i-1}e^{-\delta^{p_i}}+ \\ & \sum_{i=m+1}^{n} N_i\left(d_i\delta^{d_i-1}+2\phi_i\delta^{d_i}(\delta-D_i)\right)\Big(t_i\tau^{t_i-1}+2\beta\tau^{t_i}(\tau-\gamma_i)\Big)e^{\left[\phi_i(\delta-D_i)^2+\beta_i(\tau-\gamma_i)^2\right]}\end{aligned} \tag{45}$$

B Hypervelocity Free Fligh Aerodynamic Facility

The *Ames Research Center*, located in the Silicon Valley, was created about 80 years ago to ensure the American superiority in the aeronautic field, either civil or military. Along its history, its objectives were shifted to become a key player in the aerospace sector, as the only aeroballistic facility that belongs to the NASA. Its field of application was used during several famous missions, such as the the Apollo program, Pioneer Venus, Mars Pathfinder, Galileo or the Space Shuttle program. Nowadays, the studies carried by this research centre are mostly focused on the International Space Station, the space telescope Kepler, New Horizon, Curiosity rovers or the Lunar Atmosphere Dust Environment Explorer[9].

The facility has available several wind tunnels, among which the *Hypervelocity Free Flight Aerodynamic Facility (HFFAF)* will be introduced. (Grinstead et al., 2010) and (Wilder, 2015) described the HFFAF as the only American facility able to test aerodynamics and aerothermodynamics of a test sample with gases different from air and at a sub-atmospheric pressure. These capabilities allow then an approach of the atmospheric re-entry, especially on planets different from the Earth, where the atmospheric composition significantly varies between inner and outer planets, as it will be exposed further.

B.1 HFFAF components

The wind tunnel, depicted by Fig. 64, is composed of several parts that are a launcher tube, a separation chamber, a test section, an impact chamber and a shock tube/tunnel.

B.1.1 Launcher tubes

Three types of launching tubes can be used, depending on the requirements in terms of model velocity, size and mass. These first stages were presented by (Grinstead et al., 2010). A first possibility is the use of an *air gun launcher*, which can allow a model between 2 and 20 g to be sent at a velocity ranging between 0.2 and 0.5 km/s. This method uses a compressed air reservoir to propel the model in a similar way than what can be experienced with a blow-down wind tunnel. A second possibility is the use of a powder charge that is ignited. The expansion gases that result of the detonation are then used to propel a 0.5 to 200 g model at a velocity up to 5.4 km/s.

[9] NASA Ames Research Center website

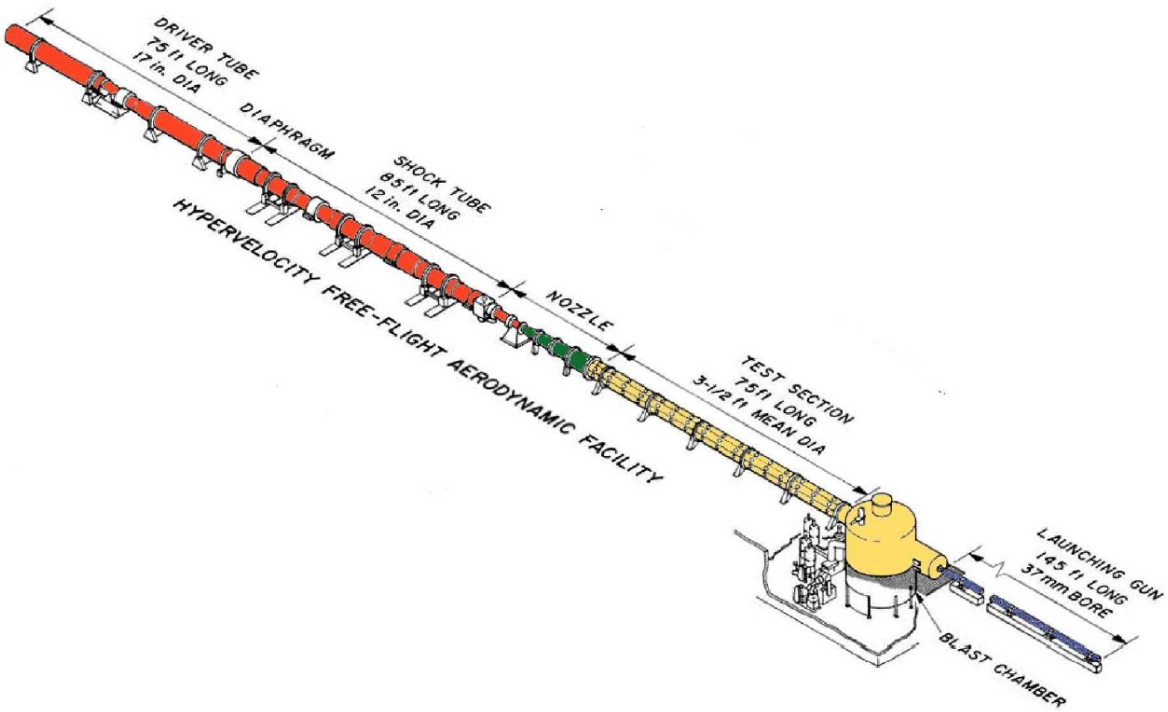

Figure 64: Sketch of the NASA Ames Hypervelocity Free Flight Aerodynamic Facility (Grinstead et al., 2010)

The last option considered by the HFFAF is the use of a light gas, hydrogen in the case of the HFFAF in a type of launcher based on the previous one, but more complex. In this type of launcher, the expanding gases resulting from the powder detonation are used to propel a deformable plastic piston in a first section of the launcher, called the pump tube. The piston compresses the light gas that, at a certain pressure, will rupture a diaphragm maintaining the launch package. A model with a mass of 0.2 to 400 g can then be propelled at a velocity ranging from 1.8 to 8 km/s. This last configuration is presented in Fig. 65.

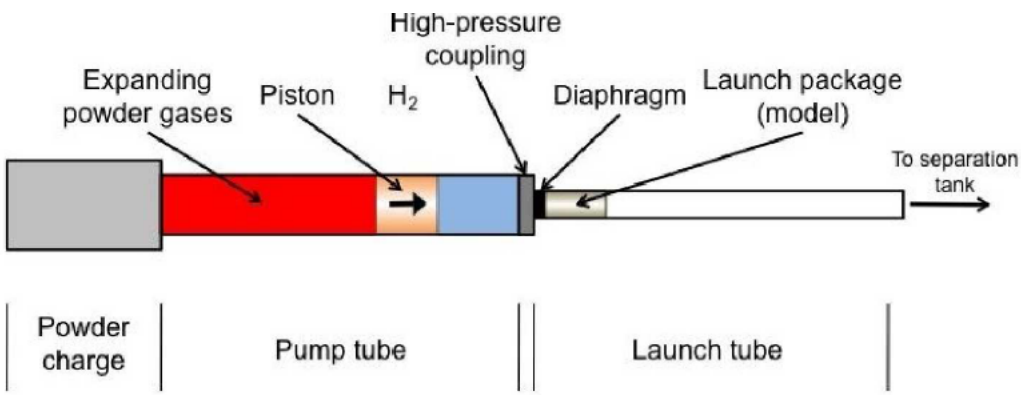

Figure 65: Launching tube using the light gas configuration (Grinstead et al., 2010)

The launched package accelerated by all these three methods are composed of the model itself, with the masses exposed for each method, and a sabot, made of several interlocking parts that hold the model until the separation chamber.

B.1.2 Separation chamber

The separation chamber is a vertical cylinder that separates the launching tube from the test section. In this dump tank, the model and the sabot will detached to each other, due to aerodynamic forces acting on the different part of the sabot. The former will pass through a conical region with a variable aperture, while the sabot will be stopped on this conical part. A thin Mylar diaphragm can be placed in this section to ensure an isolation between the test section and this separation chamber.

B.1.3 Test section

With a length of 22.8 m and a diameter of 1.1 m, the octagonal test section can be filled with different gas in order to test different atmospheric composition. Most of the tests were conducted using air for Earth re-entry experiments or carbon dioxide when the simulation of the Venusian or the Martian atmospheres were matter of interest. (Intrieri and Kirk, 1987) reported the use of several other test gases, such as hydrogen or Xenon. The measurements of the trajectory and aerodynamic coefficients are obtained thanks to a series of 16 shadowgraph stations placed 1.5 m away from each others. The aerothermodynamic measurements are obtained thanks to a group of IR cameras.

B.1.4 Impact chamber

This last section can be used for two main purposes. When the ballistic range is used alone, a set of polyethylene blocs are placed to stop the motion of the model. A second layer of steel will ensure the full stop of this model in the case where the polymer layer is not enough. When the shock tube is used, this impact chamber can be transformed into a fixed test section, where the flow over a larger model will be studied.

B.1.5 Shock tunnel

The Ames HFFAF can also use the capabilities of a shock tunnel. (Bogdanoff et al., 1992; Grinstead et al., 2010) described the geometry of the driver part of this tunnel to be 21.3 m long and have a diameter of 43.2 cm, while the driven tube is 4.7 m longer, but has a smaller diameter of 30.5 cm. The initial objective of this shock tunnel was to create a counter flow in the opposite direction of the model propelled by the ballistic range. This capability was put in standby, as well as the shock tunnel itself, in 1972. Before this date, this reflected mode shock tunnel used the combustion of a mixture of hydrogen and helium, with or without

oxygen, in its driver part. The driven part of the tunnel, separated to the driver tube by a stainless steel diaphragm and to the nozzle by a Mylar diaphragm, is filled with the desired test gas, which is usually air. Enthalpies of the order of 4,700 J/gm could then be reached at a pressure of 260 atm, or 1,900 J/gm for a wide pressure range. Depending on the nozzle, the outlet flow was able to range from 5 to 7 M. After its reactivation 17 years later, the enthalpy range was extended to 12 kJ/gm at a pressure of 408 atm.

B.2 Simulation capabilities

The purpose of the NASA Ames HFFAF is to provide the aerodynamic characteristics (lift, drag and pitching moment coefficients, stability criteria,...), aerothemodynamic characteristics, ablation behaviour and gas dynamics at hypervelocity of the tested model. The ballistic ranges have the capability to obtain Mach number between 0.5 and 20, and Reynolds number ranging from 250 to 10^7. One of the main advantage of the ballistic range is its capability to withstand pressures ranging from 760 mmHg to as low as 20 mmHg, with a very low leak rate of 10 mmHg/min. Thanks to these capabilities, several non toxic test gases can be used, even hydrogen, that would cause security concerns with other types of wind tunnels. However, as it will be exposed further, the aerodynamic tests performed on the Galileo probe were conducted using air, as reported by (Intrieri, 1988). According to (Grinstead et al., 2010), " *This facility is unique as it is the only known shock tube capable of generating shock velocities for Jovian entry*", using a test gas different from the one present on the Jovian atmosphere is very interesting, as it will be discussed further.

B.3 Summary

The Ames HFFAF uses a flying model and was used for the aerodynamic studies of several reentry vehicles and probes, such as the Apollo missions or the Galileo probe. Depending on the launching method used, a large variety of velocity can be reached by models of different masses. The measurements are obtained thanks to the analysis of shadowgraphs' pictures and IR cameras. An important consideration that must be highlight here is the consideration of air as a test gas to simulate the Jovian entry.

References

Anderson Jr, J.D., 2006. *Hypersonic and high-temperature gas dynamics*. American Institute of Aeronautics and Astronautics.

Ashby Jr, G., Love, E., Rainey, R. and Woods, W., 1969. Some topics in hypersonic body shaping.

Bavon, S., 2019. Cdf study report ice giants a mission to the ice giants-neptune and uranus. resreport 187C, ESA, 2200 AG Noordwijk The Netherlands.

Bertin, J.J., Periaux, J. and Ballmann, J., 1992. *Advances in Hypersonics: Defining the hypersonic environment*, vol. 1. Springer Science & Business Media.

Bienstock, B.J., 2004. Pioneer venus and galileo entry probe heritage. In *Planetary Probe Atmospheric Entry and Descent Trajectory Analysis and Science*, vol. 544, pp. 37–45.

Bogdanoff, D., Zambrana, H., Cavolowsky, J., Newfield, M., Cornelison, C. and Miller, R., 1992. Reactivation and upgrade of the NASA ames 16-inch shock tunnel - status report. In *30th Aerospace Sciences Meeting and Exhibit*. American Institute of Aeronautics and Astronautics.

Cain, T., 1997. Autoignition of hydrogen at high pressure. *Combustion and flame*, **111**(1-2): pp. 124–132.

Chapman, D.R., 1956. Some possibilities of using gas mixtures other than air in aerodynamic research. Tech. rep., NACA.

Chapman, D.R., 1960. *An analysis of the corridor and guidance requirements for supercircular entry into planetary atmospheres*, vol. 55. US Government Printing Office.

Collicott, H.E. and Bauer, P.E., 1983. *Entry Vehicle Heating and Thermal Protection Systems: Space Shuttle, Solar Starprobe, Jupiter Galileo Probe*. American Institute of Aeronautics and Astronautics.

Cortesi, A.F., Congedo, P.M., Magin, T.E., Van Hove, B. and Karatekin, O., 2016. Rebuilding freestream atmospheric conditions using surface pressure and heat flux data. In *8th AIAA Atmospheric and Space Environments Conference*, p. 4196.

Coutinho, J.A., Vlamos, P.M. and Kontogeorgis, G.M., 2000. General form of the cross-energy parameter of equations of state. *Industrial & engineering chemistry research*, **39**(8): pp. 3076–3082.

Curry, J.A. and Webster, P.J., 1998. *Thermodynamics of atmospheres and oceans*, vol. 65, chap. 14, pp. 386–424. Elsevier.

David C. Catling, J.F.K., 2019. *Atmospheric Evolution on Inhabited and Lifeless Worlds*. Cambridge University Press.

De Hemptinne, J.C. and Ledanois, J.M., 2012. *Select thermodynamic models for process simulation: A practical guide using a three steps methodology*. Editions Technip.

Dmitry V.Kotov, H.C.M.P.D.K.A.A., 2014. Computational challenges for simulations related to the nasa electric arc shock tube (east) experiments. *Journal of Computational Physics*, **269**: pp. 215–233.

Estela-Uribe, J., 2006. A helmholtz energy model for air and binary mixtures of nitrogen, oxygen and argon. *Fluid phase equilibria*, **243**(1-2): pp. 171–182.

Flasar, F., 1998. The composition of titans atmosphere : a meteorological perspective. *Planetary and Space Science*, **46**(9-10): pp. 1109–1124.

Gardiner Jr, W. and Kistiakowsky, G., 1961. Thermal dissociation rate of hydrogen. *The Journal of Chemical Physics*, **35**(5): pp. 1765–1770.

Grinstead, J.H., Wilder, M.C., Cornelison, C.J., Cruden, B.A. and Bogdanoff, D.W., 2010. Shock tube and ballistic range facilities at nasa ames research center. techreport, NASA Ames Research Center; Eloret Inc.

Grossir, G. and Ilich, Z., 2018. Numerical modeling of the VKI Longshot compression process. In O. Chazot and G. Grossir, eds., *Flow characterization and modeling of hypersonic wind tunnels*, vol. Lecture Series 2018/19, AVT-325, chap. 2. von Karman Institute for Fluid Dynamics.

Grossir, G., 2015. *Longshot hypersonic wind tunnel flow characterization and boundary layer stability investigations*. Ph.D. thesis, von Karman Institute for Fluid Dynamics - Université Libre de Bruxelles.

Gutsol, A., Rabinovich, A. and Fridman, A., 2011. Combustion-assisted plasma in fuel conversion. *Journal of Physics D: Applied Physics*, **44**: p. 274001.

Hofstadter, M.D., Simon, A., Reh, K. and Elliot, J., 2017. Ice giants pre-decadal study final report. *Rept. D-100520, Jet Propulsion Lab., Pasadena, CA*.

Holder, D.W. and Schultz, D.L., 1960. *On the flow in a reflected-shock tunnel*. Citeseer.

Hornung, H.G., 2010. Ground testing for hypervelocity flow, capabilities and limitations. Tech. rep., California Institute of Technology Pasadena Graduate Aerospace Labs.

Hudson, G. and McCoubrey, J., 1960. Intermolecular forces between unlike molecules. a more complete form of the combining rules. *Transactions of the Faraday Society*, **56**: pp. 761–766.

Hunt, J. and Jones, R., 1969. Use of tetrafluoromethane to simulate real-gas effects on the hypersonic aerodynamics of blunt vehicles. Tech. rep., NASA Langley Research Center,.

Hwang, Y.T. and Martin, J.J., 1964. The constant-volume heat capacity of gaseous tetrafluoromethane. *AIChE Journal*, **10**(1): pp. 89–91.

Ilich, Z.; Grossir, G.P.S.C.O., July 2017. *Experimental investigation of the VKI Longshot gun tunnel compression process*. EUCASS.

Ilich, Z., 2018. Deisgn of experiments to assess non-equilibrium nozzle flow phenomena in the VKI Longshot hypersonic tunnel. In *VKI PhD symposium*. von Karman Institute for Fluid Dynamics.

Ilich, Z., Grossir, G., Paris, S. and Chazot, O., 2019. Review of the VKI Longshot hypersonic tunnel operation for martian entries. In *AIAA Scitech*, AIAA paper 2019-1943.

Intrieri, P.F., 1988. Experimental investigation of hypersonic aerodynamics. techreport, NASA.

Intrieri, P.F. and Kirk, D.B., 1987. High-speed aerodynamics of several blunt-cone configurations. *Journal of Spacecraft and Rockets*, **24**(2): pp. 127–132.

Jacobs, P.A., 1994. Quasi-one-dimensional modeling of a free-piston shock tunnel. *AIAA Journal*, **32**(1): pp. 137–145.

Jansen, F., Chen, I. and Machonkin, M., 1989. On the thermal dissociation of hydrogen. *Journal of applied physics*, **66**(12): pp. 5749–5755.

Jargot, D., Marc, F., Miraval, S., Pilliere, F. and Robert, S., 2019. Acetylene, fiche toxicologique n^o212. *Base de donnees Fiches Toxicologiques*.

Jones, R.A. and Hunt, J.L., 1973. Measured pressure distributions of large-angle cones in hypersonic flows of tetrafluoromethane, air, and helium. Tech. rep., NASA TR R-312.

Justh, H., Justus, C. and Keller, V., 2006. Global reference atmospheric models, including thermospheres, for mars, venus and earth. In *AIAA/AAS Astrodynamics Specialist Conference and Exhibit*, p. 6394.

Justh, H.L., 2017. Neptune and titan global reference atmospheric models.

Justh, H.L. and Dwyer Cianciolo, A.M., 2017. Venus global reference atmospheric model status and planned updates. In *Venus Modeling Workshop*, vol. 2022.

Justus, C., Duvall, A. and Keller, V., 2005. Atmospheric models for mars aerocapture. In *41st AIAA/ASME/SAE/ASEE Joint Propulsion Conference & Exhibit*, p. 4106.

Justus, C., Duvall, A. and Keller, V., 2006. Atmospheric models for aerocapture. In *40th AIAA/ASME/SAE/ASEE Joint Propulsion Conference and Exhibit*. American Institute of Aeronautics and Astronautics.

Leachman, J.W., Jacobsen, R.T., Penoncello, S. and Lemmon, E.W., 2009. Fundamental equations of state for parahydrogen, normal hydrogen, and orthohydrogen. *Journal of Physical and Chemical Reference Data*, **38**(3): pp. 721–748.

Lemmon, E.W. and Tillner-Roth, R., 1999. A helmholtz energy equation of state for calculating the thermodynamic properties of fluid mixtures. *Fluid phase equilibria*, **165**(1): pp. 1–21.

Lemmon, E.W., Jacobsen, R.T., Penoncello, S.G. and Friend, D.G., 2000. Thermodynamic properties of air and mixtures of nitrogen, argon, and oxygen from 60 to 2000 k at pressures to 2000 mpa. *Journal of physical and chemical reference data*, **29**(3): pp. 331–385.

Lemmon, E.W., 1997. *A generalized model for the prediction of the thermodynamic properties of mixtures including vapor-liquid equilibrium.* Ph.D. thesis, University of Idaho.

Lind, C., 1975. What causes unconfined vapor cloud explosions. *Loss Prevention*, **9**: pp. 101–105.

Lockwood, G.J., Helbig, H.F. and Everhart, E., 1964. Measurements of thermal dissociation of hydrogen, using fast protons. *The Journal of Chemical Physics*, **41**(12): pp. 3820–3824.

Lockwood, M.K., 2003. Titan aerocapture systems analysis. In *39th AIAA/ ASME/ SAE/ ASEE Joint Propulsion Conference and Exhibit*. American Institute of Aeronautics and Astronautics.

Lukasiewicz, J., 1973. *Experimental Methods of Hypersonics*, vol. 3 of *Gas dynamics series*, chap. 1, pp. 1–23. Marcel Dekker.

Mahaffy, P.R., Webster, C.R., Atreya, S.K. and et al, 2013. Abundance and isotopic composition of gases in the martian atmosphere from the curiosity rover. *Science*, **341**(6143): pp. 263–266.

McCarty, R.D., 1981. *Selected properties of hydrogen (engineering design data)*, vol. 168. US Department of Commerce, National Bureau of Standards.

Molkov, V., 2012. Fundamentals of hydrogen safety engineering. *Bookboon. com ISBN*, pp. 978–87.

Moore, G.E. and Unterwald, F., 1964. Thermal dissociation of hydrogen. *The Journal of Chemical Physics*, **40**(9): pp. 2639–2652.

Moss, J.N., 1980. A study of the aerothermal entry environment for the galileo probe. *Entry Heating and Thermal Protection*, pp. 3–25.

Najjar, Y.S., 2013. Hydrogen safety: The road toward green technology. *International Journal of Hydrogen Energy*, **38**(25): pp. 10716–10728.

Neice, M.M., 1948. Tables and charts of flow parameters across oblique shocks. Tech. rep., NACA.

Niemann, H.B., Atreya, S.K., Bauer, S.J., Carignan, G.R., Demick, J.E., Frost, R.L., Gautier, D., Haberman, J.A., Harpold, D.N., Hunten, D.M., Israel, G., Lunine, J.I., Kasprzak, W.T., Owen, T.C., Paulkovich, M., Raulin, F., Raaen, E. and Way, S.H., 2005. The abundances of constituents of titan's atmosphere from the GCMS instrument on the huygens probe. *Nature*, **438**(7069): pp. 779–784.

Niemann, H.B., Atreya, S.K., Carignan, G.R., Donahue, T.M., Haberman, J.A., Harpold, D.N., Hartle, R.E., Hunten, D.M., Kasprzak, W.T., Mahaffy, P.R. et al., 1996. The galileo probe mass spectrometer: Composition of jupiter's atmosphere. *Science*, **272**(5263): pp. 846–849.

Niemann, H., Atreya, S., Carignan, G., Donahue, T., Haberman, J., Harpold, D., Hartle, R., Hunten, D., Kasprzak, W., Mahaffy, P. et al., 1998. The composition of the jovian atmosphere as determined by the galileo probe mass spectrometer. *Journal of Geophysical Research: Planets*, **103**(E10): pp. 22831–22845.

Olivier, H. and Gu, S., 2018. Operation, capabilities and limitations of existing hypersonic facilities. In O. Chazot and G. Grossir, eds., *Flow characterization and modeling of hypersonic wind tunnels*, vol. Lecture Series 2018/19, AVT-325, chap. 1. von Karman Institute for Fluid Dynamics.

Ordin, P., 1997. Safety standard for hydrogen and hydrogen systems: Guidelines for hydrogen system design, materials selection, operations, storage, and transportation. office of safety and mission assurance. *National Aeronautics and Space Administration, Washington DC*.

Oriani, R., 1978. Hydrogen embrittlement of steels. *Annual review of materials science*, **8**(1): pp. 327–357.

Ortiz Vega, D.O., 2013. *A new wide range equation of state for helium-4*. Ph.D. thesis, Texas A&M University.

Perry, R.W., 1964. The Longshot type of high-Reynolds number hypersonic tunnel. In *Third hypervelocity techniques symposium*, Advanced experimental techniques for study of hypervelocity flight.

Reynier, P., 2016. Survey of high-enthalpy shock facilities in the perspective of radiation and chemical kinetics investigations. *Progress in Aerospace Sciences*, **85**: pp. 1–32.

Reynier, P., 2008. Convective blockage during earth re-entry. a review. In *40th AIAA Thermophysics Conference*.

Reynier, P., 2012. Numerical reconstruction of galileo entry. In *5th International Workshop on Radiation and High Temperature Gases in Atmospheric Entry*, vol. ESA SP-714.

Saito, H., Watanabe, T. et al., 2009. Decomposition of tetrafluoromethane by water plasma generated under atmospheric pressure. *Thin Solid Films*, **518**(3): pp. 929–935.

Schmidt, R. and Wagner, W., 1985. A new form of the equation of state for pure substances and its application to oxygen. *Fluid Phase Equilibria*, **19**(3): pp. 175–200.

Seiff, A., Venkatapathy, E., Haas, B. and Intrieri, P., 1996. Galileo probe aerodynamics. In *14th Applied Aerodynamics Conference*, p. 2451.

Setzmann, U. and Wagner, W., 1991. A new equation of state and tables of thermodynamic properties for methane covering the range from the melting line to 625 k at pressures up to 100 mpa. *Journal of Physical and Chemical reference data*, **20**(6): pp. 1061–1155.

Span, R. and Wagner, W., 1996. A new equation of state for carbon dioxide covering the fluid region from the triple-point temperature to 1100 k at pressures up to 800 MPa. *Journal of Physical and Chemical Reference Data*, **25**(6): pp. 1509–1596.

Span, R., Lemmon, E.W., Jacobsen, R.T., Wagner, W. and Yokozeki, A., 2000. A reference equation of state for the thermodynamic properties of nitrogen for temperatures from 63.151 to 1000 k and pressures to 2200 mpa. *Journal of Physical and Chemical Reference Data*, **29**(6): pp. 1361–1433.

Starr, B., Westhelle, C. and Masciarelli, J., 2004. Aerocapture performance analysis for a neptune-triton exploration mission. In *AIAA Atmospheric Flight Mechanics Conference and Exhibit*. American Institute of Aeronautics and Astronautics.

Stewart, R.B. and Jacobsen, R.T., 1989. Thermodynamic properties of argon from the triple point to 1200 k with pressures to 1000 mpa. *Journal of Physical and Chemical reference data*, **18**(2): pp. 639–798.

Tegeler, C., R., S. and W., W., 1999. A new equation of state for argon covering the fluid region for temperatures from the melting line to 700 k at pressures up to 1000 mpa. *Journal of Physical and Chemical Reference Data*, **28**(3): pp. 779–850.

Tikhonov, V.I. and Volkov, A.A., 2002. Separation of water into its ortho and para isomers. *Science*, **296 5577**: p. 2363.

Twu, C.H., Coon, J.E., Kusch, M.G. and Harvey, A.H., 1994. Selection of equations of state models for process simulator. In *Simulation Science Inc. Workbook Meeting*, vol. 24.

Vitu, S., Jaubert, J.N. and Mutelet, F., 2006. Extension of the ppr78 model (predictive 1978, peng–robinson eos with temperature dependent kij calculated through a group contribution method) to systems containing naphtenic compounds. *Fluid phase equilibria*, **243**(1-2): pp. 9–28.

VonZahn, U., Kumar, S., H.Niemann and Prinn, R., 1983. *Venus*, chap. 13, pp. 299–326. Space Science Series. Donald M. Hunten.

Weimer, A.W., Dahl, J., Tamburini, J., Lewandowski, A., Pitts, R., Bingham, C., Glatzmaier, G.C. and Design, P., 2001. Thermal dissociation of methane using a solar coupled aerosol flow reactor. *Proc. US DOE Hydrogen Program Rev*, pp. 1–43.

Wilder, M.C.; Bogdanoff, D., 2015. The nasa ames hypervelocity free flight aerodynamic facility: Experimental simulation of the atmospheric break-up of meteors.

Williams, D.D.R., 2018a. Neptune fact sheet.
URL https://nssdc.gsfc.nasa.gov/planetary/factsheet/neptunefact.html

Williams, D.D.R., 2018b. Saturn fact sheet.
URL https://nssdc.gsfc.nasa.gov/planetary/factsheet/saturnfact.html

Williams, D.D.R., 2018c. Uranus fat sheet.
URL https://nssdc.gsfc.nasa.gov/planetary/factsheet/uranusfact.html